

2013 RSNA (Filtered Schedule)

**Sunday, December 01, 2013**

11:00-12:30 PM • **ICIA11** • Room: S401CD • Quantitative Medical Imaging for Clinical Research and Practice: Hands-on Workshop  
02:00-03:30 PM • **RC103** • Room: N227 • Cardiovascular Risk Assessment: The Role for the Radiologist  
02:00-03:30 PM • **RC117** • Room: S504CD • Combining In Vitro Diagnostics and Imaging for Integrated Decision Making  
02:00-03:30 PM • **RC125** • Room: S104A • Quantitative Imaging: Current and Future Practice in Radiology and Clinical Trials

**Monday, December 02, 2013**

08:30-10:00 AM • **MSMI21** • Room: S406B • Molecular Imaging Symposium: Preparing for Tomorrow: The Application of Novel and Advanced Imaging in Clinical...  
08:30-10:00 AM • **RC217** • Room: S504CD • PET-MR/Hyperpolarized MR  
08:30-10:00 AM • **RC225** • Room: N229 • Quantitative Imaging: Diffuse Lung Disease Assessment Using CT  
10:30-12:00 PM • **SSC03** • Room: S504AB • Cardiac (Quantitative Imaging)  
10:30-12:00 PM • **SSC06** • Room: E451A • Gastrointestinal (Oncology: Surveillance and Tumor Response)  
01:30-03:00 PM • **MSMI23** • Room: S406B • Molecular Imaging Symposium: Imaging Cellular Subpopulations - Current Progress and Future Directions  
01:30-02:45 PM • **PS20** • Arie Crown Theater • Monday Plenary Session  
03:00-04:00 PM • **SSE01** • Arie Crown Theater • Breast Imaging (MRI Interpretation)  
03:00-04:00 PM • **SSE19** • Room: S504CD • Nuclear Medicine (Quantitative Imaging)  
03:30-05:00 PM • **MSMI24** • Room: S406B • Molecular Imaging Symposium: Molecular Brain Imaging: From Research to Clinical Applications

**Tuesday, December 03, 2013**

08:30-10:00 AM • **RC322** • Room: E261 • Uncertainties in Imaging for Radiation Oncology: Sources and Mitigation Techniques-Incorporation of Imaging as...  
08:30-10:00 AM • **RC325** • Room: E353A • Quantitative Imaging: Functional MRI (fMRI)  
08:30-10:00 AM • **RC326** • Room: N229 • Quantitative Imaging: A Revolution in Evolution (In Association with the Society for Imaging Informatics in Me...  
10:30-12:00 PM • **SSG08** • Room: S402AB • Informatics (3D, Quantitative and Advanced Visualization)  
10:30-12:00 PM • **SSG12** • Room: N229 • Neuroradiology (Imaging of White Matter and Demyelinating Disease)  
10:30-12:00 PM • **SSG13** • Room: S403A • Physics (Quantitative Imaging I)  
04:30-06:00 PM • **RC409** • Room: E350 • Gastrointestinal: Tumor Response Assessment  
04:30-06:00 PM • **RC417** • Room: S504CD • Quantitative CT and MR Perfusion Imaging  
04:30-06:00 PM • **RC425** • Room: S404AB • Quantitative Imaging: Dynamic Contrast Enhanced MRI (DCE-MRI)

**Wednesday, December 04, 2013**

08:30-10:00 AM • **RC525** • Room: S102AB • Quantitative Imaging: Quantitative Imaging in FDG-PET  
10:30-12:00 PM • **SSK14** • Room: E451A • Musculoskeletal (Tumor II)  
10:30-12:00 PM • **SSK16** • Room: N230 • Neuroradiology (Advanced Neuroimaging of Alzheimer's Disease)  
10:30-12:00 PM • **SSK20** • Room: S403B • Physics (Quantitative Imaging II)  
03:00-04:00 PM • **SSM19** • Room: N228 • Physics (Quantitative Imaging III)

**Thursday, December 05, 2013**

08:30-10:00 AM • **RC625** • Room: N226 • Quantitative Imaging: Volumetric CT as a Biomarker for Disease  
08:30-12:00 PM • **VSCH51** • Room: E351 • Chest Series: Hot Topics in Chest Imaging: Emerging Technologies and Clinical Applications  
10:30-12:00 PM • **SSQ02** • Room: E450A • Breast Imaging (CAD/Quantitative Imaging)  
01:30-02:45 PM • **PS50** • Arie Crown Theater • Thursday Plenary Session  
03:00-04:00 PM • **SPSH52** • Room: E350 • Hot Topic Session: MR Quantification Techniques in the Liver (Fat, Iron, Fibrosis)  
04:30-06:00 PM • **RC725** • Room: E352 • Quantitative Imaging: Informatics

**Friday, December 06, 2013**

08:30-10:00 AM • **RC818** • Room: S404CD • Techniques for Quantitative Cancer Imaging: Current Status  
08:30-10:00 AM • **RC825** • Room: E263 • Quantitative Imaging: Quantitative Imaging in Ultrasound  
10:30-12:00 PM • **SST11** • Room: N230 • Neuroradiology (Quantitative Neuroimaging)

**Quantitative Medical Imaging for Clinical Research and Practice: Hands-on Workshop**

**Sunday, 11:00 AM - 12:30 PM • S401CD**



[Back to Top](#)

**ICIA11** • AMA PRA Category 1 Credit™:1.5 • ARRT Category A+ Credit:1.5

**Sonia M Pujol**, PhD  
**Katarzyna J Macura**, MD, PhD \*  
**Ron Kikinis**, MD

**LEARNING OBJECTIVES**

1) Enhance interpretation of DICOM images through the use of 3D visualization. 2) Gain experience with interactive, quantitative assessment of complex anatomical structures. 3) Present current directions of quantitative imaging as a biomarker in clinical trials.

**ABSTRACT**

Quantitative imaging has the potential to bring valuable information for the accurate interpretation of clinical data. Technological breakthroughs in medical imaging hardware and the emergence of increasingly sophisticated image processing algorithms permit the display of complex anatomical structures, and the estimation of quantitative functional parameters with increasing sensitivity and specificity. For the past 9 years, the National Alliance for Medical Image Computing (NA-MIC), one of the seven National Centers for Biomedical Computing funded by the National Institutes of Health, has converted some of the major scientific advances made by the biomedical imaging community into open-source software tools. As part of the NA-MIC toolkit, the 3D Slicer open-source software has been developed as a technology delivery platform for clinical researchers. This workshop provides an introduction to quantitative medical imaging data analysis for clinical research and practice. Cases from multiple imaging modalities and from multiple organ systems will be highlighted to illustrate the depth and breath of this field, and series of hands-on sessions using 3D Slicer will provide participants with a practical experience of quantitative image analysis. Course url: [http://www.na-mic.org/Wiki/index.php/RSNA\\_2013](http://www.na-mic.org/Wiki/index.php/RSNA_2013)

URL's  
[http://www.na-mic.org/Wiki/index.php/RSNA\\_2013](http://www.na-mic.org/Wiki/index.php/RSNA_2013)

**Cardiovascular Risk Assessment: The Role for the Radiologist**

**RC103** • AMA PRA Category 1 Credit™:1.5 • ARRT Category A+ Credit:1.5**RC103A • The Role of Carotid US****Joseph F Polak MD, MPH** (Presenter)**LEARNING OBJECTIVES**

1) Present the American Heart Association guidelines for the assessment of cardiovascular risk in individuals without clinical cardiovascular disease. 2) Define the carotid artery biomarkers:plaque and carotid artery intima media wall thickness (IMT). 3) Highlight the key elements of cardiovascular risk stratification and how imaging biomarkers can contribute. 4) Summarize the key evidence that carotid ultrasound imaging biomarkers help predict future myocardial infarctions and other cardiovascular events. 5) Describe a published carotid imaging protocol used to assess degree of cardiovascular risk in Cardiology office practices with emphasis on carotid artery intima-media thickness (IMT). 6) Weigh the advantages against the limitations of carotid ultrasound imaging biomarkers.

**ABSTRACT**

Background: Carotid ultrasound imaging as practiced in Radiology typically focuses on the detection of hemodynamically significant carotid artery stenoses in order to triage patients for carotid artery surgery. The role of carotid ultrasound imaging is, however, much broader in current clinical practices, especially those based in Cardiology. Methods: Review of the literature shows that the focus of carotid ultrasound imaging has shifted from detecting stenotic lesions in need of surgical intervention to documenting the presence of early atherosclerotic lesions. Carotid ultrasound can identify and quantify two biomarkers of use in primary prevention: early carotid artery plaques and diffuse wall intima-media thickening (IMT). Results: Early forms of carotid artery disease are associated with increased risk of all forms of first time cardiovascular events. Both IMT and plaque show evidence of risk prediction. The American Heart Association recommends carotid ultrasound evaluation of IMT and plaque in asymptomatic individuals more highly than resting or exercise electrocardiograms. Implementation of carotid IMT and carotid plaque imaging with ultrasound is still limited by a lack of standardization. This is apparent in the guidelines published by the American Society of Echocardiography. The quantitative evaluation of IMT needs to be contrasted against subjective or quantitative measurements of plaque (IMT) height. Ultimately, the value of the carotid artery biomarkers needs to be contrasted against standard risk stratification and improvement in classification of individuals as low, intermediate, or high risk. The data show promise in this regards. Conclusion: Carotid ultrasound biomarkers can be measured non-invasively without exposure to radiation. Carotid ultrasound is readily accepted by patients. The technical expertise required to perform these measurements is much more stringent that would appear at first glance.

**RC103B • The Role of Cardiac CT****John J Carr MD, MS** (Presenter)**LEARNING OBJECTIVES**

1) Discuss the utility of CT to detect and characterize coronary artery disease and subclinical disease. 2) Discuss CT findings predictive of cardiovascular risk factors.

**ABSTRACT**

Cardiac CT, without and with intravenous contrast, has for the first time provided a non-invasive measurements of coronary plaque in healthy people. We now have strong evidence that subclinical coronary artery disease by CT strongly predicts future clinical events but perhaps more importantly is consistent with :pathologic studies indicating that coronary artery disease begins in childhood and progresses over decades before resulting in clinical disease. This presentation will review the evidence that calcified plaque by CT is the single:strongest predictor of 5 year risk of acute myocardial infarction and:cardiovascular death. Likewise, CT angiography has provided new insights into features of coronary plaque (positive remodeling, low attenuation and spotty calcifications) that places individuals at high risk for clinical events. Beyond dramatic reductions in radiation exposure, new computational techniques are allowing CT to provide precise estimates of coronary blood flow, a:physiologic measure important for patient management.: Lastly, we will discuss how physicians should use every chest CT to help patients and their healthcare teams better understand their cardiovascular risk and guide clinical care.

**RC103C • The Role of Cardiac MRI****David A Bluemke MD, PhD** (Presenter) \***LEARNING OBJECTIVES**

1) Discuss use of MRI to assess the cardiovascular disease to detect and characterize early, subclinical disease. 2) Present information on left ventricular mass, volumes and myocardial scar as risk factors, as derived from large population-based studies.

**ABSTRACT**

Cardiovascular MRI has key characteristics of precision in disease detection combined with lack of radiation exposure. As a result, MRI has found tremendous use not only in evaluating sick patients, but also in screening for disease in individuals who may be healthy but who are at risk for cardiovascular disease. This presentation will review results from large population based trials that have used MRI to detect early, subclinical cardiovascular disease. Left ventricular mass in particular has proven to be an extremely powerful biomarker to identify individuals at risk for heart failure. Common risk factors, such as diabetes and smoking, have tremendous adverse effect on myocardial remodeling that have now been quantified. Myocardial scar detection with MRI is used routinely in the clinic, and its role in identifying early disease in asymptomatic individuals will also be discussed.

**Combining In Vitro Diagnostics and Imaging for Integrated Decision Making**

Sunday, 02:00 PM - 03:30 PM • S504CD

**RC117** • AMA PRA Category 1 Credit™:1.5 • ARRT Category A+ Credit:1.5**Moderator****Sanjiv S Gambhir**, MD, PhD \***RC117A • Combining In Vitro and In Vivo Diagnostics for Monitoring Response to Anti-cancer Therapies****Sanjiv S Gambhir MD, PhD** (Presenter) \***LEARNING OBJECTIVES**

1) Understand biomaker discovery for response to therapy applications. 2) Understand how animal models are used for validating biomarkers. 3) Learn relative advantages of In Vitro vs. In Vivo diagnostics. 4) Understand a specific application in EGFR targeted Lung Cancer Therapy.

**RC117B • In-Vivo, Near-Vivo, and On-Vitro Diagnostics: The Overlap****Richard Levenson MD** (Presenter) \*

#### LEARNING OBJECTIVES

1) Appreciate the challenges confronting rigorous correlation between pathology and radiology findings and the potential benefit to both disciplines if better, high-resolution correspondences are established, perhaps via machine-learning-based image segmentation tools. 2) Understand the potential that in-vivo microscopy holds for integrating pathology and radiology diagnostic procedures. 3) Learn about virtual autopsy procedures (combined post-mortem CT and tissue sampling) and their role in improving quality control. 4) And possibly hear about new technology that should allow comparison of PET tracer gross anatomic location with cellular-scale imaging (work in progress).

### RC117C • Combining In Vivo and In Vitro Diagnostics for Lung Cancer Detection

**Viswam S Nair MD** (Presenter)

#### LEARNING OBJECTIVES

1) To understand how blood biomarker integration may improve clinical diagnosis for solitary pulmonary nodules. 2) To understand how circulating tumor cells may be helpful in diagnosing malignant nodules of the lung.

#### ABSTRACT

Current data from CT screening studies suggest that they improve survival for high risk patients with a lung nodule. Yet, this comes at considerable cost, both to the patient as a result of unnecessary procedures and for the medical system delivering care. Non-invasive circulating biomarkers that augment current clinical diagnostic algorithms provide one solution to these issues. The specific case of circulating tumor cells will be discussed.

## Quantitative Imaging: Current and Future Practice in Radiology and Clinical Trials

**Sunday, 02:00 PM - 03:30 PM • S104A**

**RS PH BQ**

[Back to Top](#)

**RC125 • AMA PRA Category 1 Credit™:1.5 • ARRT Category A+ Credit:1.5**

#### Director

**Michael F McNitt-Gray**, PhD \*

### RC125A • RSNA Perspective and Initiatives

**Daniel C Sullivan MD** (Presenter)

#### LEARNING OBJECTIVES

1) Describe the benefits of implementing more quantitative image interpretation in clinical radiology practice. 2) Understand the activities that RSNA supports to help move the profession of radiology from a primarily qualitative interpretation paradigm to a more quantitative-based interpretation model. 3) Describe the challenges of extracting uniform, standardized quantitative measures from clinical imaging scans.

#### ABSTRACT

The RSNA Strategic Plan strives to advance the radiological sciences and foster the development of new technologies in part by promoting the quantification of imaging results. The added value of quantification in both research and clinical environments is likely to increase as health care initiatives place increased pressure on radiologists to provide decision support for evidence-based care. There remain substantial barriers to the widespread use of quantitative measures in clinical radiology including inherently large number of variables that impede validation of specific metrics, diversity of proprietary industry platforms, and lack of acceptance by radiologists. A critical barrier to the implementation of QI in radiology is the lack of standardization among vendor platforms. Collaboration in the pre-competitive space is challenging yet crucial to address standardization, and integrating quantitative measurement into workflow will be necessary for wide adoption. The obstacles to overcome with practicing radiologists are a distrust of the reliability of QI and the fear of losing value of radiologists' expertise through automation and commoditization. The Quantitative Imaging Biomarkers Alliance (QIBA) was officially launched in 2007 as a means to unite researchers, healthcare professionals, and industry stakeholders in the advancement of quantitative imaging. QIBA's mission is to: Improve the value and practicality of quantitative biomarkers by reducing variability across devices, patients and time. QIBA's six active technical committees (DCE-MRI, fMRI, FDG-PET, volumetric CT, COPD-Asthma, US shear-wave speed) develop QIBA Profiles (i.e., documents) of standardized specifications for image acquisition, collection, and post-processing.

### RC125B • NCI's Quantitative Imaging Network (QIN): Progress and Impact on Clinical Trials

**Paula M Jacobs PhD** (Presenter)

#### LEARNING OBJECTIVES

1) Describe various methods for prediction and measurement of therapy response. 2) Understand which imaging modalities and software tools are best suited for this clinical goal. 3) Understand the complexity of quantitative imaging methodology and how to compare the performance of different. 4) Understand how NCI Research Networks function to create a consensus on imaging methodology and public resources to meet these aims. 5) Learn about NCI funding opportunities for this research area.

### RC125C • American College of Radiology Imaging Network/Eastern Cooperative Oncology Group (ACRIN/ECOG) Perspective

**Mitchell D Schnall MD, PhD** (Presenter)

#### LEARNING OBJECTIVES

1) Identify the importance of quantitative imaging principles in the setting of clinical trials. 2) Identify conditions required for successful application of quantitative imaging principles. 3) Analyze quantitative imaging techniques and apply this knowledge to protocol development in the setting of clinical trials.

## Molecular Imaging Symposium: Preparing for Tomorrow: The Application of Novel and Advanced Imaging in Clinical Oncology

**Monday, 08:30 AM - 10:00 AM • S406B**

**OI MI BQ**

[Back to Top](#)

**MSMI21 • AMA PRA Category 1 Credit™:1.5 • ARRT Category A+ Credit:1.5**

#### Moderator

**Ronald L Korn**, MD, PhD

### MSMI21A • Fluorescence and Optoacoustic Imaging Heads to the Clinics

**Vasilis Ntziachristos PhD** (Presenter) \*

#### LEARNING OBJECTIVES

1) Learn the technology basics and assess the current state of the art in fluorescence and optoacoustic imaging. 2) Understand the imaging performance achieved and major improvements over past approaches. 3) Learn on how this new-generation imaging

performance offers a paradigm shift in optical and clinical imaging. 4) Link the developments described to unique contrast generation in clinical and pre-clinical applications. 5) Gain insights into current clinical pilot studies using these approaches.

## MSMI21B • CT Biomarkers and How to Use Them

**Kenneth Miles** (Presenter) \*

### LEARNING OBJECTIVES

1) Describe the oncological imaging biomarkers available from CT. 2) Demonstrate knowledge of the processes required for qualification of CT biomarkers in oncological drug development and clinical practice. 3) Compare the applications of CT biomarkers for prognosis, response prediction and response assessment.

### ABSTRACT

By measuring size and attenuation with or without contrast material, CT can provide a range of oncological biomarkers including T-stage, RECIST, enhancement, CT perfusion and CT texture analysis. Implementation of these biomarkers requires prior assessments of technical/biological performance and establishment of biomarker performance characteristics. For clinical applications, assessments of therapeutic and health impact are also required. Technical/biological validation includes assessments of test-retest performance and identification of relevant biological correlates. Evaluations of biomarker performance should report cross-validated diagnostic/prognostic thresholds, hazard ratio and biomarker prevalence. Based on these parameters, modelling studies can evaluate the potential therapeutic and health impacts that would result from clinical deployment. Current evidence supporting the use of CT biomarkers in drug development and clinical practice are summarised.

## MSMI21C • The Use of Novel PET Tracers. What is in the Pipeline for Approval

**Jonathan E McConathy** MD, PhD (Presenter) \*

### LEARNING OBJECTIVES

1) Describe the PET tracers in late phase clinical trials for oncologic imaging in terms of their molecular targets and potential clinical indications. 2) Identify the major regulatory and financial challenges encountered during the translation of PET tracers into widespread clinical use. 3) Compare the properties, strengths, and weaknesses of PET tracers for prostate cancer imaging as case studies.

### ABSTRACT

Positron emission tomography (PET) with the glucose analogue 2-deoxy-2-[F-18]fluoro-D-glucose (FDG) combined with computed tomography (CT) is currently the workhorse for clinical molecular imaging in oncology. While very successful, FDG-PET/CT has limitations in certain cancers and provides a readout of only one aspect of cancer biology. Novel PET tracers have great promise to improve diagnostic imaging, and a wide range of small molecule, peptide, antibody, and nanoparticle-based PET tracers are in development for oncologic imaging. This presentation will provide an overview of PET tracers in late phase clinical development with an emphasis on mechanism of action and potential clinical indications. Additionally, some of the key challenges to the widespread clinical use of PET tracers including regulatory and financial issues will be reviewed. Finally, several classes of PET tracers for prostate cancer imaging will be discussed in greater depth to illustrate key points.

## MSMI21D • Systems Diagnostics - The Future of Diagnostic Medicine?

**Michael D Kuo** MD (Presenter) \*

### LEARNING OBJECTIVES

1) To understand systems diagnostics as a new diagnostics paradigm. 2) To explore clinical applications and future directions of systems diagnostics.

## PET-MR/Hyperpolarized MR

**Monday, 08:30 AM - 10:00 AM • S504CD**

**NM** **MR** **BQ**

[Back to Top](#)

**RC217 • AMA PRA Category 1 Credit™:1.5 • ARRT Category A+ Credit:1.5**

**Moderator**

**Heike E Daldrup-Link**, MD

## RC217A • Hyperpolarized 13C MR-A Complementary Method to PET for Imaging in Vivo Metabolism

**Daniel M Spielman** PhD (Presenter)

### LEARNING OBJECTIVES

1) Assess the basic principles of hyperpolarized 13C MRS, including sample preparation, image acquisition, and data analysis. 2) Differentiate metabolic parameters measurable by hyperpolarized 13C MRS from those obtained with PET. 3) Compare PET versus hyperpolarized 13C MRS sensitivities, spatial resolution, and temporal resolution.

## RC217B • MR/PET, A New Perspective of Molecular Imaging

**Claus D Claussen** MD (Presenter)

### LEARNING OBJECTIVES

1) To learn about the evolution of MR/PET. 2) To become familiar with current MR/PET imaging strategies. 3) To be informed about clinical applications of MR/PET.

## RC217C • The Emerging Clinical Role of Hyperpolarized 13C MR in Prostate Cancer Imaging

**John Kurhanewicz** PhD (Presenter) \*

### LEARNING OBJECTIVES

1) Understand the clinical need and biochemical rationale for the use of hyperpolarized [1-13C] pyruvate for prostate cancer imaging. 2) Demonstrate a multi-hyperpolarized probe approach for simultaneously measuring prostate cancer metabolism and tumor micro-environment. 3) Demonstrate the utility of hyperpolarized 13C MR for measuring prostate cancer aggressiveness and response to therapy. 4) Demonstrate the safety, clinical feasibility, sensitivity and resolution, and future availability of clinical hyperpolarized 13C MR.

## RC217D • Brain Dedicated PET-MRI -How Far Are We?

**Zang-Hee Cho** PhD (Presenter)

### LEARNING OBJECTIVES

1) For the study of neurochemical and molecular activities in the human brain In-Vivo. 2) Roles of the ultra-high field MRI and high resolution brain PET and their fusion product.

### ABSTRACT

Last decade or so nuclear medicine or molecular imaging has progressed substantially, especially with new brain dedicated PET such as HRRT and the ultra-high field MRI such as 7.0T. Combination of the two, that is HRRT-PET and 7.0T MRI MRI, designed for the brain dedicated molecular imaging began to provide a number of markedly improved images hitherto unavailable by the conventional systems. In this talk, recent development of PET-MRI fusion Imaging focused onto the study of a number deep brain structures such as the hippocampus, the thalamus and brainstem would be discussed. For instance, brainstem molecular imaging of the raphe nuclei began to show individually resolved raphe nucleus glucose and serotonin transporter activities and suggesting us the potentials of the technique for to the study of the emotional and affect related disorders.

## Quantitative Imaging: Diffuse Lung Disease Assessment Using CT

Monday, 08:30 AM - 10:00 AM • N229

[PH](#) [CT](#) [BQ](#) [CH](#)

[Back to Top](#)

**RC225** • AMA PRA Category 1 Credit™:1.5 • ARRT Category A+ Credit:1.5

**Director**

**Michael F McNitt-Gray**, PhD \*

### RC225A • The Role of Quantitative CT in the Assessment of Diffuse Lung Disease

**Jonathan G Goldin** MBChB, PhD (Presenter)

#### LEARNING OBJECTIVES

1) Identify the application of quantitative imaging principles in the assessment of patients with Diffuse Lung Disease. 2) Identify conditions required for successful application of quantitative imaging principles. 3) Analyze quantitative imaging techniques and apply this knowledge to protocol development and patient management in the setting of both clinical workup and clinical trials involving patients with Diffuse Lung Disease.

### RC225B • Quantitation in the Assessment of COPD

**David A Lynch** MBBCh (Presenter) \*

#### LEARNING OBJECTIVES

1) Describe the methodology and limitations of non-invasive imaging in quantifying lung structure. 2) Describe the opportunities for non-invasive imaging in understanding the structure of the lung, and how that relates to phenotyping subjects for clinical trials and longitudinal studies. 3) Understand the clinical relevance of quantitative imaging of COPD. 4) Learn how to interpret quantitative CT results in the lung.

#### ABSTRACT

COPD is characterized on CT by emphysema, bronchial wall thickening, and small airway abnormalities. These morphologic findings may be quantified and grouped into phenotypes, with different clinical presentations and prognosis. Clinicians are increasingly using these quantitative imaging techniques to study COPD. This course will provide information on the results of large-scale clinical trials ongoing in COPD. The limitations and sources of variation of current quantitative imaging methods will be discussed. Relationships between quantitative CT measures, genetic markers, and clinical abnormalities will be stressed.

### RC225C • Standardization of Imaging and Measurement Protocols

**Matthew S Brown** PhD (Presenter) \*

#### LEARNING OBJECTIVES

1) Understand sources of quantitative lung CT measurement variation including technical, physiologic, and algorithmic. 2) Review strategies for standardization across multiple sites and imaging platforms. 3) Assess the impact on sample size in multicenter clinical trials.

## Cardiac (Quantitative Imaging)

Monday, 10:30 AM - 12:00 PM • S504AB

[MR](#) [BQ](#) [CA](#)

[Back to Top](#)

**SSC03** • AMA PRA Category 1 Credit™:1.5 • ARRT Category A+ Credit:1.5

**Moderator**

**E. Kent Yucel**, MD

**Moderator**

**Suhny Abbara**, MD \*

**Moderator**

**Pamela K Woodard**, MD \*

### SSC03-01 • Role of 4D Flow MRI in Detecting Hemodynamic Changes in Patients with Pulmonary Arterial Hypertension

**Pegah Entezari** MD (Presenter); **Susanne Schnell**; **Naomi C Chesler** PhD; **Christopher J Francois** MD; **Alejandro Roldan** PhD; **Oliver Wieben** PhD; **Jeremy D Collins** MD\*; **James C Carr** MD\*; **Alex Barker**; **Michael Markl** PhD

#### PURPOSE

To evaluate peak velocity, net flow, vessel diameter and wall shear stress (WSS) in the proximal pulmonary arteries of normotensive controls and patients with pulmonary arterial hypertension (PAH) using 4D flow MRI.

#### METHOD AND MATERIALS

With IRB approval, 10 patients (age: 57±10, 5 females) and 9 volunteers (age: 40 ±12, 6 females) were scanned on a 3T MR system. Time-resolved 3D pulmonary flow was measured using 4DMRI with full coverage of the right ventricular outflow tract, pulmonary trunk (PT) and right and left pulmonary branches (RPA and LPA). Net flow and maximum velocity were quantified at the level of PT, RPA and LPA. WSS and vessel diameter were also measured in analysis planes positioned at these three levels in both groups.

#### RESULTS

Net flow in PAH patients (PT: 52.7±11, LPA: 21.5±5, RPA: 26.2±7 ml/cycle) was significantly lower compared to controls (PT: 68.3±13, LPA: 29.3±7, RPA: 32.7±5 ml/cycle, p-value< 0.05). The same pattern was observed for peak velocity in PAH patients (PT: 0.5±0.1, LPA: 0.3±0.1, RPA: 0.4±0.1 m/s) compared to the controls (PT: 0.8±0.1, LPA: 0.7±0.2, RPA: 0.9±0.2 m/s, p-value< 0.05). In addition, PAH arteries had a significantly larger diameter (PT: 3.4±0.5, LPA: 2.3±0.3, RPA: 2.4±0.3 cm) compared to the normal population (PT: 2.6±0.2, LPA: 1.8±0.2, RPA: 1.7±0.3 cm, p-value< 0.001). As shown in Figure 1, PAH patients had reduced WSS at all three measurement positions, compared to volunteers.

#### CONCLUSION

4D flow MRI illustrates distinct hemodynamic changes in PAH patients compared to a normal population. The significant reduction in net flow, peak velocity and an increase in PA lumen diameter in patients resulted in decreased WSS values, as compared to normal

volunteers.

#### CLINICAL RELEVANCE/APPLICATION

Pulmonary hypertension is associated with right heart failure, but its effect on arterial diameter and hemodynamic factors (i.e. velocity, flow, WSS) and their role in disease progression is not clear

### SSC03-02 • Serum Biomarkers of Atherosclerosis and Myocardial Remodeling: Correlation with Quantitative Imaging Markers of Coronary Heart Disease at Cardiac CT

**Lucas L Geyer MD (Presenter) \***; **Balazs Ruzsics**; **Aleksander Krazinski**; **Justin R Silverman**; **Christopher L Schlett MD, MPH**; **U. Joseph Schoepf MD \***; **Ullrich Ebersberger MD**; **Fabian Bamberg MD, MPH \***; **Maximilian F Reiser MD**; **Michael R Zile MD**

#### PURPOSE

We aimed at correlating the plasma levels of several novel circulating biomarkers of atherosclerotic disease activity and myocardial remodeling with quantitative imaging markers of coronary heart disease obtained by coronary CT angiography (cCTA).

#### METHOD AND MATERIALS

In an IRB-approved, HIPAA compliant study, 75 patients with suspected coronary artery disease underwent contrast enhanced, retrospectively ECG-gated coronary dual-source CT angiography. Patients were evaluated for the type of coronary plaque and the presence and severity of coronary artery stenosis on a per patient and per segment basis. Semi-automated software was used for measuring the volume of non-calcified and mixed plaques; lipid-rich and fibrous contents were differentiated. Cardiac function parameters were obtained using cine CT reconstructions across the RR cycle. Plasma samples were collected from each patient and a cytokine and protease profiling panel was performed by multiplex analysis. The plasma concentrations of seven biomarkers with a reported relationship with atherosclerosis and myocardial remodeling were measured: TNF $\alpha$ , IL-6, IL-8, matrix metalloproteinase (MMP)-2, MMP-3, MMP-7, MMP-8. Data were analyzed using Spearman's rank correlation coefficient and Mann-Whitney-U-Test.

#### RESULTS

Data of 61 men and 14 women (59 $\pm$ 10 years) were evaluated. 60/75 patients showed atherosclerotic changes in at least one vessel based on cCTA. 34/75 had significant (>50%) stenosis in at least one coronary artery. 46 non-calcified, 129 calcified, and 86 mixed plaques were identified. We found a statistically significant ( $p$

#### CONCLUSION

Our study suggests that elevated levels of MMP-8 are associated with greater atherosclerotic plaque volume at cCTA. Moreover, IL-8 and TNF $\alpha$  may indicate more active myocardial remodeling with higher myocardial mass at CT.

#### CLINICAL RELEVANCE/APPLICATION

Integration of quantitative cardiac CT imaging with novel serum biomarkers of atherosclerosis and myocardial remodeling may enhance insights into the patho-mechanisms of coronary heart disease.

### SSC03-03 • Coronary Artery Calcification Scoring with CT Scanners from Four Different Vendors Results in Different Scores

**Martin J Willemink MD (Presenter)**; **Richard A Takx MD**; **Mathias Prokop MD, PhD \***; **Johan De Mey \***; **Marco Das MD \***; **Pim A De Jong MD, PhD**; **Ricardo P Budde MD, PhD**; **Arnold Schilham PhD**; **Ronald L Bleys MD, PhD**; **Nico Buls DSc, PhD \***; **Joachim E Wildberger MD, PhD**; **Tim Leiner MD, PhD \***

#### PURPOSE

Coronary artery calcifications have emerged as an important biomarker for cardiovascular risk stratification. New guidelines recommend evaluation of these calcifications using cardiac computed tomography (CT) in asymptomatic adults with low-to-intermediate and intermediate cardiovascular risk, concerning approximately 40% of the United States adult population. Treatment strategies depend on coronary artery calcification scores on CT. However, it is unknown whether different new generation CT scanners result in similar Agatston scores. Therefore, the purpose was to determine the inter-vendor variability of coronary artery calcifications expressed as Agatston scores with state-of-the-art CT scanners from the four major vendors.

#### METHOD AND MATERIALS

We evaluated the differences in coronary calcium scores between state-of-the-art CT scanners from four different vendors using fifteen ex-vivo human hearts placed in a commercially available anthropomorphic chest phantom. These hearts were scanned with unenhanced prospectively ECG-triggered step-and-shoot protocols at equal radiation dose settings. Thickness and increment of slices were 3mm. Agatston scores, calcification volume and mass scores were quantified with clinically used semi-automatic software from the same vendor as the CT system. Differences were analyzed with the Friedman test (significance level  $P$

#### RESULTS

Fourteen hearts had coronary calcifications. Agatston scores, calcification volume and mass scores differed significantly ( $P$ 3, respectively. Median (interquartile range) calcification mass scores were 70 (27-245), 84 (42-326), 85 (43-337), and 69 (35-246) mg, respectively.

#### CONCLUSION

CT scanners from different vendors result in significantly different Agatston scores, calcification volume scores and mass scores.

#### CLINICAL RELEVANCE/APPLICATION

Dependent on the CT vendor of a hospital, differences in coronary calcium scoring may result in different treatment strategies.

### SSC03-04 • Impact of Iterative Reconstruction on CT Coronary Calcium Quantification

**Akira Kurata (Presenter)**; **Anoeshka S Dharampal MD**; **Admir Dedic MD**; **Pim Feyter MD, PhD**; **Marcel L Dijkshoorn RT \***; **Gabriel P Krestin MD, PhD \***; **Koen Nieman MD**

#### PURPOSE

Coronary artery calcium (CAC) score by computed tomography (CT) is widely used for cardiovascular risk stratification. Iterative reconstruction algorithms reduce image noise and potentially decrease radiation exposure. We evaluated the influence of sonogram-affirmed iterative reconstruction (SAFIRE) on the CCS score.

#### METHOD AND MATERIALS

In 70 consecutive patients, who underwent CAC imaging by 128-slice dual-source CT, CAC volume, mass and Agatston score were calculated from images reconstructed by filtered back projection (FBP) without and with incremental degrees of iterative reconstruction (SAFIRE algorithm: 10-50%). We used the repeated measuring test and the Steel-Dwass test for multiple comparisons of values and the difference ratio among different SAFIRE groups, using the FBP (0% SAFIRE) as reference.

#### RESULTS

The median Agatston score (range) decreased with incremental IR: 163 (0.1 ~ 3393.3), 158.4 (0.3 ~ 3079.3), 137.7 (0.1 ~ 2978.0), 120.6 (0 ~ 2783.6), 102.6 (0 ~ 2468.4), and 84.1 (0 ~ 2186.9) for 0% (FBP), 10%, 20%, 30%, 40%, and 50% SAFIRE, respectively (Figure 1;  $P$

#### CONCLUSION

SAFIRE noise reduction techniques significantly affected the coronary calcium quantification, with potential clinical consequences.

#### CLINICAL RELEVANCE/APPLICATION

Iterative reconstruction techniques should not be used, because it significantly reduced quantitative coronary calcium quantification.

### SSC03-05 • Higher Myocardial Extracellular Volume Fraction in Women than Men: Study by Contrast Enhanced Cardiac Magnetic Resonance Imaging

**Shi-Jun Zhang** (Presenter) ; **Sheng Hong Ju** MD, PhD

#### PURPOSE

To investigate whether the myocardial extracellular volume fraction (ECV) of women differs from that of men in healthy population.

#### METHOD AND MATERIALS

Institutional review board approval and informed consent were obtained. Twenty-eight healthy volunteers (11 men and 17 women, aged 19 to 63 years) were recruited and underwent MRI scan with a 0.15 mmol/kg intravenous bolus of Gd-DTPA. A mid-cavity short-axis plane was selected for T1 mapping precontrast and repetitively after contrast injection, using the modified Look-Locker inversion recovery (MOLLI) sequence. Regions of interest (ROIs) were selected from four segments (the septal, anterior, lateral and inferior wall of the left ventricular) within the myocardium for ECV calculating in each person. The ECV was calculated as:  $ECV = \frac{R_{1m} - R_{1b}}{R_{1b}} (1 - \text{hematocrit})$ , where  $R_{1m}$  is the myocardial contrast partition coefficient, and was calculated by relating change in longitudinal relaxation rate ( $R_1 = 1/T_1$ ) of myocardium ( $R_{1m}$ ) versus that of left ventricular blood pool ( $R_{1b}$ ). Independent-samples  $t$  tests were applied to compare ECV between the two sexes groups on both per-segment and per-person basis.

#### RESULTS

Three out of the 112 segments were excluded from two men due to severe artifact, remaining 41 segments in men and 68 segments in women. The mean values ( $\pm$ standard deviation) of ECV within the septal, anterior, lateral and inferior left ventricular wall were  $0.238 \pm 0.023$ ,  $0.235 \pm 0.024$ ,  $0.245 \pm 0.032$  and  $0.240 \pm 0.022$  in the 11 men, while in the 17 women, the values were  $0.273 \pm 0.023$ ,  $0.275 \pm 0.033$ ,  $0.279 \pm 0.025$  and  $0.276 \pm 0.034$ . The mean difference (95% confident interval, 95%CI) for the four segments between the two sexes groups were 0.034 (0.016-0.053), 0.040 (0.016-0.063), 0.034(0.012-0.057) and 0.036 (0.010-0.063). The overall mean ECV values of these two groups on per-segment basis were  $0.239 \pm 0.025$  and  $0.275 \pm 0.029$ ,  $P < 0.001$ . The per-person ECV were calculated as the arithmetic mean value of the ROIs from the 4 segments, and the mean values of the two groups were  $0.239 \pm 0.024$  and  $0.275 \pm 0.024$ ,  $P = 0.001$ .

#### CONCLUSION

Women's myocardial extracellular volume fraction is higher than men's in healthy population.

#### CLINICAL RELEVANCE/APPLICATION

The higher myocardial ECV in healthy women than men indicates studies ideally consist of subgroups of each gender may help to interpret the research and clinical results involving myocardial ECV.

### SSC03-06 • Automatic Quantification of Blood Flow from Real-time Phase-contrast MRI

**Markus Huellebrand** (Presenter) ; **Anja Hennemuth** MS ; **Jens Frahm** PhD \* ; **Lennart Tautz**

#### PURPOSE

2D phase-contrast (PC) MRI is an established technique for the analysis of vascular hemodynamics. A recently developed real-time MRI technique allows for respective acquisitions under free breathing and without the need for ECG synchronization. However, quantitative evaluations become more complicated than for conventional methods because of potential changes in contrast, the management of multiple cycles without manual interference, and the influence of respiratory displacements. In order to overcome such problems, we developed a new method for the automatic analysis of blood flow parameters from real-time PC MRI.

#### METHOD AND MATERIALS

Real-time 2D PC MRI of the ascending aorta was performed in 5 healthy subjects (mean age 25 years) were at 3-T (TrioTim, Siemens, Erlangen, Germany). Acquisitions were based on a highly undersampled radial FLASH sequence with and without a bipolar flow-encoding gradient ( $VENC=200$  cm/s, flip angle  $10^\circ$ ) and image reconstruction by regularized nonlinear inversion. The spatial resolution was  $1.33 \times 1.33 \times 6.0$  mm<sup>3</sup> and the temporal resolution corresponded to 40 ms. The images were analyzed with use of the research software prototype CAIPI. After an initial segmentation of the aortic vessel wall, the vessel contour is automatically propagated to all frames using a registration based on a quadrature filter. The results of the automatic analysis were compared to the manual results of three experts.

#### RESULTS

The segmentation results of the three observers and the automatic segmentation (duration  $39 \pm 4$  s) were compared pair-wise. The average dice coefficient between observers and the algorithm was  $0.86 \pm 0.04$ , the inter-observer comparison was  $0.92 \pm 0.03$ . The average symmetric absolute surface distance error was  $1.09 \pm 0.4$  mm for the algorithm and  $0.71 \pm 0.22$  mm for the observers. The mean absolute error of the stroke volume was  $4.67 \pm 2.28$  ml for the algorithm and  $6.14 \pm 3.5$  ml for the observers.

#### CONCLUSION

The comparison of the manual and automatic quantification shows good agreement. Because no manual correction is needed, the proposed method is suited for the automatic analysis of the temporal evolution of flow velocities, peak velocities, stroke volumes and flow rates over multiple cardiac cycles.

#### CLINICAL RELEVANCE/APPLICATION

Automatic quantification of real-time 2D PC MRI enables analysis of patients with aperiodic heartbeats (e.g. arrhythmias) and monitoring of hemodynamic responses to stress or physiologic maneuvers.

### SSC03-07 • Normal Diastolic and Systolic Myocardial T1 Times at 1.5 T: Correlations and Blood Normalization

**Ursula Reiter** (Presenter) ; **Gert Reiter** \* ; **Katrin Dorr** MD ; **Andreas Greiser** PhD \* ; **Ralph Maderthaler** MD ; **Michael H Fuchsjaeger** MD

#### PURPOSE

To evaluate regional differences between systolic and diastolic myocardial longitudinal relaxation time (T1), and to investigate variances of myocardial T1 values associated with T1 time of blood to derive relations between blood normalized systolic and diastolic myocardial T1 times in healthy subjects.

#### METHOD AND MATERIALS

In the current prospective study, approved by the local ethical review board, 40 healthy subjects (20 female, 20 male; age range 20-35 years) underwent ECG-gated 1.5 T magnetic resonance imaging. A modified Look-Locker inversion recovery (MOLLI) sequence was used to acquire basal, mid-ventricular and apical short-axis myocardial T1 maps in systole and diastole. Regional myocardial T1 times were evaluated in 16 AHA-segments, blood T1 values were derived from blood pool in the center of the left ventricular cavity. Linear regression slopes between myocardial and blood T1 values were employed to normalize measured myocardial T1 values to the mean blood T1 time of the study population. Means of T1 values were compared by t-test, considering  $p < 0.05$  as significant.

#### RESULTS

Mean myocardial T1 times ( $984 \pm 28$  ms in diastole,  $959 \pm 21$  ms in systole) as well as all segmental T1 values in diastole and systole differed significantly ( $p_2 = 0.53$  for diastole,  $R^2 = 0.52$  for systole): After blood normalization variances of segmental and mean myocardial T1 times decreased (to 17 ms in diastole and 13 ms in systole in case of mean myocardial T1 times) and significant differences in segmental and mean myocardial T1 times with gender completely disappeared. Blood normalized diastolic and systolic myocardial T1 values strongly correlated with each other on segmental ( $r = 0.72$ ) as well as mean myocardial ( $r = 0.89$ ) level.

#### CONCLUSION

In normal myocardium, diastolic and systolic myocardial T1 times significantly differ but strongly correlate with each other. Besides elimination of gender differences in myocardial T1 values, blood normalization reduces variability of myocardial T1 times.

#### CLINICAL RELEVANCE/APPLICATION

Blood normalization allows improving the definition of threshold values to distinguish normal from pathologically affected myocardium in diastole and systole.

### SSC03-08 • 4-Dimensional Magnetic Resonance Velocity Mapping Based Evaluation of Elevated Mean Pulmonary Arterial Pressure: Comparison of Vector, Streamline and Particle Trace Flow Visualization

**Ursula Reiter** (Presenter) ; **Gert Reiter** \* ; **Gabor Kovacs** MD ; **Aurelien F Stalder** \* ; **Mehmet A Gulsun** \* ; **Andreas Greiser** PhD \* ; **Horst Olschewski** MD ; **Michael H Fuchsjaeger** MD

#### PURPOSE

To compare relative period of existence of vortical blood flow in the main pulmonary artery in patients with pulmonary hypertension (PH) from velocity vector field, streamline and particle trace visualization of time resolved three-dimensional (4D) magnetic resonance phase-contrast imaging (MR-PCI) data and to compare their linear relationship with invasively determined mean pulmonary arterial pressure (mPAP).

#### METHOD AND MATERIALS

This prospective study was approved by the local ethical review board. 23 patients with manifest PH underwent right heart catheterization (RHC) and 4D MR-PCI of the main pulmonary artery. Blood flow patterns were visualized as 3D velocity vector fields projected on 2D anatomical images (3D-vector visualization), as 3D streamlines and as 3D particle traces and evaluated for period of existence of vortical blood flow ( $t_{\text{vortex}}$  in percent of the cardiac interval) in the main pulmonary artery. Dependence of  $t_{\text{vortex}}$  on visualization and relation to mPAP were analyzed by means of correlation, linear regression and Bland-Altman analysis.

#### RESULTS

$t_{\text{vortex}}$  derived from different visualizations strongly correlated ( $r = 0.94$  for 3D-vector versus streamline and  $r = 0.92$  for 3D-vector versus particle trace visualization). Bias and 95%-limits-of-agreement were -4% and  $\pm 14\%$  for comparison 3D-vector versus streamline visualization and were -3% and  $\pm 15\%$  for 3D-vector versus particle trace visualization. In all techniques  $t_{\text{vortex}}$  showed strong correlation with mPAP with small standard errors from regression lines ( $r = 0.96$ , SE = 3.4 mmHg for 3D-vector,  $r = 0.95$ , SE = 3.6 mmHg for streamline, and  $r = 0.92$ , SE = 4.4 mmHg for particle trace visualization).

#### CONCLUSION

Although periods of existence of vortical blood flow determined from 3D-vector visualization correlated best with mPAP, visualization of streamlines and particle traces provide similar results.

#### CLINICAL RELEVANCE/APPLICATION

4D velocity mapping represents an emerging tool in the analysis of PH hemodynamics and enables estimation of elevated mPAP irrespectively of flow visualization technique.

### SSC03-09 • 3T 1H-MR Spectroscopy of Myocardial Steatosis: Relationship to Fat Depots throughout the Body

**Radwa A Noureldin** MD, MSc (Presenter) ; **Ronald Ouwerkerk** PhD ; **Roderic I Pettigrew** MD, PhD ; **Ahmed M Gharib** MBChB

#### PURPOSE

To quantify amount of fat accumulated in the heart using high field MRH1 and to determine its relationship to metabolic lipid profile and other fat depots in the human body.

#### METHOD AND MATERIALS

After IRB approval, ninety HIPAA-compliant subjects, not known to have cardiac disease, underwent 1H-MRS using wide bore 3T scanner. B0 shimming parameters were optimized with a rapid B0 mapping method. MRS of heart was performed using ECG gated PRESS breath navigated technique, TR/TE = 1R-R/30ms. PRESS voxel was located in the septum at isovolumic phase of diastole planned on a 4-chamber SSFP with saturation slabs across subcutaneous and pericardial fat. The same sequence was used for musculoskeletal 1H-MR; PRESS voxel targeting the vastus lateralis, tibialis anterior and soleus muscles. Fat was quantified with Amares/MRU1 and related to water in unsuppressed spectra. Axial images of the heart were obtained at end systole for pericardial fat quantification. Axial T1 weighted images at L4-L5 level were acquired for abdominal fat measurement. All subjects had lipid profile assessment including serum cholesterol, HDL, LDL and serum triglycerides and were obtained within one month of the scan.

#### RESULTS

#### CONCLUSION

1H-MR spectroscopy quantifies ectopic fat deposition in the heart. In population with no cardiac disease, myocardial steatosis is correlated with high circulating triglycerides, musculoskeletal fat other fat depots in the human body.

#### CLINICAL RELEVANCE/APPLICATION

1H-MR spectroscopy is an important tool to investigate and monitor the effects of circulating serum lipids on fat metabolism and its accumulation within cardiac muscle and other ectopic fat depots.

## Gastrointestinal (Oncology: Surveillance and Tumor Response)

Monday, 10:30 AM - 12:00 PM • E451A

[RO](#) [OI](#) [BQ](#) [GI](#)

[Back to Top](#)

**SSC06** • AMA PRA Category 1 Credit™:1.5 • ARRT Category A+ Credit:1.5

#### Moderator

**Bonnie N Joe**, MD, PhD

#### Moderator

**Seong Ho Park**, MD \*

#### Moderator

**Erik K Paulson**, MD

### SSC06-01 • Multimodality Multiparametric Imaging for Prediction of Response and Survival after Radioembolization of Liver Metastases

**Fabian Morsbach** (Presenter) ; **Bert-Ram Sah** ; **Niklaus G Schaefer** MD ; **Thomas Pfammatter** MD ; **Caecilia S Reiner** MD ; **Hatem Alkadhi** MD

#### PURPOSE

To determine prospectively, in patients with liver metastases, the best predictor for response and survival to transarterial radioembolization (TARE) comparing multi-phase CT, perfusion CT, and 99mTc-MAA SPECT.

#### METHOD AND MATERIALS

Forty consecutive patients (mean age 61 years) with liver metastases undergoing multi-phase CT, CT perfusion and 99mTc-MAA SPECT were included, who all underwent TARE with 90Yttrium microspheres. Arterial perfusion (AP) acquired from perfusion CT, HU values from arterial phase (aHU) and portalvenous phase from multi-phase CT, and 99mTc-MAA uptake ratio from SPECT were calculated. Morphologic response was evaluated 4 months after TARE based on RECIST 1.1 criteria. One-year survival was calculated with Kaplan-Meier survival curves, Cox proportional hazard model was used to determine predictors of survival.



## RESULTS

We found significant differences between responders and non-responders for AP from perfusion CT ( $38 \pm 15$  ml/100ml/min vs  $12 \pm 6$  ml/100ml/min, P20ml/100ml/min showed a significantly ( $P=0.010$ ) higher one-year survival (mean survival 345 days vs 205 days), whereas an aHU value  $>55$ HU did not result in a statistically significant difference in survival ( $P=0.123$ ). Cox proportional hazard model revealed AP as the only significant ( $P=0.004$ ), independent predictor of survival.

## CONCLUSION

Compared to arterial and portal-venous enhancement as well as to the  $^{99m}\text{Tc}$ -MAA uptake-ratio of liver metastases, the AP from CT perfusion is the best predictor for morphologic response and one-year survival to TARE.

## CLINICAL RELEVANCE/APPLICATION

Perfusion CT can be used to differentiate between patients most likely to respond to transarterial radioembolization.

### SSC06-02 • Validation of Best Surrogate Markers of DCE-US to Predict PFS for Different Anti-angiogenic Treatments

**Nathalie B Lassau MD, PhD (Presenter) \*** ; **Michele Kind MD** ; **Valerie Vilgrain MD** ; **Joelle Lacroix MD** ; **Sophie Taieb MD** ; **Serge Koscielny**

## PURPOSE

The dynamic contrast enhanced ultrasonography (DCE-US) has been used in several monocentric studies to evaluate tumor response to anti-angiogenic treatments. The prospective multicentre French National Program for the Evaluation of DCE-US has studied the technique in different tumor types and anti-angiogenic treatments.

The aim was identify perfusion parameters to predict tumor response to different anti-angiogenic treatments

## METHOD AND MATERIALS

DCE-US were performed at baseline and at 4 time-points (Day 7, 15, 30, 60). At each examination, we quantified 7 DCE-US parameters. We also estimated the variation between baseline and each post-baseline time-point. The main endpoint was freedom from progression assessed according to RECIST. We first selected the best parameters: for each parameter and each time point, we studied the trend between the parameter value and freedom from progression. After, the best cut-points were searched through a grid search. The best single cut-point was that with the lowest P-value for progression free survival. We performed analyses according to the treatment and type of tumor, looking for the groups of patients that contribute the most to the heterogeneity.

## RESULTS

A total of 1968 DCE-US were performed in 539 patients. The median follow-up was 1.65 year. The mean transit time (MTT) was the only significant parameter at day 7 ( $P=0.002$ ). The best cut-point to predict tumor progression was 12 seconds ( $P=0.02$ ), a MTT  $>12$ s being of good prognosis. Variations from baseline were significant at day 30 for several parameters. The area under the curve (AUC) was the parameter with the lowest P-value ( $P=0.00004$ ); Patient with a decrease of more than 40 % had a better prognosis. The groups defined accordingly were different for both FFP ( $P=0.009$ ) and OS (0.03). The analyses according to treatment suggested heterogeneity which could be attributed to 81 RCC patients treated by Sunitinib. We performed a separate analysis of this group: the best cutoff for AUC at 30 days was 0.1, corresponding to a decrease of 90%.

## CONCLUSION

DCE-US is the first functional imaging technique that validated predictors of tumor progression in a large multicentric cohort.

## CLINICAL RELEVANCE/APPLICATION

A large multicentric study confirms the potential of DCE-US to monitor different anti-angiogenic treatments in different type of tumors.

### SSC06-03 • Acoustic Radiation Force Impulse Elastography for the Prediction of Chemotherapeutic Response in the Patients with Liver Metastases from Colon Cancer

**Jae Young Lee MD (Presenter)** ; **Soo Yeon Kang** ; **Se Hyung Kim** ; **Joon Koo Han MD** ; **Byung Ihn Choi MD, PhD \***

## PURPOSE

To investigate if and when acoustic radiation force impulse (ARFI) elastography can predict chemotherapeutic response in patients with liver metastasis from colon cancer.

## METHOD AND MATERIALS

The institutional review board approved this prospective study and informed consents were observed in all patients. 45 untreated metastatic liver tumors from colon cancer (mean,  $3.6 \pm 1.9$  cm; =3 nodules per patient) of 26 patients (M:F=16:10; mean age, 58.6  $\pm$  9.6 years) were included in this study. ARFI elastography was performed before chemotherapy and 48 hours, 1 week, 2 weeks and 4 weeks after chemotherapy for the same liver tumors along with measurement of tumor diameter. Shear wave velocities were obtained from the center, 12 o'clock, 3 o'clock, 6 o'clock and 9 o'clock direction within a tumor, two times per measurement point (total, 10). Responders and nonresponders were determined by RECIST 1.1 criteria on CT taken 2 month after the start of chemotherapy. Paired t-test was used for statistical analysis.

## RESULTS

Responders ( $n=10$ ) showed significant interval drop in elasticity of metastatic liver tumors between pre-chemotherapy and post-48hr (mean difference,  $-0.23$  m/s; 95% CI,  $-0.42$  to  $-0.04$  m/s) ( $P=0.016$ ). There was no significant interval change between pre-chemotherapy and other time points in responders. No significant interval change between pre and any time points in nonresponders ( $n= 16$ ) was noted. Rather, elasticity in liver tumors in nonresponders increased 48 hours after chemotherapy (mean difference,  $0.08$ m/s; 95% CI,  $-0.21$  to  $0.39$  m/s) ( $P=0.54$ ). Significant size change of liver tumors in diameter was detected since 1 week after chemotherapy only in responders.

## CONCLUSION

ARFI elastography might be used as a biomarker to predict chemotherapeutic response as early as 48 hours after initiation of chemotherapy in patients with colon cancer liver metastasis

## CLINICAL RELEVANCE/APPLICATION

ARFI elastography might be used as a biomarker to predict chemotherapeutic response as early as 48 hours after initiation of chemotherapy in patients with colon cancer liver metastasis.

### SSC06-04 • Diagnosis of Complete Response in the Colorectal Cancer Liver Metastasis (CRCLM) after Chemotherapy: Which Imaging Modality Should Be Used?

**Min Jung Park (Presenter)** ; **Mi-Suk Park MD** ; **Seong Ho Park MD \*** ; **Won Jae Lee MD** ; **Min Ju Kim** ; **Sung Eun Rha MD** ; **Chang Hee Lee MD** ; **Yoon Jin Lee MD** ; **Sumi Park** ; **Yang Shin Park MD** ; **Nurhee Hong MD**

## PURPOSE

To compare the accuracy of CT and MRI with liver-specific contrast agent for the evaluation of complete response in CRCLM after chemotherapy in a retrospective multicenter setting and to find out alternative role of non-contrast enhanced MRI (NE-MR) with Diffusion-weighted imaging (DWI) for the evaluation of complete response in CRCLM after chemotherapy

## METHOD AND MATERIALS

Among patients treated for CRCLM between 2008 and 2011 at eight hospitals in Korea, 90 patients (63men, 27women; mean age, 57 years; age range, 36-77 years) with the following criteria were retrospectively included: fewer than 10 liver metastases (LM) before chemotherapy; neoadjuvant chemotherapy followed by liver resection; disappearance of at least one LM on post-chemotherapy

multidetector CT portal venous phase images with slice thickness=5mm; post-chemotherapy gadolinium acid-enhanced MRI including DWI of b-value=500sec/mm<sup>2</sup>; time interval=4weeks between post-chemotherapy CT and MRI; follow-up at least 1 year after surgery. We retrospectively evaluated 445 LM in these patients on CT and MRI. Pathologic report of surgical specimen, sonographic finding on radiofrequency ablation and follow-up CT or MRI were served as reference standard. The diagnostic accuracies of MRI and CT were determined and compared using the McNemar test.

#### RESULTS

In diagnosing complete response after chemotherapy, gadolinium acid-enhanced MRI showed significantly higher accuracy (89%), sensitivity (75%), and specificity (94%) compared to CT (59%; 91%; 49%), respectively (P

#### CONCLUSION

MRI with liver-specific contrast agent is more accurate than CT for the evaluation of complete response in CRCLM after chemotherapy. And NE-MR with DWI could be an alternative tool as it is more accurate than CT.

#### CLINICAL RELEVANCE/APPLICATION

MRI with liver-specific contrast agent and diffusion weighted imaging is more accurate than CT for the evaluation of complete response in colorectal cancer liver metastasis after chemotherapy.

### SSC06-05 • Formula-based Lesion Volume Estimation: Evaluation of the Agreement with Software-based Volumetry

**Melvin D'Anastasi MD (Presenter) \***; **Ruediger P Laubender MA, MPH \***; **Julia Lynghjem \***; **Volker Heinemann MD \***; **Maximilian F Reiser MD**; **Anno Graser MD \***

#### PURPOSE

To evaluate the agreement between true tumor volume and tumor volume derived from (i) a new formula based on longest lesion (RECIST) diameter, (ii) a new formula based on longest diameter and longest orthogonal (WHO) diameter.

#### METHOD AND MATERIALS

89 baseline and follow-up CTs were available in 20 patients with metastatic colorectal cancer from the randomized phase II multicenter CIOX trial. Target lesions were defined at baseline and followed over time. Lesions were evaluated by (i) semi-automated volumetry using Siemens Syngo.via and (ii) volumetric assessment using a newly developed formula based on manual measurement of the longest diameter and the longest orthogonal diameter. True, WHO- and RECIST-based volumes were calculated. We compared the agreement of the true volume to the WHO-based volume and RECIST-based volume. We also compared the agreement between true and WHO-based volume relative changes by means of the intraclass correlation.

#### RESULTS

A total of 151 lesions were evaluated. Using a variance components model it was shown that the difference between true and RECIST-based volume is statistically significant ( $p < 0.001$ ) indicating a substantial constant bias. The same model showed a difference between true and WHO-based volume, which was not statistically significant ( $p = 0.50$ ), indicating no substantial constant bias. Scatter-plots show that the RECIST-based volume overestimates lesion volume. The intraclass correlation between true and WHO-based volume relative changes was 0.95, showing nearly perfect agreement between methods.

#### CONCLUSION

Our proposed formula, if based on WHO-measurements, allows for a very good estimate of relative volume changes (the RECIST-based formula overestimates the true volume).

#### CLINICAL RELEVANCE/APPLICATION

Volumetric tumor information, in particular relative changes in volume during therapy, can be approximated using the proposed WHO-based formula if no volumetric software is available.

### SSC06-06 • Novel Diffusion Kurtosis Imaging for Improved Evaluation of Treatment Response of Hypervascular Hepatocellular Carcinoma

**Satoshi Goshima MD, PhD (Presenter)**; **Yoshifumi Noda MD**; **Hiroshi Kondo MD**; **Hiroshi Kawada MD**; **Haruo Watanabe MD**; **Masayuki Kanematsu MD**; **Yukichi Tanahashi MD**; **Nobuyuki Kawai MD**; **Kyongtae T Bae MD, PhD \***

#### PURPOSE

To determine the value of diffusion kurtosis imaging (DKI) of the liver for improved evaluation of treatment response of hypervascular hepatocellular carcinoma (HCC).

#### METHOD AND MATERIALS

During a five-month period, we prospectively recruited 62 patients with treated or untreated hypervascular HCC (48 men and 14 women; mean age, 73.4 years; range, 49-86 years) and evaluated their MR images. DKI was performed with a respiratory-triggered single shot echo-planar sequence at multiple b values (0, 100, 500, 1000, 1500, and 2000 sec/mm<sup>2</sup>). The duration of this imaging acquisition was five minutes. We computed the mean kurtosis (MK) and apparent diffusion coefficient (ADC) (10<sup>-3</sup> mm<sup>2</sup>/s) over regions of interest encompassing the entire tumor using MATLAB software (Mathworks, Natick, Mass). The diagnostic performance of MK and ADC values for the evaluation of HCC viability were compared.

#### RESULTS

MR image acquisition and analysis were successful in all our study patients. Forty-nine HCCs were completely necrotic: 10 after transcatheter arterial chemoembolization (TACE) and 39 after radiofrequency ablation (RFA), whereas 22 HCCs revealed local recurrences: 18 after TACE and 4 after RFA. On the other hand, 41 HCCs remained untreated. MK was significantly higher in the untreated and local recurrent HCCs (0.81 +/- 0.11) than the necrotic HCCs (0.57 +/- 0.11) ( $P < 0.001$ ). Mean ADC value was significantly lower in the untreated and local recurrent HCCs (1.44 +/- 0.42) than the necrotic HCCs (1.94 +/- 0.52) ( $P < 0.001$ ). For the evaluation of HCC viability comparing between the MK and ADC, the sensitivity, specificity, and area under the ROC curve for the MK (85.7%, 98.0%, and 0.95; cutoff value of 0.710) were greater than those of the ADC (79.6%, 68.3%, and 0.77; cutoff value of 1.535).

#### CONCLUSION

Our study findings suggest DKI is superior to conventional diffusion MRI analysis for the evaluation of posttherapeutic response of HCC.

#### CLINICAL RELEVANCE/APPLICATION

When MRI is performed to evaluate the posttherapeutic response of HCC, diffusion kurtosis imaging may improve the diagnostic confidence of lesion characterization over conventional diffusion imaging.

### SSC06-07 • Heterogeneity Analysis of Tumor Perfusion for Monitoring Antiangiogenic Therapy in Hepatocellular Carcinoma Using Fractal Analysis

**Koichi Hayano MD (Presenter)**; **Sang Ho Lee PhD**; **Hiroyuki Yoshida PhD \***; **Dushyant V Sahani MD**

#### PURPOSE

Noninvasive imaging biomarkers that can quantitatively monitor physiologic changes in tumor microenvironment in response to antiangiogenic therapies will be of significant value. No in vivo study showed whether angiogenic agents can change the heterogeneity of tumor blood physiology. The purpose of this study is to evaluate the change of heterogeneity in tumor perfusion during antiangiogenic therapy using fractal dimension analysis in hepatocellular carcinoma patients treated with bevacizumab.

#### METHOD AND MATERIALS

Twenty-three patients (15 men, 8 women; mean age: 61.0 years) with advanced HCC underwent CT perfusion (CTP) at baseline and 2 weeks after administration of bevacizumab. Perfusion color maps of blood flow (BF) generated by the perfusion software (CT Perfusion 3;

GE) were saved in a grayscale format, and were loaded onto ImageJ (NIH), and fractal analyses were applied to perfusion maps using a plugin ImageJ software (FracLac, version 2.5). Differential box count method was applied, and fractal dimension and lacunarity were calculated as heterogeneity parameters. The baseline and percent change of heterogeneity parameters were compared with clinical response and PFS at 6 months.

#### RESULTS

This study included 12 clinical responders and 11 non-responders. 11 patients were PFS > 6 months, whereas 12 were PFS

#### CONCLUSION

Fractal analysis demonstrated that a patient whose BF heterogeneity in tumor was improved during antiangiogenic therapy could show a longer PFS. Homogenization of blood physiology may reflect an important process in normalization of tumor vasculature during antiangiogenic treatment.

#### CLINICAL RELEVANCE/APPLICATION

Fractal analysis of CT perfusion can be a new noninvasive biomarker for antiangiogenic therapy.

### SSC06-08 • Significance of Pelvic Imaging in Computed Tomographic Surveillance of Hepatocellular Carcinoma

**Kazim Narsinh MD (Presenter) ; Iris M Otani MD ; Cynthia S Santillan MD ; Claude B Sirlin MD \***

#### PURPOSE

To retrospectively determine the frequency and clinical significance of the findings and recommendations derived from pelvic CT performed as part of multiphasic CT surveillance imaging for hepatocellular carcinoma (HCC) in patients at risk for the development of HCC.

#### METHOD AND MATERIALS

The study was HIPAA-compliant and approved by the institutional review board with waiver of informed consent. The cohort was comprised of 602 patients with either cirrhosis and/or hepatitis B who were referred for routine HCC surveillance by hepatologists from an academic medical center in southern California. Multiphasic acquisitions were performed using a multidetector 16-slice or 64-slice helical CT scanner (GE Lightspeed) to obtain non-contrast, arterial, portal venous, and delayed phase images. Reports from the initial abdominopelvic CT scan for each patient obtained between 2002-2007 were retrospectively reviewed for extrahepatic findings in the pelvis.

#### RESULTS

Screening was performed in 602 patients (mean age 54 years). Of these patients, 389 (65%) were male and 213 (35%) were female. Logistic regression indicated a lower likelihood of pelvic findings in patients that were young (

#### CONCLUSION

Pelvic CT included at the time of HCC surveillance does not uncover a statistically significant number of incidental pelvic findings that impact patient care. In light of the increased ionizing radiation dose to patients and unnecessary healthcare costs associated with pelvic CT imaging in this context, routine surveillance of patients with known risk factors for HCC should be performed with multiphasic abdominal CT only.

#### CLINICAL RELEVANCE/APPLICATION

Pelvic CT does not detect clinically meaningful pelvic pathology with sufficient frequency to warrant its routine inclusion in HCC surveillance protocols.

### SSC06-09 • Accuracy of mRECIST versus RECIST 1.1 in Predicting Outcome in Hepatocellular Carcinoma Treated with Sorafenib

**Giulia Gallusi ; Rossella Di Miscio ; Michele Di Martino (Presenter) ; Concetta V Lombardo ; Adolfo Attili ; Carlo Catalano MD**

#### PURPOSE

To compare RECIST1.1 and mRECIST ability in the estimation of the response to therapy in patients with advanced HCC treated with Sorafenib.

#### METHOD AND MATERIALS

From August 2008 to July 2012, 58 cirrhotic patients with advanced HCC received Sorafenib at starting dose of 400 mg bid and were followed until death occurred. Using RECIST1.1 and mRECIST, 27 patients who had undergone a 4-phase CT scan/dynamic MR before and after (30-100 days) the start of treatment were retrospectively analysed. RRR was evaluated according to RECIST1.1 and mRECIST, to determine the ability of each method in predicting the response of HCC to Sorafenib, taking OS as end-point.

#### RESULTS

The objective response [OR= complete response (CR) + partial response (PR)], stable disease (SD) and progressive disease (PD) rates according to RECIST1.1 and mRECIST were 14%, 25%, 59% and 25%, 18%, 55%, respectively. In CR+PR versus SD+PD patients, median OS was 24.3 months (both with RECIST1.1 and mRECIST) versus 10.9 (with RECIST1.1) and 10.1 months (with mRECIST). OR was significantly associated with OS only according to mRECIST (p=0.007).

#### CONCLUSION

RRR according to mRECIST, but not to RECIST1.1, sensibly correlates to outcome in cirrhotic patients with HCC treated with Sorafenib.

#### CLINICAL RELEVANCE/APPLICATION

mRecist evaluation may help to select patient who try benefit from Sorafenib treatment

## Molecular Imaging Symposium: Imaging Cellular Subpopulations - Current Progress and Future Directions

**Monday, 01:30 PM - 03:00 PM • S406B**

**OI** **MI** **BQ**

[Back to Top](#)

**MSMI23 • AMA PRA Category 1 Credit™:1.5 • ARRT Category A+ Credit:1.5**

**Moderator**

**Michael D Kuo, MD \***

**MSMI23A • Using Imaging to Track the In Vivo Contribution of Lgr5 Stem Cells in GI Cancer**

**Nick Barker PhD (Presenter)**

#### LEARNING OBJECTIVES

1) To learn about in vivo lineage tracing as a technique to document endogenous stem cell activity.

#### ABSTRACT

Lgr5 Stem Cells in Epithelial Self-Renewal and Cancer Nick Barker: Institute of Medical Biology, 8A Biomedical Grove, 06-06 Immunos, Singapore 138648 The intestinal epithelium is subjected to a constant barrage of mechanical and chemical assault, imposing a requirement for regular self-renewal. This renewal is driven by a small population of adult stem cells residing in epithelial pockets known as crypts of Lieberkuhn. Lgr5 is a Tcf/?-catenin (Wnt) target gene specifically expressed on crypt-base columnar cells located at the base of the intestinal crypts. Employing in vivo lineage tracing we have proven these cells to be the stem cells of the small intestine and colon.

The same rapid turnover of the intestinal epithelium also makes it particularly susceptible to cancer-forming mutation. Using Lgr5-CreERT2 mice to selectively induce deletion of the APC tumor suppressor gene in the intestinal stem cells, we recently proved that these Lgr5+ve stem cells are the cell-of-origin of colon cancer. This work also revealed the presence of a minor population of Lgr5+ve cells within intestinal tumors. Multicolor lineage tracing from these tumor-resident Lgr5+ve cells has demonstrated these to be cancer stem cells contributing to tumor growth in vivo.

## **MSMI23B • CLARITY and Beyond: Towards Complete Structural and Molecular Investigation of Large-Scale Intact Biological Systems**

**Kwanghun Chung** PhD (Presenter)

### LEARNING OBJECTIVES

1) To understand the limitations of current imaging-based approaches in understanding disease processes. 2) To understand how CLARITY overcomes these limitations and allows cellular and subcellular imaging/molecular phenotyping while maintaining a whole system-wide perspective. 3) To explore potential clinical applications and future directions of CLARITY.

## **MSMI23C • Imaging Immune Cell Subsets Using ImmunoPET**

**Anna M Wu** PhD (Presenter) \*

### LEARNING OBJECTIVES

1) To delineate the advantages and disadvantages of using an antibody-based imaging approach for cell tracking. 3) To identify appropriate combinations of antibody formats and radionuclides for specific immunoPET applications.

### ABSTRACT

Antibodies are attractive candidates as imaging agents due to their exquisite specificity. Recent advances in protein engineering have enabled optimization of antibodies for noninvasive imaging applications such as immunoPET, through reduction of immunogenicity, acceleration of clearance to enable rapid, same-day imaging, and provision of site-specific radioconjugation. Broader availability of non-standard PET radionuclides, including Cu-64, Zr-89, and I-124 and others, has expanded the range of biological targets and processes that can be imaged. The cell-surface CD markers provide a well-characterized set of targets that can be used to distinguish lineage, differentiation, and activation state of hematopoietic and immune cells. Corresponding antibodies can readily be converted into engineered fragments for PET imaging, and can be used to profile immune responses such as expansion, trafficking, homing, and activation of immune cell subsets. Examples of profiling immune cells and responses in mouse models will be presented, as well as the potential for clinical translation.

## **MSMI23D • New Strategies for Using Smart MRI Contrast Agents for Monitoring Cell Therapy**

**Michael T McMahon** PhD (Presenter)

### LEARNING OBJECTIVES

1) Describe the Chemical Exchange Saturation Transfer (CEST) MRI contrast mechanism and how to modify an imaging sequence to obtain this contrast. 2) List the properties that make a compound a successful CEST MRI contrast agent. 3) Describe the various methods to employ CEST MRI contrast for monitoring cell therapy.

### ABSTRACT

Hydrogels have facilitated cell therapies by protecting therapeutic cells from immune responses and providing a physical cue to support the grafts. A non-invasive imaging technique that allows the monitoring of engrafted cell viability is needed as these therapies move into the clinic. Chemical Exchange Saturation Transfer (CEST) imaging is sensitive to changes in pH and ion concentrations, and as a result is well suited as a tool to obtain information on the status of these cells. We have incorporated organic CEST contrast agents into alginate hydrogels for this purpose and have developed a magnetization transfer image collection scheme suitable for obtaining high quality CEST contrast maps in the abdomen. The in vivo results upon transplanting these hydrogels into mice will be discussed.

## **Monday Plenary Session**

Monday, 01:30 PM • Arie Crown Theater



[Back to top](#)

**PS20 • AMA PRA Category 1 Credit**™: 1.25 • **ARRT Category A+** Credit: 1  
To receive credit, relinquish attendance voucher at end of session.

### **Presiding**

**Sarah S Donaldson, MD, Palo Alto, CA**  
*President, Radiological Society of North America*

### **Presentation of the Alexander R. Margulis Award for Scientific Excellence**

### **Presentation of Honorary Memberships**

**Gabriel P Krestin**, MD, PhD \*, *Rotterdam, NETHERLANDS*

**Anne W Lee**, MD, *Shenzhen, Guangdong, CHINA*

**Malgorzata Szczerbo-Trojanowska**, MD, *Lublin, POLAND*

### **Introduction by**

**Sarah S Donaldson**, MD, *Palo Alto, CA*

## **Eugene P. Pendergrass New Horizons Lecture: Normal and Neoplastic Stem Cells: Implications for the Radiological Sciences**

**Irving L Weissman**, MD \*, *Stanford, CA*

### **Introduction by**

**Sarah S Donaldson**, MD, *Palo Alto, CA*

### LEARNING OBJECTIVES

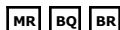
Research that bears on the earliest stages of cancer development as well as the sequelae of cancer treatment is of import not only to radiation oncologists but to diagnostic radiologists as well. Our investigation into blood-forming stem cells (HSC) and their non-self-renewing progeny hold promise for (1) regenerating the hematopoietic system after chemotherapy and radiation for cancer, (2) replacing genetically defective or otherwise damaged blood-forming systems, and (3) understanding the stages of hematopoiesis that harbor the earliest stages of pre-leukemia.

Following embryonic development, most of our tissues and organs are continuously regenerated from tissue/organ specific stem cells. The principal property that distinguishes such stem cells from their daughter cells is self-renewal; when stem cells divide they give rise to stem cells (by self-renewal) and progenitors (by differentiation). In most tissues only the primitive stem cells self-renew. Stem cell isolation and transplantation is the basis for regenerative medicine. For example, prospectively isolated blood forming [hematopoietic] stem cells [HSC] are cancer-free even when isolated from marrow or mobilized blood containing cancer cells; autologous pure HSC transplants into women with metastatic breast cancer to rescue them from high dose chemotherapy in a phase 1/2 trial resulted in 33% overall survival, compared to 6% for unpurified mobilized peripheral blood. This is contrary to conventional wisdom only because the titles of most mobilized blood transplants are still called HSC transplants, even in major journals that should know better. Still, the therapy began in the 1996-8 trial has not been extended to extended phase 3 trials, largely because

most oncologists counsel against it, and the company with the rights to use it does not offer it. Pure HSC in allogeneic transplants can give graft vs host free hematopoietic regeneration, and because the host has a donor immune system, it cannot reject any organ, tissue, or tissue stem cell transplant from the HSC donor. The failure of extension of HSC transplantation clinically has blocked the testing of such protocols in humans. Nevertheless, if it is extended to it's logical conclusion, in the next decades the organ and tissue donors will not be living people, but pluripotent stem cell lines that can generate HSC and organ-specific stem cells. Because total body irradiation (TBI) is the preferred method to condition for HSC transplants, it could become a major clinical entity for the radiation therapy community. Self-renewal is dangerous, and therefore strictly regulated. Poorly regulated self-renewal can lead to the genesis of cancer stem cells, the only self-renewing cells in the cancer. In myelogenous leukemia the developing cancer clones progress at the stage of HSC, until they become fully malignant. At this point, the leukemia stem cell moves to a stage of a downstream progenitor that has evaded programmed cell death and programmed cell removal, while acquiring self-renewal. While there are many ways to defeat programmed cell death and senescence, there appears to be one dominant method to avoid programmed cell removal the expression of the cell surface don't eat me protein CD47, the ligand for macrophage SIRP-alpha. All cancers tested express CD47 to overcome expression of eat me signals such as calreticulin. Antibodies that block the CD47-SIRP-alpha interaction enable phagocytosis and killing of the tumor cells in vitro and in vivo. In primary human cancers of all types transplanted from patients to immune deficient mice orthotopically, anti-CD47 eliminates all metastases, but often requires local resection or radiotherapy to remove bulky tumors that grow faster than the macrophages can eat them. The anti-CD47 therapies are expected to be in phase 1 trials in early 2014.

## Breast Imaging (MRI Interpretation)

Monday, 03:00 PM - 04:00 PM • Arie Crown Theater



[Back to Top](#)

**SSE01** • AMA PRA Category 1 Credit™:1 • ARRT Category A+ Credit:1

**Moderator**

**Constance D Lehman**, MD, PhD \*

**Moderator**

**Elizabeth A Morris**, MD

### **SSE01-01 • Lesion Characteristics, Malignancy Rate, and Follow-up of BI-RADS 3 Lesions Identified on Breast MRI: Implications for MRI Interpretation and Management**

**Sona A Chikarmane** MD (Presenter) ; **Catherine S Giess** MD ; **Patricia S Poole** MD ; **Dorothy A Sippo** MD ; **Robyn L Birdwell** MD

#### PURPOSE

To 1) evaluate the incidence of BI-RADS 3 assessment in screening and diagnostic breast MRI; 2) review types of findings considered BI-RADS 3; and 3) determine outcomes of BI-RADS 3 studies, including BI-RADS upgrades, downgrades and biopsy results.

#### METHOD AND MATERIALS

IRB approved, retrospective review of breast MRI database (2009-2011) with 5778 studies in 3360 patients, was performed to identify all breast MRIs assigned BI-RADS 3 for one or both breasts. 679/5778 (11.8%) studies had at least one BI-RADS 3 finding. Cases in which initial BI-RADS 3 assessment was given prior to 2009 were excluded. Breast MRI reports and electronic medical record were reviewed to obtain patient demographics and outcome data including tissue diagnosis, imaging and/or clinical stability for at least 24 months, or decrease/resolution during imaging surveillance.

#### RESULTS

570 findings (483 studies) were assigned initial BI-RADS 3 assessment during study period. Indications (n=483) included 257 (53%) high risk screening and 226 (47%) diagnostic studies. BI-RADS 3 lesions (n=570) included mass (171, 30%), focus (141, 24.7%), moderate/marked background parenchymal enhancement [BPE] (131, 23%), NMLE (96, 16.8%), post-treatment changes (18, 3%), and other (13, 2.5%). Outcomes data was available in 508/570 (89%) lesions, including 408 (72%) without imaging evidence of malignancy > 24 months, 29 (5%) prophylactic mastectomy (all benign), and 71 (12%) upgraded to BI-RADS 4, with 11 cancers. Cancer rate for BI-RADS 3 lesions was 2.1% (11/508); all invasive cancers were diagnosed in < 12 months of surveillance and in women with genetic mutation or personal history of breast cancer. Cancer morphology (n=11) included mass (3, 27%), focus (4, 36.5%), and ductal or linear NMLE (4, 36.5%). No cancer was detected in cases of moderate/marked BPE.

#### CONCLUSION

Approximately 12% of breast MRI studies had findings assessed as BI-RADS 3, with a 97.9% negative predictive value for cancer. Although it may interfere with cancer detection, marked diffuse background enhancement does not require a BI-RADS 3 assessment. Strict adherence to the BI-RADS lexicon may reduce inappropriate BI-RADS 3 assessments for lesions with more suspicious imaging findings.

#### CLINICAL RELEVANCE/APPLICATION

In a population with an elevated breast cancer risk, breast MRIs assigned BI-RADS 3 assessment had an acceptably low cancer rate which may be further reduced by careful adherence to BI-RADS lexicon.

### **SSE01-02 • Probably Benign Lesions Detected at Dynamic Contrast Enhanced Breast MRI: Prevalence of BIRADS III Diagnoses and Malignancy Rate**

**Yunus Alparslan** (Presenter) ; **Simone Schradung** MD ; **Christiane K Kuhl** MD \*

#### PURPOSE

Aim of this study was to analyze the malignancy rate of MRI-BIRADS III lesions.

#### METHOD AND MATERIALS

Between 06-2010 and 12-2011 a total of 3154 breast MRI studies were performed at our institution. Among those 107 MRI studies in 107 patients (3.4%) were rated as MR-BIRADS III and were further analyzed. The time interval between the initial MRI and the follow-up examination, BIRADS category in the follow-up study and histologic results of possible biopsies were recorded to calculate the malignancy rate of BIRADS 3 lesions.

#### RESULTS

Follow up MRI was performed in 87% (93/107) of the 107 patients after a mean time interval of 10 month (median 9.6, range [4;25]). At this follow up exams MR-BIRADS 3 lesions were stable or regressive and downgraded to BIRADS 1/2 in 96% (89/93). MR-guided biopsy was performed by patients request in 7 of these stable lesions. All of these yielded benign changes at histology, including 2 papillomas. Four MR-BIRADS III lesions were progressive (4%) and upgraded to MR-BIRADS IV in the follow up exam. All of those underwent MR-guided vacuum biopsy. Histology revealed an invasive lobular carcinoma (pT1b, 0.7 cm, pN0 (0/2sn), G2) in one, borderline lesions in two patients (atypical ductal hyperplasia and papilloma) and benign changes in one patient (adenosis). Accordingly the malignancy rate of MR-BIRADS III lesions was 1.1% (1/93).

#### CONCLUSION

In concordance with prior studies the malignancy rate of MRI findings categorized as MR-BIRADS III is low. MR-follow up is a valid approach in the management of these lesions.

#### CLINICAL RELEVANCE/APPLICATION

The malignancy rate of MR-BIRADS III lesions is low. To avoid early invasive tissue sampling, the observation with short-term MR-follow up is a valid approach in the management of these lesions.

### SSE01-03 • Can Breast Cancer Molecular Subtype Help Select Patients for Preoperative MRI?

**Lars J Grimm MD (Presenter) \*** ; **Mary Scott Soo MD** ; **Jay A Baker MD \*** ; **Karen S Johnson MD \***

#### PURPOSE

To determine whether breast cancer molecular subtype can help predict which patients will benefit from preoperative breast MRI.

#### METHOD AND MATERIALS

305 consecutive preoperative breast MRIs were retrospectively reviewed. Patients with prior breast cancer therapy or surgery were excluded. The presence of multicentric/multifocal disease, contralateral disease, skin/nipple involvement, chest wall/pectoral muscle invasion, and lymph node involvement was correlated with the pathology report. Estrogen receptor (ER), progesterone receptor (PR), and human epidermal growth factor receptor-2 (HER2) status were recorded from the pathology report. Molecular subtypes were defined as luminal A (ER+ and/or PR+, HER2-), luminal B (ER+ and/or PR+, HER2+), HER2 (ER- and PR-, HER2+), and basal (ER-, PR-, and HER2-). MRI findings that could potentially alter clinical management were correlated with molecular subtypes.

#### RESULTS

The 305 cases were classified as 202 (66.2%) luminal A, 33 (10.8%) luminal B, 17 (5.6%) HER2, and 53 (17.4%) basal subtype. Multicentric/multifocal disease was significantly more commonly ( $p=0.015$ ) detected by MRI in luminal B (16/33, 48.5%) and HER2 (10/17, 58.8%) subtypes, compared to luminal A (62/202, 30.7%) or basal (13/53, 24.5%) subtypes. Compared to luminal A subtype, preoperative MRI was 2.1 ( $p=0.049$ , 95% confidence interval [95% CI], 1.0-4.5) and 3.2 times ( $p=0.022$ , 95% CI, 1.2-9.3) more likely to detect multicentric/multifocal disease in luminal B and HER2 subtypes respectively. Although there was no significant difference ( $p=0.167$ ) between lymph node involvement among all groups, luminal B (14/33, 42.4%) subtype was 2.4 times ( $p=0.026$ , 95% CI, 1.1-5.2) more likely to have lymph node involvement than luminal A (47/202, 23.3%) subtype. There was no significant difference in contralateral disease, skin/nipple involvement, or chest wall/pectoral muscle invasion between subtypes.

#### CONCLUSION

Preoperative breast MRI is significantly more likely to detect multicentric/multifocal disease in luminal B and HER2 molecular subtype breast cancer, while lymph node involvement is more commonly detected in luminal B than luminal A molecular subtype breast cancer.

#### CLINICAL RELEVANCE/APPLICATION

Breast cancer molecular subtypes could help tailor utilization of pre-operative breast MRI.

### SSE01-04 • Does Breast Biopsy Affect Lesion Enhancement Characteristics or Accuracy of Tumor Measurement on MRI?

**Nikki Tirada MD (Presenter)** ; **Anjeza Chukus MD** ; **Stuart S Kaplan MD \***

#### PURPOSE

The objective of this study is to determine the effect ultrasound, stereotactic, and MRI-guided biopsy may have on lesion morphology, size measurement, and qualitative and quantitative dynamic kinetic features. It is our hypothesis that inflammatory changes and possible tumor burden reduction related to biopsy will alter tumor appearance on MRI. Discordance in imaging characteristics can lead to inaccuracy of size measurement and tumor extension, which could have significant impact on surgical and treatment planning.

#### METHOD AND MATERIALS

A retrospective review of patients who had contrast-enhanced Breast MRI performed either before or after biopsy of a suspicious lesion between January 2010 and January 2013 were included in the study. Patients who had neo-adjuvant chemotherapy prior to MRI were excluded. Imaging characteristics evaluated include time-signal intensity curve and changes in degree of enhancement were evaluated. In patients who also underwent surgical excision, the size of tumors measured on MRI was compared with pathology measurement. Using a paired Student's t test, differences were considered significant where  $P < 0.05$ . Approval for this study was obtained from Mount Sinai Medical Center Institutional Review Board.

#### RESULTS

To date, we have identified 36 eligible patients. The mean age was 58.2 years. 8 of 36 lesions (22%) demonstrate changes in enhancement pattern after biopsy: 3 lesions (8.3%) with homogenous washout kinetics became heterogeneous, 3 lesions (8.3%) with homogenous washout became persistent, 1 lesion (2.8%) with progressive curve became plateau, and 1 lesion (2.8%) with plateau became indeterminate (hematoma cavity). There was no significant difference between radiologic and pathologic size of the tumor (2.47 vs 2.31;  $P = 0.69$ ).

#### CONCLUSION

Breast biopsy leads to changes in enhancement pattern but does not significantly impact the accuracy of diagnosis or tumor size measurement.

#### CLINICAL RELEVANCE/APPLICATION

Breast MRI is frequently performed after the diagnosis of breast cancer has been established. Therefore, it is important to assess any potential effect prior biopsy may have on imaging characteristics

### SSE01-05 • Breast MRI Background Parenchymal Enhancement and Tumor Characteristics

**Janice S Sung MD (Presenter)** ; **Jennifer Brooks PhD** ; **Valencia King MD** ; **Jennifer B Kaplan MD** ; **Eve Burstein** ; **Mark E Robson MD \*** ; **Jonine L Bernstein** ; **Malcolm Pike** ; **Elizabeth A Morris MD**

#### PURPOSE

To examine the relationship between fibroglandular tissue (FGT) and background parenchymal enhancement (BPE) on MRI and histopathological and immunohistochemical features of breast cancers.

#### METHOD AND MATERIALS

IRB approved retrospective review identified 712 women diagnosed with unilateral invasive ductal breast carcinoma consecutively between February 2008 and February 2011 who had a pre-treatment MRI of the unaffected breast, were not taking hormonal medications, and did not have a prior history of breast cancer. Women with unknown menopausal status or with tumors with unknown receptor status or tumor grade were excluded ( $N=51$ ). Clinicopathologic data was obtained from the electronic medical records. Two breast imaging radiologists blinded to clinical data independently assessed BPE and FGT using BI-RADS criteria. Odds ratios (OR) and 95% confidence intervals (CI) were generated using logistic regression models adjusting for age, menopausal status and body mass index.

#### RESULTS

Of 661 tumors, 522 (79%) were estrogen receptor positive (ER+), 491 (74%) progesterone receptor positive (PR+) and 117 (18%) human epidermal growth factor receptor positive (HER2+). Women with dense breasts (heterogeneously/extremely dense) were more likely to have ER+ (OR=1.6, 95% CI 1.0, 2.5,  $p=0.05$ ) or PR+ tumors (OR=1.7, (1.1, 2.7),  $p=0.01$ ) compared to women with less dense breasts (predominantly fatty/scattered fibroglandular densities). Women with dense breasts were less likely to have triple negative breast cancer compared to luminal A (OR=0.5, (0.3, 0.8),  $p=0.008$ ). No association between these factors and BPE was observed. Results did not differ when stratified by menopausal status.

#### CONCLUSION

FGT on MRI is associated with an increased likelihood of having ER+ and PR+ breast cancer, which is consistent with some studies that have shown a similar association between mammographic density and ER+ disease. No association between BPE and subtype was

observed.

#### CLINICAL RELEVANCE/APPLICATION

FGT on MRI may be a much greater risk factor specific to ER/PR+ disease. Although BPE has been shown to be a breast cancer risk factor, this appears to be independent of subtype.

### SSE01-06 • Prepectoral Edema as a Morphological Sign in MR-mammography

**Clemens G Kaiser MD, BA (Presenter) ; Michael Herold ; Julia Krammer MD ; Matthias Dietzel MD ; Pascal A Baltzer MD ; Klaus Wasser MD ; Stefan O Schoenberg MD, PhD \* ; Werner A Kaiser MD, PhD**

#### PURPOSE

Morphological and kinetic signs of breast lesions contribute to diagnosis and differential diagnosis in MR-Mammography. Prepectoral edema in patients without any history of previous biopsy, operation, radiation or chemotherapy has been detected as a new diagnostic Sign during clinical routine. The purpose of this study was to evaluate the role of this morphological sign in the differential diagnosis of breast lesions.

#### METHOD AND MATERIALS

Between 11/2001 and 10/2006 a total of 1109 MRM exams have been performed in our institution. Patients had no previous operation, biopsy, intervention, chemotherapy, hormone replacement therapy or previous mastitis. 162 patients with 180 lesions were included and histologically correlated by operation (124 patients / 136 lesions) or corebiopsy (38 patients / 44 lesions) in our hospital. The evaluations were performed by 4 experienced radiologists in consensus.

#### RESULTS

180 evaluated lesions included 104 malignant lesions (93 invasive; 11 non-invasive cancers) and 76 benign lesions. The prepectoral edema Sign was seen in 2.6 % of benign lesions (2/76), none of the DCIS-cases (0/11) and 25.8 % of malignant lesions (24/93). Prepectoral edema were found significantly more frequently in poorly-differentiated cancers [(33.9 %; 19/56 vs. 13.9 % (5/36)] as well as in presence of lymphangiosis [(53.8 %; 14/26) vs. (9.8 %; 4/41)], positive lymphnodes [(44.4 %; 12/27) vs. (19.4 %; 12/62)], size of tumor above 2 cm [(47.1 %; 16/34) vs. (13.8 %; 8/58)], pectoralis infiltration [(80.0 %; 4/5) vs. (22.7 %; 20/88)], presence or absence of prominent vessels [(44.4 %; 20/45) vs. (8.3 %; 4/48)] and the presence of the hook sign [(60.9 %; 14/23) vs. 14.5 %; 10/69]. The prepectoral edema Sign was not statistically associated to tumor-type, presence or absence of additional DCIS, receptor status, number of lesions, margin, form, enhancement pattern and curve-type.

#### CONCLUSION

The Prepectoral Edema Sign seems to be a highly reliable indicator for tumors with malignant prognosis.

#### CLINICAL RELEVANCE/APPLICATION

Perifocal edema is a very powerful sign towards malignancy in the differential diagnosis of breast lesions in MR-Mammography.

## Nuclear Medicine (Quantitative Imaging)

Monday, 03:00 PM - 04:00 PM • S504CD



[Back to Top](#)

**SSE19 • AMA PRA Category 1 Credit™:1 • ARRT Category A+ Credit:1**

#### Moderator

**Andrew Quon, MD**

#### Moderator

**Amir H Khandani, MD**

### SSE19-01 • Integration of Automated Quality Control Using Image Classification into a CAD System for Bone Scan Lesion Detection

**Keith W Henkel MS, BEng (Presenter) \* ; Matthew S Brown PhD \* ; Jonathan G Goldin MBChB, PhD ; Grace Kim MD ; Katherine Yang \* ; Bharath Ramakrishna ; Greg Chu ; Richard Pais**

#### PURPOSE

The aim of this research is to develop an automated bone scan image classifier for quality control as a pre-processing step prior to application of a CAD lesion detection system. As quantitative image analysis of bone scans becomes increasingly useful in clinical trials, so does the need to define quality bone scans in such a way that it predicts images' usability for an automated lesion detection system.

#### RESULTS

Based on review of the CAD segmentation, 35.5% of the 833 images were usable. In the test data set, images were split by those performed on ADAC machines (n=30), and those performed on other machines (n=803). To confirm the algorithm identified in the training set, its sensitivity and specificity were compared against the usability predictive power of the individual parameters. Overall, the manufacturer (ADAC vs. not ADAC) appeared to have a low classification accuracy, but there was not enough data in the ADAC dataset reach a firm conclusion. In the other machine group, pixel spacing also showed a low classification accuracy (sensitivity of 0.889, specificity of 0.702). The image type most commonly associated with usable images (ORIGINAL / PRIMARY / WHOLE BODY / EMISSION) had a very high classification accuracy with a sensitivity of 0.918 and a perfect specificity (no false negatives) of 1.000. Image Type is defined in DICOM Part 3: Information Object Definitions, and had a perfect specificity. Image size (256 by 1024 pixels as usable, others as requiring manual review) had a sensitivity of 0.968 and specificity of 0.985 in predicting image usability, the largest individual parameter sensitivity.

The combination of manufacturer, image type, and image size provide the best criteria for identifying quality bone scans: a sensitivity of 0.973 and a perfect specificity of 1.000. Further classification of images by pixel spacing (the last step of the algorithm identified in the training data set) actually had no further effect on the sensitivity and specificity. Images incorrectly identified as usable (n=7) were not usable due to extravasation hindering anatomic segmentation or due to missing anatomy with two notable exceptions: a pair of blood pool NM images. Including all images performed on ADAC scanners, for which the sample size was too small to identify an association, 56 of 833 images (6.7%) would require review via a non-automated process to determine usability of an image.

#### CONCLUSION

The question of how to approach quality control of medical images for use in automated systems appears to have an answer in traditional image classification. Close regulation of consistent scanner use, delay times from injection of radiotracer to acquisition of image, and varying doses received across time points, though not completely irrelevant, are not as significant factors in identifying quality images as simple DICOM header values like image type, image size, and manufacturer. Based on the inefficacy of including pixel spacing as a step in classifying the images of the test set, further evidence will be sought to determine if including the parameter is redundant or not.

#### METHODS

Acceptable bone scan image quality was defined in terms of usability for processing by an CAD lesion detection system currently in use in clinical trials (see Brown et al. Computer-aided quantitative bone scan assessment of prostate cancer treatment response. Nuclear Medicine Communications. 33(4):384-394, April 2012.). The CAD system atlas-based segmentation of anatomic landmarks and normal bone has been observed to fail when non-standard and/or non whole-body DICOM images are acquired, i.e., for secondary screen captures, spot views, tomos, key images, etc. Such images are unusable by CAD processing required in clinical trials and are thus considered of unacceptable quality. From a training set of over 3,000 images (Phase 2 multi-center clinical trial of VEGFR-2 inhibitor in prostate cancer), four technical

imaging parameters from the DICOM header were identified as features to classify image quality as acceptable or not: (1) image size, (2) image type, (3) pixel spacing, and (4) manufacturer. In the training data set, the best correlations with usability were found by differentiating by manufacturer first, then by a combination of image type, image size, and pixel spacing. While additional factors such as radiotracer dosage and timing may affect the quality of a bone scan, they are not consistently available within the DICOM header and are prone to manual entry error, and therefore have been excluded from analysis.

To test the imaging parameter features, 833 images from 25 patients across 23 sites were analyzed from a different multi-center Phase 2 prostate cancer clinical trial. Each of the images was processed by the CAD lesion detection system, and usability was determined as defined above. Statistically, sensitivity and specificity are reported to test the association between classified image quality and CAD usability.

### **SSE19-02 • QIBA2 FDG PET Reading Study: Variability of Liver FDG Uptake Measurements across Different Sites**

**Joo Hyun O MD (Presenter) ; Edward A Eikman MD ; Jaime L Montilla-Soler ; Paul E Kinahan PhD \* ; James M Mountz MD, PhD ; Eric Perlman ; John Sunderland PhD ; Heather Jacene MD ; Nathan C Hall MD, PhD \* ; Michael V Knopp MD, PhD ; Abdel K Tahari MD, PhD ; Ronald Boellaard PhD ; Otto S Hoekstra MD ; Li Huo ; Hye Ok Kim ; Sun Young Chae ; Sae Jung Na ; Sung Hoon Kim ; Mike Satheke ; Moses Modiselle ; Sally Barrington ; Andrew M Scott ; Sam Berlangieri ; Andrew Quon MD ; Jeffrey P Leal BA ; Muhammad A Chaudhry MD,MBBS ; Richard L Wahl MD \***

#### **PURPOSE**

To determine the variability in measurement of FDG uptake in normal liver background in identical human PET studies analyzed by differing readers, software and performance sites.

#### **METHOD AND MATERIALS**

Baseline and post-therapy FDG PET/CT images of a single patient were distributed digitally to 15 sites in North America, Europe, Africa, Asia and Australia in an IRB approved study. Readers at each site measured the background activity by placing a 3 cm diameter spherical volume of interest (VOI) in right side of the liver. Workstation software from 8 different vendors were used for the quantification. The standard uptake value (SUV) and SUV corrected for lean body mass (SUL) were measured using local standard approaches.

#### **RESULTS**

The liver background SUV ranged from 1.47 to 2.19 at baseline with standard deviation (SD) of 0.16; and ranged from 1.80 to 2.96 (SD 0.26) at follow-up. The liver SUL measurements ranged from 0.91 to 1.56 (SD 0.12) at baseline; and from 1.20 to 2.02 (SD 0.17) at follow-up.

#### **CONCLUSION**

SUV and SUL measurements of the normal liver derived from the same set of FDG PET/CT images showed generally similar, but not consistently the same, values. The cause of the variance of liver measurements is likely due to both human VOI selection methods and software differences.

#### **CLINICAL RELEVANCE/APPLICATION**

These results indicate that varying quantitative results can be extracted from identical PET/CT images and suggest the need to more fully standardize the PET analytic process.

### **SSE19-03 • Impact of 4D PET-CT on SUV Quantification in Lung Tumors: How Many Phase-bins?**

**Carlo Cavedon DPhil (Presenter) ; Emanuele Zivelonghi ; Stefania Guariglia ; Maria Grazia Giri ; Daniela Grigolato ; Michele Zuffante ; Marina Cucca ; Marco Ferdeghini MD**

#### **PURPOSE**

To find the optimal number of phase bins in respiratory-gated PET-CT (4D PET-CT) in order to improve SUV quantification in lung tumors while preserving signal-to-noise ratio.

#### **METHOD AND MATERIALS**

28 patients with lung tumors were studied with 18F-FDG 4D PET-CT. Only patients that showed respiratory-induced tumor motion greater than 5 mm were enrolled. 4D PET-CT was performed by means of a Philips Gemini BigBore TOF scanner and the Varian RPM respiratory gating system. 3.0 MBq/kg, 2 min/bed and retrospective-mode for both PET and CT modalities were used. Images were reconstructed using 1 (no sorting) up to 10 phase bins. SUV<sub>max</sub> values within the lesion were studied as a function of the number of phase-bins. The lower number of phase bins that allowed SUV quantification no smaller than 90% compared to the gold standard (10 phases) was considered as optimal. Lesion volumes were estimated by three different segmentation methods: fixed SUV=2.2 threshold, 40% of SUV<sub>max</sub> isocontour and gradient-based method. These volumes were also studied as a function of the number of phase bins.

#### **RESULTS**

SUV<sub>max</sub> measured at max exp was on average 63.2% higher in the gated acquisition (10 phases) compared to the non-gated case (range 11.5%-328.3%). The underestimation of SUV in non-gated PET-CT was strongly dependent on lesion volume and location, small lesions in the lower lung region being the most affected. When comparing 4D PET-CT in 4 and 10 phases, the underestimation reduced to 12.3% (range 2.0%-37.7%). The corresponding value for 6 and 10 phase bins was 6.9% (range 0.0%-23.3%). Volumes estimated by the fixed-threshold method increased with the number of phase bins, SUV<sub>max</sub> percentage-based volumes decreased and gradient-based volumes did not show a unique trend.

#### **CONCLUSION**

4D PET-CT offers an advantage in 18F-FDG SUV quantification for tumors that move with respiration. The balance between acquisition/reconstruction time, SNR and accuracy of SUV estimation seems to be achievable using 4 to 6 phase bins, depending on lesion volume and location. SUV-based volume quantification obtained by multiple segmentation methods is less prone to inconsistent results when respiratory gating is used.

#### **CLINICAL RELEVANCE/APPLICATION**

4D PET-CT can improve SUV quantification in tumors that move with respiration. This might be especially useful when metabolic data are used to help delineate reference volumes in Radiation Oncology.

### **SSE19-04 • Impact of a New Respiratory Amplitude-based Gating Technique (HD-Chest) in Evaluation of Subdiaphragmatic PET Lesions**

**Axel Van Der Gucht (Presenter) ; Benjamin Serrano ; Florent Hugonnet ; Benoit Paulmier ; Nicolas Garnier ; Marc Faraggi \***

#### **PURPOSE**

PET acquisition requires several minutes which can lead to respiratory motion blurring, partial volume effect and SUV under-estimation. To avoid these artifacts, conventional 10-minute Phase-Based Respiratory Gating (PBRG) can be performed but is time-consuming and difficult with a non-compliant patient. HD-Chest is an amplitude-based gating method which keeps 35% of the counts at the end of expiration to minimize respiratory motion. We estimated the impact of HD-Chest on subdiaphragmatic lesion detectability and quantification.

#### **METHOD AND MATERIALS**

Our study consisted of 30 patients for a total of 76 hepatic and 26 perihepatic lesions. Each patient underwent 3 acquisitions on a Siemens Biograph mCT (4 rings and time-of-flight): a Standard free breathing Whole Body (SWB, 5 to 7 steps / 2.5 min per step, 3.3 ± 0.4 MBq/Kg of 18F-FDG), a 10-min PBRG with six bins and a 5-min HD-Chest. All gated acquisitions were performed with an ANZAI respiratory gating system. SUV<sub>max</sub> and Target to Background Ratio (TBR, expressed as SUV<sub>max</sub> of lesions / SUV<sub>mean</sub> in healthy liver) were compared.



## RESULTS

All 93 lesions in SWB images were detected in the gated images. PBRG and HD-Chest respectively revealed 5 and 9 new lesions and relocated 7 and 8 lesions. Localization remained uncertain for 2 lesions in both gated methods. Four lesions revealed by HD-Chest were missed by PBRG in 3 non-compliant patients. Compared to SWB, TBR but not SUVmax increased significantly with PBRG (respectively  $40 \pm 62\%$ ,  $p$

## CONCLUSION

A better detection rate, a better coregistration, a higher contrast, a reduction of the acquisition time by up to 50% compared to PBRG make of HD-Chest the first choice respiratory-gated PET protocols in the evaluation of subdiaphragmatic lesions.

## CLINICAL RELEVANCE/APPLICATION

Compared to phase-based respiratory gating, HD-Chest enhances detectability, image quality and reduces acquisition time without compromising quantification in evaluation of subdiaphragmatic lesions.

### **SSE19-05 • Quantification of Treated Volumes and Correlation with Functional and Morphologic Target Volume Estimation in SIRT of the Liver**

**Michael P Wissmeyer MD (Presenter) ; Valentina Garibotto ; Pietro Mjano MD ; Romain Breguet MD ; Christoph D Becker MD ; Osman Ratib MD, PhD \* ; Sylvain Terraz MD**

## PURPOSE

To quantify treated volumes and compare them with morphologic and functional target volume estimation algorithms in patients undergoing SIRT.

## METHOD AND MATERIALS

We evaluated 28 consecutive patients scheduled for SIRT due to hepatocellular carcinoma or liver metastases from other tumors into this pilot study. Treated liver volumes were calculated using a threshold based semi-automatic delineation technique on post-interventional Y-90 SPECT-CT. The pre-interventional target volumes and Y-90 activities were estimated by manual delineation on contrast enhanced CT and on pre-therapeutic Tc-99m-MAA SPECT-CT by two experienced observers. Additionally, the expected lung dose was determined on the base of the lung shunt fraction as derived from planar whole-body MAA-images. Treated and target volumes, Y-90 activities and lung doses were compared using correlation coefficients (cc) and a paired two sided t-test.

## RESULTS

7 patients were excluded because of too high hepato-pulmonary shunt fractions. In 7 other patients with bilobar treatment, functional target volumes could not be drawn on the MAA-SPECT/CT due to technical reasons. In the remaining 14 patients, estimated mean $\pm$ SD treated liver volume was  $1247\pm 533$ ml using a threshold of  $24.2\pm 9.1\%$  of maximum counts for semi-automatic volume estimation. Absolute counts were not useful for threshold selection. Estimated target volumes (ml), calculated Y-90 activities (GBq), and lung doses (Gy) were  $1344\pm 524$ ,  $3.62\pm 1.37$ , and  $13.03\pm 8.35$  for CT, compared to  $1352\pm 664$ ,  $3.62\pm 1.69$ , and  $12.35\pm 7.54$  for MAA-SPECT-CT. Overall, morphologic (cc=0.88;  $p=0.185$ ) and functional (cc=0.92;  $p=0.177$ ) target volumes correlated well with treated volumes, with a slight but not statistically significant advantage for the functional approach ( $p=0.125$ ).

## CONCLUSION

Treated liver volumes can be quantified easily on the post-interventional Y-90 SPECT-CT using a threshold based semi-automatic approach. Functional and morphologic pre-therapeutic target volume estimation correlates well with the treated volumes, with a slight advantage of the functional technique, most probably due to patients presenting with perfusion patterns differing from the expected vascular anatomy.

## CLINICAL RELEVANCE/APPLICATION

Functional target volume estimation correlates slightly better with treated liver volumes in SIRT than the morphologic approach and is an important adjunct to depict unexpected liver perfusion patterns

### **SSE19-06 • Integrated PET/CT Color Scale Response Assessment Workflow**

**Joseph Colao BS (Presenter) ; Alin Chirindel MD ; Joo Hyun O MD ; Steve Cho MD \***

## PURPOSE

Assessment of tumor response to therapy by FDG PET/CT image sets from various time points can be often tedious and time consuming, especially in complex patients with multiple lesions or subtle changes. We developed and applied an integrated color-coded PET/CT image visualization workflow incorporating the tumor uptake at two time points to allow the reader to efficiently and accurately assess the relative PET tumor response to therapy.

## METHOD AND MATERIALS

Using MIM 5 imaging software (MIM Software <sup>TM</sup>), we analyzed FDG PET/CT image sets from two time points for 6 melanoma and 6 lymphoma cases. With technical support from MIM, we created a workflow that deformed the baseline PET and CT to the follow-up images. The SUV in each voxel of the deformed baseline PET was subtracted from each voxel's SUV in the follow-up PET. Each PET voxel was assigned a color based on its subtraction value, and the colored images were fused with the follow-up CT image set to create an anatomical view of the relative SUV changes. The colors corresponding to each subtraction value were based on a 20-color scale for positive and negative absolute and percent SUV change from baseline to follow-up. Two readers with third reader adjudication reviewed all 12 cases to determine if the response of the lesions with the greatest SUV values from baseline (max of 2 per organ) were accurately depicted by the color scale by comparing it to traditional gray-scale PET/CT visualization and ROI SUV values.

## RESULTS

The number of lesions analyzed per patient ranged from 1 to 5 for each based on the state of the patient's disease. The readers found that integrated PET/CT color scale images accurately depicted the approximate SUV changes for 26 of the 28 index lesions. The less clear color scale representations occurred because of small errors in the deformable registration in a lung nodule and with development of tumor necrosis.

## CONCLUSION

The integrated color scale PET/CT tumor response image sets provides an efficient and reliable method of determining the approximate tumor SUV changes associated with disease progression or treatment response for the major index lesions in our pilot study of metastatic melanoma or lymphoma patients.

## CLINICAL RELEVANCE/APPLICATION

Integrated color scale PET/CT representation can be a helpful aid to quickly judge and approximately quantify tumor response to therapy, especially in cases difficult to assess by current methods.

### **Molecular Imaging Symposium: Molecular Brain Imaging: From Research to Clinical Applications**

**Monday, 03:30 PM - 05:00 PM • S406B**



**MSMI24 • AMA PRA Category 1 Credit <sup>TM</sup>:1.5 • ARRT Category A+ Credit:1.5**

**Moderator**

**Satoshi Minoshima, MD, PhD \***

[Back to Top](#)

#### LEARNING OBJECTIVES

1) To discuss molecular brain imaging technologies that have been translated from research developments to clinical applications.

#### ABSTRACT

### MSMI24A • Amyloid Imaging: Translational Research to Clinical Applications

**Alexander Drzezga MD (Presenter) \***

#### LEARNING OBJECTIVES

1) Pathophysiological background: Role of amyloid-aggregation in the development of Alzheimer's disease. Concept of modern anti-amyloid therapy options. Time course of amyloid-aggregation as compared to the appearance of clinical symptoms. Value of amyloid-imaging as compared to other biomarkers of Alzheimer's disease. 2) Methodological principles of amyloid imaging: Development, mechanism, available tracers. Proof of concept, in vivo versus ex vivo histopathological confirmation. 3) Clinical value and interpretation of amyloid-imaging results, pitfalls and artefacts, value of amyloid-imaging with regard to early diagnosis, differential diagnosis and therapy monitoring. 4) Amyloid imaging in comparison to other imaging biomarkers (MRI, FDG-PET), value of multioimodal imaging.

### MSMI24B • How Molecular Imaging Contributes to Movement Disorders? Current and Future

**Kirk A Frey MD, PhD (Presenter) \***

#### LEARNING OBJECTIVES

View learning objectives under main course title.

### MSMI24C • Quantitative Analysis and Interpretation of Molecular Brain Imaging

**Satoshi Minoshima MD, PhD (Presenter) \***

#### LEARNING OBJECTIVES

1) To explain various quantification methods applied in the field of molecular brain imaging. 2) To discuss how such quantification methods can be used in clinic.

### MSMI24D • Making Molecular Brain Imaging Available in the Clinic: FDA and CMS

**Peter Herscovitch MD (Presenter)**

#### LEARNING OBJECTIVES

1) To discuss new molecular brain imaging techniques that are available in the clinic. 2) To explain how basic research has been translated to clinical applications. 3) To discuss approval processes that are necessary to establish clinical molecular brain imaging.

## Uncertainties in Imaging for Radiation Oncology: Sources and Mitigation Techniques-Incorporation of Imaging as a Biomarker in RT

**Tuesday, 08:30 AM - 10:00 AM • E261**

**PH RO BQ**

[Back to Top](#)

**RC322 • AMA PRA Category 1 Credit™:1.5 • ARRT Category A+ Credit:1.5**

**Co-Director, Moderator  
Robert Jeraj**

#### LEARNING OBJECTIVES

1) Anatomical imaging in treatment response (RECIST, volumetrics). 2) PET in treatment response assessment (PERCIST etc) with uncertainties. 3) MRI in treatment response assessment. 4) Imaging biomarkers.

### RC322A • Introduction to Biomarkers

**Robert Jeraj (Presenter)**

#### LEARNING OBJECTIVES

1) Imaging biomarkers and surrogate endpoints. 2) Prentice's criteria vs real world. 3) Imaging biomarker characteristics. 4) Imaging biomarker validation and qualification.

### RC322B • PET Assessment/Uncertainties

**Paul E Kinahan PhD (Presenter) \***

#### LEARNING OBJECTIVES

1) Understand the advantages and disadvantages of PET/CT as a biomarker for radiation oncology. 2) Understand sources of bias and variance in PET/CT imaging, both in data acquisition and analysis. 3) Understand the limitations of functional PET/CT techniques currently being used to evaluate treatment effect.

### RC322C • MRI Assessment/Uncertainties

**Edward F Jackson PhD (Presenter)**

#### LEARNING OBJECTIVES

1) Understand the physical principles of functional MR techniques currently being used to evaluate treatment effect. 2) Understand selected applications of each of these techniques to the assessment of radiation therapy. 3) Understand current limitations of each of the techniques.

URL's

web.me.com/efjackson

## Quantitative Imaging: Functional MRI (fMRI)

**Tuesday, 08:30 AM - 10:00 AM • E353A**

**PH MR BQ**

[Back to Top](#)

**RC325 • AMA PRA Category 1 Credit™:1.5 • ARRT Category A+ Credit:1.5**

**Director  
Michael F McNitt-Gray, PhD \***

## RC325A • Quality Assessment and Quantitation of Language and Motor fMRI

James T Voyvodic PhD (Presenter)

### LEARNING OBJECTIVES

1) Understand the major sources of variance in fMRI results. 2) Be aware of post-processing approaches for reducing variance and improving reproducibility. 3) Understand the quality assessment methods used to measure sources of variance within individual patient scans. 4) Appreciate how to evaluate whether a particular patient fMRI scan meets the quality assessment criteria necessary for obtaining quantitative fMRI measurements within clinically useful reproducibility margins.

### ABSTRACT

Many different variables affect clinical fMRI mapping of language and motor function, including behavioral task performance, head motion, tissue pathology, physiological variables, scanner performance, and software analysis methods. In order to achieve reproducible quantitative clinical fMRI results it is important to assess each of the major sources of variability, and to reduce unwanted signal variability where possible. This presentation will focus on identifying specific quality assessment criteria necessary to obtain reproducible quantitative fMRI results. It will also discuss the quantitative precision that can be expected for clinical fMRI results if the quality assessment criteria have been met. By establishing objective quality assessment criteria and validated reproducibility constraints, clinicians should be able to evaluate the quantitative confidence (i.e. margin of error) of the fMRI results for individual patient scans. Such guidelines are essential to enable quantitative measurements of the laterality, location, and spatial extent of clinically important functional brain areas. <http://hawking.biac.duke.edu/RSNA>

## RC325B • More Quantitative fMRI Paradigms for Presurgical Mapping of the Visual System

Edgar A Deyoe PhD (Presenter) \*

### LEARNING OBJECTIVES

1) Review the functional organization of the human visual cortex. 2) Become familiar with state-of-the-art methods for presurgical mapping of the visual system with fMRI. 3) Learn of new methods for visualizing and interpreting fMRI brain maps of the visual system. 4) Become aware of interpretational issues such as neurovascular uncoupling that can significantly affect interpretation in a presurgical mapping context.

### ABSTRACT

The complexity of MRI technology and the wealth of new information it provides can leave clinicians hard pressed to stay abreast of the latest developments and applications, especially since the field continues to evolve at a brisk pace. The goal of this session will be to review clinically relevant aspects of fMRI methods and their use in mapping the visual system to aid diagnosis of vision-related CNS diseases and to assist treatment planning, delivery and followup. The session will include a review of fundamental organizational principles of the human visual system with an emphasis on those properties that may be particularly relevant for clinical applications. Some principles, such as retinotopic organization may be generally familiar, but the ability to map this organization in detail quantitatively in individual patients and its utility in specific clinical applications is likely to be novel. Unique methods will be described for visualizing this organization both within the brain and as it relates to the patient's visual field and scotomata. The session will describe specific clinical applications of visual system mapping with fMRI and will present case studies to highlight such applications. Also, included is a description of methodology aimed at streamlining the clinical workflow and highlighting practical issues that should be considered to obtain high quality data with clinical patients. The overall goal is to show how it is possible to spend as little as 10 minutes of fMRI scan time yet obtain information that can be invaluable for diagnosis and treatment of patients with brain tumors, arteriovenous malformations, epilepsy and other pathologies that can impact central visual pathways.

## RC325C • BOLD Cerebrovascular Reactivity Mapping as Applied to Brain Tumor fMRI

Jay J Pillai MD (Presenter) \*

### LEARNING OBJECTIVES

1) Understand the role of breath hold cerebrovascular reactivity (BH CVR) mapping in the assessment of neurovascular uncoupling potential. 2) Appreciate how neurovascular uncoupling may affect the reliability of BOLD fMRI activation maps. 3) Describe how BH CVR mapping can be performed in brain tumor patients.

### ABSTRACT

The phenomenon of neurovascular uncoupling (NVU) is an important limitation of blood oxygen level dependent (BOLD) functional MRI (fMRI). One effective and practical method for assessment of risk of NVU is BOLD breath hold cerebrovascular reactivity (BH CVR) mapping. BH CVR mapping, similar to MR perfusion methods, allows assessment of regional hemodynamic impairment that may result in NVU and thus may lead to false negative activation on task-based sensorimotor or language fMRI that may be used for presurgical mapping in patients with brain tumors and other resectable brain lesions. However, unlike MR perfusion imaging, which assesses static or baseline perfusion to brain tumors and peritumoral regions, BOLD BH CVR mapping enables a dynamic assessment of cerebrovascular response, and its results can be applied to any task-based activation map. This lecture will describe the technique of BH CVR mapping, some of its strengths and limitations, and include cases in which interpretation of clinical fMRI exams has been affected by the additional information provided by these maps.

## Quantitative Imaging: A Revolution in Evolution (In Association with the Society for Imaging Informatics in Medicine)

Tuesday, 08:30 AM - 10:00 AM • N229



[Back to Top](#)

RC326 • AMA PRA Category 1 Credit™:1.5 • ARRT Category A+ Credit:1.5

### Co-Moderator

Luciano M Prevedello, MD, MPH

### Co-Moderator

Adam E Flanders, MD

### LEARNING OBJECTIVES

1) Develop an understanding of what quantitative imaging is and how it may revolutionize the way we practice diagnostic radiology today. 2) Learn the research advances and the current clinical applications of this technology. 3) Appreciate the current challenges involved in using these tools clinically and understand the steps required for a successful clinical implementation.

### ABSTRACT

Medicine has undergone a gradual evolution in which diagnostic imaging has become the centerpiece in establishing a clinical diagnosis and in assessing disease response. In recent years, the focus has changed such that for some disease categories (e.g. oncology) we now perceive medical imaging as a phenotypic expression of the genetic makeup of that disease. To that end, imaging now serves as a biomarker of genetic disease subtypes with features that may offer clues to understanding the natural behavior of the disease and specific changes that may occur as part of a therapeutic response. It is now well recognized that there is a substantial amount of objective information contained within diagnostic imaging studies that can be exploited beyond the level of simple measurements. The extraction of quantitative and semi-quantitative information from imaging studies that is both useful and reproducible is the challenge and opportunity for clinical trials research and radiologic reporting today and in the future. This session will explore the revolution and evolution of quantitative imaging; providing attendees with research advances, clinical applications, and the challenges of clinical implementation.

## RC326A • What is Quantitative Imaging?

**Katherine P Andriole** PhD (Presenter)

#### LEARNING OBJECTIVES

1) Be able to describe what is meant by quantitative imaging. 2) Understand existing issues in implementing quantitative imaging techniques in the clinical arena as well as in the research realm, and see how informatics tools may help. 3) Be aware of on-going international efforts to address current challenges and to move quantitative imaging forward.

#### ABSTRACT

Quantitative imaging has rapidly evolved in recent years from a promising research activity to an essential clinical tool. Physicians consider the objective metrics obtained from imaging studies, in making critical patient management decisions. What is meant by quantitative imaging will be described using illustrative real-world use cases. Existing issues including technical as well as workflow challenges will be discussed. An introduction to imaging informatics tools and techniques such as standards, integration, data mining, cloud computing, ontologies, data visualization and navigation tools, and business analytics applications that may assist in filling current gaps in the clinical implementation of quantitative imaging will be given. An overview of activities of the RSNA's Quantitative Imaging Biomarkers Alliance (QIBA), an international initiative whose goal is to optimize the potential of quantitative imaging, including a description of the data warehouse project will be provided.

### RC326B • Informatics Approaches to Enable Quantitative Imaging in Real World Radiology Practice

**Daniel L Rubin** MD,MS (Presenter) \*

#### LEARNING OBJECTIVES

1) To highlight limitations in current radiological quantitative imaging practice and identify opportunities for improvement through informatics. 2) To introduce Annotation and Image Markup (AIM) as a new standard for capturing and sharing quantitative imaging metadata. 3) To demonstrate new AIM-enhanced tools that can streamline and improve quantitative imaging assessment and workflow for the radiologist.

#### ABSTRACT

Radiology practice is increasingly a quantitative endeavor. Radiologists frequently need to measure the length of lesions to track treatment response or measure the size of structures to for diagnostic assessment. Current practices of quantitation are cumbersome; measurements are recorded as screen captures that cannot be processed by machine, and the numbers must be transcribed into a radiology report. It is currently exceedingly difficult to create structured databases of quantitative image information for discovery about how, say, change in tumor size over time relates to drug treatment. Quantitative imaging is currently at best a labor-intensive process and at worst error-prone. We have been developing informatics methods to streamline the electronic capture of quantitative imaging results as image metadata in structured format that can be easily processed by computers. Tools that we are producing will allow the radiologist to perform quantitative imaging assessment in their current routine workflow measuring lesions on the PACS, while simultaneously their measurements will be captured and transmitted in standardized formats to applications that can automate accurate reporting, analysis, and decision support. In the future such tools will even help researchers to discover new ways that quantitative signals in images can improve assessment of treatment and prediction of disease course.

### RC326C • QI Clinical Use Cases Outside of Oncology

**Eliot L Siegel** MD (Presenter) \*

#### LEARNING OBJECTIVES

1) Understand the use of quantitative imaging outside of oncology. 2) Learn how to apply these QI techniques to current radiology practice.

## Informatics (3D, Quantitative and Advanced Visualization)

**Tuesday, 10:30 AM - 12:00 PM • S402AB**

**IN** **CT** **BQ**

[Back to Top](#)

**SSG08 • AMA PRA Category 1 Credit™:1.5**

#### Moderator

**Asim F Choudhri**, MD

#### Moderator

**Safwan Halabi**, MD

### SSG08-01 • Gray-matter Volumetry Predicts Decline of Intelligence Quotient in Children with Sickle Cell Disease

**Rong Chen** PhD (Presenter) ; **Michal Arkuszewski** ; **Jaroslawn Krejza** MD ; **Edward H Herskovits** MD, PhD ; **Elias R Melhem** MD, PhD

#### PURPOSE

For children with sickle cell disease (SCD), we aim to differentiate those with decline of intelligence-quotient (IQ) from counterparts without decline, based on structural magnetic-resonance (MR) imaging volumetry

#### METHOD AND MATERIALS

This prospective cohort study included 25 children with SCD, homozygous for hemoglobin S, with no history of stroke. We administered the Kaufman Brief Intelligence Test (K-BIT) to each child at yearly intervals for 2-4 years. Each child underwent MR examination within 30 days of the baseline K-BIT evaluation date. We calculated K-BIT change rates, and used rate of change in K-BIT to classify children into two groups: a decline group and a non-decline group. We then generated predictive models to predict the group-membership variable (K-BIT decline / non-decline) based on regional gray-matter volumes computed from structural MR images.

#### RESULTS

We identified six gray-matter structures (the left median cingulate gyrus, the right middle occipital gyrus, the left inferior occipital gyrus, the right fusiform gyrus, the right middle temporal gyrus, the right inferior temporal gyrus) that, when assessed for volume at baseline, are jointly predictive of whether or not a child would suffer subsequent K-BIT decline. Based on these six regional GM volumes, maternal education, and the baseline K-BIT, we built a prognostic model using the K\* algorithm. The accuracy, sensitivity and specificity were 0.84, 0.75 and 1.0, respectively.

#### CONCLUSION

Structural MR imaging predicts subsequent IQ decline for children with SCD.

#### CLINICAL RELEVANCE/APPLICATION

Structural MR derived features can be used as a biomarker to predict subsequent IQ decline for children with SCD.

### SSG08-02 • Heterogeneity as Biomarker in Tumour Imaging

**Lejla Alic** ; **Jifke F Veenland** PhD (Presenter)

#### PURPOSE

Tumour heterogeneity could be a valuable biomarker for differentiation, grading, response monitoring and outcome prediction. Many

quantitative techniques have been described, however in clinical practice these methods are scarcely used. The aim of this study is to evaluate the performance of the described methods and to identify the bottlenecks for the implementation in clinical practice.

#### METHOD AND MATERIALS

We searched OVID, EMBASE, and Cochrane CENTRAL up to 24 March 2013. Heterogeneity analysis methods were classified into four categories, i.e., non-spatial methods (NSM), spatial grey level methods (SGLM), fractal analysis (FA) methods, and filters and transforms (FandT).

#### RESULTS

From 6908 potentially relevant publications, 183 studies were included. The number of studies has been increasing steadily since 2009. Generally, 60 % studies use NSM, 49% use SGLM, 11 % use FA, and 28% use FandT. Differential diagnosis, grading or outcome prediction was the goal in 86% studies, 36% studies were based on MRI, and 88% studies were conducted retrospectively. Tumours in the breast and brain together cover 49% of the studies.

No relation was found between the discriminative power and the quantification methods used, or between the discriminative power and the imaging modality. The reported AUC ranged from 0.5 to 1 with a median of 0.89. A negative correlation was found between the AUC and the number of features estimated per tumour, which is presumably caused by overfitting in small datasets. In only 53.4% of the classification studies, the use of cross-validation was reported. None of the publications report the use of an external validation set to test their findings. Retrospective analyses were conducted in 60% of the studies without a clear description of the inclusion criteria. Only 12% of the studies had a prospective study design. Almost none of the papers evaluated the incremental value of the heterogeneity biomarker on top of clinical established markers.

#### CONCLUSION

To enable the translation of imaging biomarkers from the research stage to clinical practice, research should focus more on prospective studies, use external datasets for validation, and focus on the added value of the proposed heterogeneity biomarker on top of the clinical established markers.

#### CLINICAL RELEVANCE/APPLICATION

Heterogeneity has the potential of a valuable biomarker.

### **SSG08-03 • Effective Staging of Fibrosis by the Selected Texture Features of Liver: Which One Is Better, CT or MR Imaging?**

**Xuejun Zhang** PhD (Presenter) ; **Yufan Zeng** ; **Hiroshi Fujita** PhD ; **Yan Wen** ; **Liling Long** MD ; **Yu Huang** MMed

#### PURPOSE

Different types of datasets acquired from CT and MR images are investigated to select the optimal parameters for the classification of texture patterns of hepatic fibrosis using in Computer-aided Diagnosis.

#### METHOD AND MATERIALS

149 patients were scanned by MDCT and 218 patients were performed abdominal examination using 1.5T and 3T superconducting MR scanners. All the cases are verified by needle biopsies as the gold standard of our experiment, ranging from 0(no fibrosis) to 5(cirrhosis). For each case, at least four sequenced phase images are acquired: pre-contrast, arterial, portal venous and delayed phase. 15 texture features calculated from gray level co-occurrence matrix (GLCM) are extracted within an ROI in liver as one set of input vectors. Each combination of these input subsets is checked by using support vector machine (SVM) with leave-one-case-out method to differentiate fibrosis into two groups: normal or abnormal. 10 ROIs in liver are manually picked up dispersedly by experienced radiologist from each sequenced image and each item in 15 features is averaged by 10 ROIs in each case to reduce the validation time. The number of input items  $n$  is selected from the combinations of 15 features exhaustively. ( $2^{15}-1$  different combinations obtained, where  $n \in [1,15]$ )

#### RESULTS

According to the accuracy rate (AR) calculated from each combination, the optimal number of texture features to classify liver fibrosis degree is from 4 to 7, no matter what modalities are used. The overall performance calculated by the average sum of maximum AR value of all 15 types number of features is 66.83% in CT images, while 68.14%, and 71.98% in MR images (Fig.1a), respectively; among 15 texture features, mean gray value and entropy are in most common used in 3 datasets. Correlation has the lowest AR value and is abandoned to be used in all datasets. AR value tends to increase with the injection of contrast agency, and both CT and MR images reach highest performance in equilibrium phase as shown in Fig.1b.

#### CONCLUSION

Comparing the accuracy of classification on two modalities, we should reveal that MR images have an advantage over CT images, while 3T MRI is better than 1.5T MRI to detect liver fibrosis. The texture analysis is effective in equilibrium phase than in other phased images.

#### CLINICAL RELEVANCE/APPLICATION

MR can demonstrate fibrotic texture efficiently and equilibrium phase image is recommended as a main tool for interpretation of cirrhosis.

### **SSG08-04 • The Development of a Methodology to Simulate 3D Models of Benign and Malignant Breast Masses**

**Eman Shaheen** (Presenter) ; **Chantal Van Ongeval** MD ; **Frederik De Keyzer** ; **Kenneth C Young** PhD ; **David Dance** PhD ; **Hilde Bosmans** PhD \*

#### PURPOSE

Breast cancer remains a major health concern and a leading cause of cancer mortality among women. The commonly used screening mammography has limited sensitivity for small lesions detection due to anatomical noise. Therefore, new breast imaging modalities with proven superiority for lesion detection may remedy this shortcoming in breast cancer screening and diagnosis. Clinical trials are very expensive, giving rise to alternative dedicated simulation studies for the investigation of new modalities in terms of lesion detectability. Here, we present a new method to create more clinically-relevant 3D models of benign and malignant breast masses for use in simulation studies.

#### METHOD AND MATERIALS

Breast MRI cases with histologically-proven malignant masses, imaged with a 3D contrast enhanced acquisition, were collected. Each mass was manually segmented in three reconstructed orthogonal planes (sagittal, transversal, coronal), and then combined with logical OR, resampled to have isotropic voxel sizes in 3D space, then meshed. Due to the low resolution of MRI images, most of these masses had well defined borders. In order to create spiculated masses, suspicious for malignancy, the segmented model was used as nucleus with branches grown on the surface. The branches had different lengths, bifurcations, orientations and thicknesses. The clinical appearance of these models was assessed by inserting each mass model into 2D digital mammography and breast tomosynthesis (BT) images using a previously-validated simulation framework. Each 2D and BT was shown to an expert radiologist who scored the BIRADS (scale 1-5) and the realism of the simulated mass (scale 1-10, 10=definitely real).

#### RESULTS

Preliminary results for the benign category (well defined borders) with 7 simulated masses showed a BIRADS score between 2 and 3, and an average realism score of 8.1 (range 8-9) for 2D and 7.9 (7-9) for BT. For the malignant category with 8 spiculated masses, the BIRADS score was between 4 and 5, and the average realism score was 8.3 (8-9) in 2D and 7.6 (7-9) in BT.

#### CONCLUSION

A new method to simulate 3D models, based on an atlas of real lesions, with variety of shapes and degree of malignancies was presented with promising results.

#### CLINICAL RELEVANCE/APPLICATION

The proposed 3D mass models are promising candidates to create enriched databases for virtual clinical trials and observer detectability studies to optimize the performance of mammography systems.

## SSG08-05 • Tumor Heterogeneity Assessed with First Order Histogram Features in Dependence from Image Resolution: A Point to Be Considered in Clinical Routine?

**Matthias Benndorf** MD (Presenter) ; **Martin Soschynski** ; **Sabine Bucher** ; **Marisa Windfuhr-Blum** PhD ; **Mathias F Langer** MD, PhD ; **Elmar C Kotter** MD, MSc \*

### PURPOSE

Measurement of tumor heterogeneity in contrast enhanced MRI is a promising method to obtain additional information about prognosis, tumor type and therapy response. One way to describe heterogeneity is by histogram analysis of the tumor signal intensities. Our aim was to analyze to what extent image resolution affects first order histogram features, using breast MRI examinations.

### METHOD AND MATERIALS

32 consecutively histopathologically (n=25) or by means of follow up (n=7, one year imaging follow up was considered sufficient) verified breast MRI lesions >9mm were retrospectively analyzed. Parameters of our scanner protocol were: 1.5T, TE: 4.76ms, TR: 11ms, matrix: 480x512. Analysis was performed in early enhancement phase subtraction images. The cross sectional image showing the largest axial tumor diameter was rescaled with a bicubic interpolation function 10 times in decreasing 5% steps. This resulted in a dataset of 352 images. Within each of these images the tumor was manually delineated and the raw signal intensity matrix obtained. Mean, standard deviation, skewness, kurtosis, empirical Shannon entropy [ $-1 \times Sp(a) \times \log(p(a))$ ] and uniformity [ $Sp(a)^2$ ] then were analyzed in dependence from image resolution.

### RESULTS

We demonstrate that histogram features mean, standard deviation, skewness and kurtosis are robust to changes in resolution, with  $P > 0.4$  for analysis of variance (anova) comparisons between resolutions for the single feature. Entropy however decreases with decreasing resolution (P

### CONCLUSION

The Shannon entropy within tumors decreases with decreasing image resolution, whereas basic distribution information like mean and standard deviation remain relatively stable. Uniformity behaves inversely to entropy.

### CLINICAL RELEVANCE/APPLICATION

When interpreting studies about diagnostic performance of histogram analysis, one should consider the imaging protocol used in the respective study. Image resolution affects entropy estimates.

## SSG08-06 • Differential Diagnosis of Benign and Malignant Brain Tumors by Use of Texture Analysis on FDG-PET Images

**Shoji Kido** MD, PhD (Presenter) ; **Akiko Katamoto** BS ; **Rui Xu** ; **Yasushi Hirano**

### PURPOSE

To develop the computer-aided diagnosis (CAD) method by use of texture analysis and pattern classification technique to analyze F-18-fluorodeoxy-glucose (FDG) uptake distribution of brain tumors for differential diagnosis of malignancy and benignancy on FDG-PET images.

### METHOD AND MATERIALS

We used consecutive 24 patients with brain tumors (10 benign and 14 malignant cases). Each patient underwent MRI and PET scans continuously. In the PET images, it is difficult to determine the contours of tumors in many cases. So, MR images were used for determination for tumor regions on PET images. In the first step, each patient of MR image data was superimposed to PET image data by use of a three-dimensional registration algorithm. After manual segmentation of tumor regions on MR images, tumor regions on PET images were segmented based on those on MR images. Texture features representing FDG uptake distributions were obtained from these tumor regions on PET images. From these texture features, four optimal parameters to distinguish malignancy from benignancy were selected. For pattern classification technique, we used a support vector machine (SVM) as a classifier. We classified 24 tumors into benign and malignant cases with the SVM by a leave-one-out method. The performance of our CAD method was compared with a maximum standard uptake value ( $SUV_{max}$ ) based method that was generally used in clinical diagnosis.

### RESULTS

The accuracy rate of our CAD method for all cases was 91.7% (22/24 cases). The accuracy rate for benign cases was 80.0% (8/10 cases), and that for malignant cases was 100.0% (14/14 cases). On the other hand, the accuracy rate of  $SUV_{max}$  based method for all cases was 62.5% (15/24 cases). The accuracy rate for benign cases was 20.0% (2/10 cases), and that for malignant cases was 92.9 % (13/14 cases). The performance of our CAD method was superior to that of the  $SUV_{max}$  based method ( $P < 0.05$ ).

### CONCLUSION

The CAD method for differential diagnosis of brain tumors on FDG-PET images by use of texture analysis and the SVM classifier indicated high performance compared with the  $SUV_{max}$  based method. This method is feasible for assisting radiologists in the differential diagnosis of brain tumors on FDG-PET images.

### CLINICAL RELEVANCE/APPLICATION

The CAD method by use of texture analysis and the SVM classifier on FDG-PET images improves the abilities of radiologists for differential diagnosis of malignant and benign tumors on FDG-PET images.

## SSG08-07 • Quantification of the Distribution and Extent of Automatically Classified Small Pulmonary Arteries and Veins on Volumetric Chest CT

**Seyoun Park** ; **Sang Min Lee** MD ; **Namkug Kim** PhD (Presenter) ; **Joon Beom Seo** MD, PhD ; **Joon Ho Choi** MD

### CONCLUSION

Our automatic vessel classification-based quantification approach may be useful for assessing the status of many pulmonary disease, considering the spatial distribution and extents of automatically classified, small pulmonary arteries and veins.

### Background

As one of meaningful indicators for assessing the status of pulmonary circulation in various pulmonary diseases, analysis of the distribution and extent of small pulmonary vessels is necessary. We developed a quantitative analysis method for determining the total vascular structure in 3D from volumetric chest CT.

### Evaluation

Non-contrast volumetric chest CT scans with sub-millimeter thickness of 29 patients with chronic obstructive pulmonary disease (COPD) were used for this study. We extracted vessels as 3D points from volumetric CT images. A minimum spanning tree of pulmonary arteries and veins were then generated by construction energy minimization from extracted points. This tree was divided into smaller branches by cutting the mediastinal region. The arteries and veins were then separately collected to observe distributions. From the distal to proximal surfaces, we extracted 6 offset surfaces at 5mm intervals and detected intersecting points with vascular trees. At each point, vascular direction was estimated using neighbor vessel points. Finally, vascular radii were computed by fitting cylinders at each center. Quantitative measures were computed such as the number of vessels and the mean diameters. We collected several quantitative measures such as the mean diameter, cross-sectional area with the inner pulmonary surface. The diameters of vessels are  $1.544 \pm 0.158$ ,  $1.823 \pm 0.093$ ,  $1.934 \pm 0.079$ ,  $1.968 \pm 0.073$ ,  $1.977 \pm 0.082$ , and  $1.994 \pm 0.092$ mm (mean $\pm$ SD) from distal to proximal surfaces with 5 mm intervals, respectively. Among those, the diameters of only arteries of 29 patients' lungs are  $1.513 \pm 0.159$ ,  $1.840 \pm 0.105$ ,  $1.929 \pm 0.076$ ,  $1.960 \pm 0.073$ ,  $1.958 \pm 0.085$  and  $1.960 \pm 0.093$ mm at the surfaces, respectively.

### Discussion

This method is especially useful in artery and vein classification and could be possible to evaluate etiology and progress of many

pulmonary diseases such as pulmonary hypertension, interstitial lung disease and COPD using volumetric chest CT.

### SSG08-08 • Quantitative Analysis of Infectious Lung Disease from Serial PET-CT Scans in Small Animal Models

**Brent Foster** (Presenter) ; **Ulas Bagci** PhD, MSc ; **Ziyue Xu** PhD ; **Awais Mansoor** PhD ; **Brian Luna** ; **Bappaditya Dey** ; **Colleen Jonsson** ; **William Bishai** ; **Sanjay K Jain** MD ; **Daniel J Mollura** MD

#### PURPOSE

To develop a complete image analysis and quantification framework that accurately determines disease severity and its progression in pulmonary infections using three small animal models (rabbit, ferret, and mouse).

#### METHOD AND MATERIALS

We designed a fast and robust automated image analysis platform with a quantification tool that facilitates accurate quantification of pulmonary lesions, and an image registration pipeline that supports a volumetric comparison of all serial scans using PET and CT images. The proposed method for analysis contained three steps: (i) the lung was segmented via an interactive region growing method (ii) mathematical morphology was then applied to this binary mask to remove all non-lung regions from the images; and (iii) then the affinity propagation based clustering algorithm was used on all PET images to precisely segment the high uptake regions. The proposed framework was tested using sequentially acquired CT and PET images. The rabbits were infected with Mycobacterium tuberculosis (TB) (92 PET-CT scans). The ferrets were injected with the H1N1 influenza virus (44 PET-CT scans), and the mice were infected with an aerosolized respiratory pathogen (24 PET-CT scans). Segmentations were evaluated by expert radiologists and compared with ground truth segmentations.

#### RESULTS

Each small animal model was evaluated within the same animal type and the Dice Similarity Coefficient (DSC), and the Hausdorff distance (HD) were used for evaluation of the proposed method. The estimated lesion volume sizes from CT and PET images, estimated from the proposed method and the ground truth ( $R^2=0.8922$ , p

#### CONCLUSION

The proposed computational framework can increase the efficiency and quality of pre-clinical findings relative to clinical standards and decrease the inter-observer variation from manual quantification methods that can obscure findings.

#### CLINICAL RELEVANCE/APPLICATION

This framework can be applied clinically for accurate, efficient, and robust quantification of infectious diseases using longitudinal PET-CT images.

### SSG08-09 • Computerized Differentiation of Regional Patterns of Diffuse Infiltrative Lung Disease for Iodine Quantification in Dual-energy CT Using SVM Classifier and a Hybrid Segmentation Method

**Jangpyo Bae** MS (Presenter) ; **Yongjun Chang** ; **Jung Won Moon** ; **Ho Yun Lee** MD ; **Namkug Kim** PhD

#### PURPOSE

To construct the computerized differentiation framework to quantify the iodine concentration according to the regional patterns of diffuse infiltrative lung disease (DILD) in dual-energy CT.

#### METHOD AND MATERIALS

Volumetric CT scans of thirty patients with diffuse interstitial lung disease (DILD) were performed by a 64-multi detector row dual energy CT scanner (Siemens Definition Flash) with in 0.75mm collimation at dept. of radiology, Samsung Medical Center. Two hundred seventy one rectangular regions of interest (ROIs) with 20x20 pixels, consisting of each 57 ROIs representing three regional disease patterns (ground-glass opacity; GGO; reticular opacity; RO; and consolidation; CONS) and 100 ROIs for normal region were marked at dual-energy CT images of various DILD by two experienced radiologists with consensus. Twenty eight density, textural and shape features (histogram, gradient, run-length, co-occurrence matrix, cluster, and top-hat) were calculated and employed to characterize the ROIs by a SVM classifier with sequential forward selection method which differentiate the ROI into each class. The lung segmentation was performed with a hybrid method using rib information and an inverse level set of which parameters were adjusted with the density histogram of lung region. In addition, five folding cross validation with twenty repetitions were performed for average ROI based accuracy. To validate the region based accuracy, 40 slices were randomly selected from 20 patients and drawn by two radiologists with consensus, which was compared with the computerized method.

#### RESULTS

The accuracies of the classification of ROIs and whole lung region were  $87.61 \pm 0.76$  and  $74.20 \pm 4.62$ , respectively. The region based accuracies of normal, RO, GGO and CONS were  $77.04 \pm 4.50$ ,  $37.69 \pm 12.20$ ,  $62.38 \pm 9.53$  and  $45.03 \pm 13.18$ .

#### CONCLUSION

The proposed classification methods showed clinically applicable accuracy. In addition, the proposed segmentation method was effective in the lung with DILD in dual energy CT.

#### CLINICAL RELEVANCE/APPLICATION

This method is useful in computer aided differentiation and quantification of regional disease patterns of diffuse infiltrative lung disease in dual energy CT images.

## Neuroradiology (Imaging of White Matter and Demyelinating Disease)

Tuesday, 10:30 AM - 12:00 PM • N229

BQ NR

[Back to Top](#)

SSG12 • AMA PRA Category 1 Credit™:1.5 • ARRT Category A+ Credit:1.5

Moderator

Aaron S Field, MD, PhD

Moderator

Christopher D Lascola, MD

### SSG12-01 • A Capillary Phantom for Quantitative DTI Assessment: A Method for Normalization of Diffusion Tensor Parameters

**Damien P Galanaud** MD, PhD (Presenter) \* ; **Omid Khalilzadeh** MD, MPH ; **Julien Dinkel** MD ; **Irene S Wang** MD ; **Paulette Onorato** PhD ; **Rajiv Gupta** PhD, MD

#### PURPOSE

Although quantitative diffusion tensor imaging (DTI) shows great potential for the assessment of white matter pathologies, no consensus exists on a standardized method of calculating DTI measurements. Quantitative DTI measurements cannot be compared between patients scanned with different acquisition parameters. In this study, we evaluated the feasibility of using water-filled arrays of glass capillaries to construct a DTI phantom. A multivariate method to normalize DTI measurements based on the acquisition parameters is proposed and tested.

#### METHOD AND MATERIALS

The phantom was constructed using arrays of glass capillaries oriented at 6 different directions: one set in the center and 5 at radial orientations. The capillary arrays at different orientations had different inner diameters (20, 40, 50, 100, 150, and 200um). DTI data of

212 healthy subjects were also analyzed. Phantom was scanned with the same scanners and acquisition parameters, as that of healthy individuals. The repetition time (84-105ms), b values (700-100s/mm<sup>2</sup>), field strength (1.5-3T), slice thickness (3-5mm), number of diffusion directions (11-64), relaxation time (5700-13000ms) and echo time (84-105ms) varied across different scans. The fractional anisotropy and principal eigenvectors of the diffusion tensors were calculated in different capillary sets in the phantom and 20 different white matter brain tracts. The correlation between DTI measurements of different white matter tracts and the phantom glass capillaries, scanned with the same acquisition parameters, was assessed.

#### RESULTS

There was a significant association between DTI measurements of various white matter tracts and different sets of phantom capillaries, scanned with the same acquisition parameters. A multivariate-regression model with age, gender, head motions and rotation angle, different acquisition parameters and diffusion tensor parameters of the phantom capillaries could explain 77-86% of variability in diffusion tensor measurements of the white matter tracts. The standardized residual values were calculated and the normal ranges for DTI parameters at different white matter tracts were estimated.

#### CONCLUSION

This study presents a practical and accurate model for standardization of diffusion tensor parameters.

#### CLINICAL RELEVANCE/APPLICATION

The capillary phantom introduced in this study can make DTI measures comparable between different acquisition settings

### **SSG12-02 • Investigation of Influences of the Magnetic Field Inhomogeneity Due to the Subject Positioning on the Apparent Diffusion Coefficient in the Cerebral Cortex Using MRI Simulator**

**Daigo Ushijima** (Presenter) ; **Seiji Kumazawa** PhD ; **Hidetake Yabuuchi** MD ; **Masafumi Ohki**

#### PURPOSE

In the study of neurodegenerative diseases, apparent diffusion coefficient (ADC) values in the cerebral cortex are investigated using diffusion-weighted images (DWIs). However, DWIs suffer from geometric distortion due to magnetic field inhomogeneity (MFI) caused by susceptibility effect. It is known that the cortical ADC values increase due to contamination of signal intensity in cerebrospinal fluid by distortion. It is reported that distribution of MFI depends on the subject positioning in the static field. The purpose of this study was to investigate influences of the MFI which depends on the subject positioning on the cortical ADC values using MRI simulator.

#### METHOD AND MATERIALS

We investigated the differences of ADC values in the cortex among the different patterns of MFI using digital brain phantom. We calculated MFI depending on the subject position in the static field by using the Susceptibility-Voxel Convolution method. We generated different three patterns of MFI: no inhomogeneity, and two different patterns of inhomogeneities. In each pattern of MFI, DWI was generated by MRI simulator according to single-shot echo-planar imaging sequence, and ADC map was generated from DWIs. In our simulator, the diffusion coefficient of cortex was set to  $0.89 \times 10^{-3} \text{ mm}^2/\text{s}$ . We compared ADC values in six cortical regions of interest among different three patterns of MFI.

#### RESULTS

In the cortical region close to frontal sinus, the average of ADC value in no inhomogeneity was  $1.017 \times 10^{-3} \text{ mm}^2/\text{s}$ , and was higher than ideal ADC value in the cortex. The average of ADC values in other two patterns of MFI were  $1.114 \times 10^{-3}$  and  $0.952 \times 10^{-3} \text{ mm}^2/\text{s}$ , respectively. These ADC values showed significant differences among different three patterns of MFI. Although the ADC values showed statistically no significant differences in the other regions among them, ADC values showed the variation.

#### CONCLUSION

We have investigated influences of the MFI on the cortical ADC values using MRI simulator. Our results suggest that ADC values in the cortical region might vary due to MFI which depends on the subject positioning in the static field.

#### CLINICAL RELEVANCE/APPLICATION

In interpretation of cortical ADC values in neurodegenerative diseases, influences of the MFI should be taken into account in changes of ADC values.

### **SSG12-03 • Microstructural Integrity of Brain White Matter in Non-demented Older Adults Is Associated with Frequency of Cognitive Activity in Late Life**

**Christopher M Barth** ; **Robert S Wilson** PhD ; **Shengwei Zhang** BS, BEng ; **David A Bennett** MD ; **Konstantinos Arfanakis** PhD (Presenter)

#### PURPOSE

The purpose of this study was to test the hypothesis that more frequent late life cognitive activity in a community sample of non-demented elderly subjects is associated with greater brain microstructural integrity, as assessed by diffusion tensor imaging (DTI).

#### METHOD AND MATERIALS

A community sample of non-demented elderly subjects (N = 379) ( $82 \pm 7$  years of age) participating in the Rush Memory and Aging Project was included in this study. All participants rated how often they were involved in various cognitively stimulating activities from childhood to middle-age (past cognitive activity, PCA), as well as within the last year (late life cognitive activity, LLCA). Participants also rated the availability of cognitive resources (CR) in their home during childhood and adulthood. T1-weighted MPRAGE, T2-weighted FLAIR and SE-EPI DTI data were collected on all participants using a 1.5 Tesla MRI scanner. White matter hyperintense (WMH) lesions were automatically segmented based on MPRAGE and FLAIR data. Correction for bulk motion and distortions due to eddy-currents and field non-uniformities, B-matrix reorientation, and diffusion tensor calculation, were all conducted using TORTOISE. The fractional anisotropy (FA), trace of the diffusion tensor, axial (AD) and radial diffusivity (RD) were calculated in each voxel. Tract-Based Spatial Statistics was used to test for voxel-wise associations of DTI parameters with LLCA, while controlling for age, sex, level of education, the presence of WMHs, PCA and CR. The null distribution was generated using the randomise tool and 5000 permutations. Differences were considered significant at p

#### RESULTS

Higher frequency of LLCA was associated with higher FA values in the corpus callosum and white matter of the left brain hemisphere, and generally lower trace, AD, and RD in the thalamus.

#### CONCLUSION

The present work suggests that a higher frequency of LLCA in community-dwelling non-demented elderly adults may be associated with greater microstructural integrity in white matter of the corpus callosum and left brain hemisphere.

#### CLINICAL RELEVANCE/APPLICATION

Frequent late life cognitive activity may play a role in protecting the microstructure of brain white matter.

### **SSG12-04 • Cerebral Microbleeds Are Related to Loss of White Matter Structural Integrity: The Rotterdam Scan Study**

**Saloua Akoudad** ; **Marius De Groot** MSC ; **Aad Van Der Lugt** MD, PhD ; **Wiro Niessen** PhD ; **Mohammad A Ikram** ; **Meike W Vernooij** MD (Presenter)

#### PURPOSE

Cerebral microbleeds (CMBs) are highly frequent in the general population and are increasingly recognized as a manifestation of cerebral small vessel disease (CSVD). Although CMBs appear as focal lesions on imaging, it remains unclear whether the underlying CSVD is also restricted to that focal area or that it affects the brain more diffusely. We investigated whether the presence, number, and location of microbleeds is related to loss of microstructural integrity of brain white matter, as measured by diffusion tensor imaging (DTI).



## METHOD AND MATERIALS

A total of 4493 Rotterdam Scan Study participants underwent brain MRI to determine microbleed status. With DTI, global fractional anisotropy (FA) and mean diffusivity (MD) were measured in normal-appearing white matter. Multiple linear regression models, adjusted for age, sex, cardiovascular risk factors, white matter lesions and infarcts were applied to investigate the independent association between microbleeds and integrity of brain white matter. Analyses were repeated after stratification by apolipoprotein E  $\epsilon$ 4 (APOE  $\epsilon$ 4) carriership.

## RESULTS

Presence of microbleeds was related to a lower mean FA and higher mean MD, in a dose-dependent manner, and was already apparent for a single CMB microbleed (standardized FA: -0.13, 95% CI -0.21; -0.05; MD: 0.12, 95% CI 0.05; 0.19). For lobar microbleeds alterations in DTI measurements were solely driven by APOE  $\epsilon$ 4 carriers.

## CONCLUSION

Presence of microbleeds relates to poorer microstructural integrity of brain white matter, independent of cardiovascular risk and other markers of CSVD. Our data suggest that microbleeds reflect diffuse brain pathology, even when just a single microbleed is present.

## CLINICAL RELEVANCE/APPLICATION

Microbleeds have emerged as a novel marker of small vessel disease. Our data indicate that the pathology underlying microbleeds is much more widespread than the focal lesions seen on MRI.

## SSG12-05 • Molecular Magnetic Resonance Myeloperoxidase Imaging Is Sensitive to Treatment Effects of Glatiramer Acetate in Murine Multiple Sclerosis

**Benjamin Pulli MD (Presenter) ; Gregory R Wojtkiewicz MSc ; Muhammad Ali MBBS ; Lionel A Bure MD ; John Chen MD, PhD**

\*

## PURPOSE

Treatment effects in multiple sclerosis (MS) are difficult to quantify. We hypothesized, that MPO-Gd (bis-5HT-DTPA-Gd), a molecular MRI probe sensitive and specific for the inflammatory enzyme myeloperoxidase (MPO), can detect therapeutic effects of glatiramer acetate (GA), a current first-line drug in MS, on the molecular level non-invasively.

## METHOD AND MATERIALS

Thirty female SJL mice were induced with experimental autoimmune encephalomyelitis, a mouse model of MS, and treated with either GA (150  $\mu$ g/day) or saline from day 1 post induction onwards. To determine effects of GA on MPO, mice underwent MRI at 4.7T with MPO-Gd at the disease peak (day 12). Lesion numbers and volume were quantified at 60 minutes post MPO-Gd injection. MPO activity assay and flow cytometry of brain leukocytes were also performed.

## RESULTS

Disease severity was ameliorated with GA treatment ( $p < 0.01$ ; **figure, C**). MPO-Gd enhanced MRI detected decreased number of lesions ( $6.0 \pm 0.9$  vs.  $2.4 \pm 0.5$ ,  $p < 0.01$ ), and smaller total ( $669 \pm 198$  vs.  $123 \pm 42$  mm<sup>2</sup>,  $p < 0.05$ ) and mean ( $109 \pm 23$  vs.  $48 \pm 8$ ,  $p < 0.05$ ) lesion volumes with GA compared to saline-treated mice (**A+B**). Brain homogenates of GA-treated mice had  $60 \pm 9\%$  MPO activity compared to saline-treated mice ( $p < 0.05$ ; **D**). Flow cytometry revealed a reduced number of Ly-6C-high inflammatory monocytes in the brain with GA treatment ( $8.1 \pm 1.4$  vs.  $3.9 \pm 0.6 \times 10^4$  cells/brain,  $p < 0.05$ ; **E**). No significant effect of GA on neutrophils could be detected ( $3.9 \pm 0.9$  vs.  $3.0 \pm 0.7 \times 10^4$  cells/brain,  $p = 0.48$ ; **E**). Flow cytometry also revealed that MPO is mostly secreted by Ly-6C high monocytes ( $60 \pm 1.7\%$ ), followed by neutrophils ( $32 \pm 2,3\%$ ; **F**). This reduction in MPO-secreting inflammatory monocytes explains our MRI finding of reduced MPO activity *in vivo*.

## CONCLUSION

GA, a current first-line drug in MS directly affects monocyte subsets, decreasing the number of MPO-secreting inflammatory monocytes entering the brain. MPO-Gd enhanced MRI is sensitive to these effects of GA and provides a novel way to monitor treatment effects at the molecular level in this disease. This could advance our understanding of the molecular events over the course of MS.

## CLINICAL RELEVANCE/APPLICATION

Upon translation, treatment efficacy of GA, which reduces MPO-positive monocytes and thus MPO activity in the brain, could be monitored with MPO-Gd.

## SSG12-06 • Diffusion Variations of Normal-appearing White Matter in Multiple Sclerosis Using Diffusional Kurtosis Imaging

**Lemei Tang MD (Presenter) ; Ni m Fei MA ; Feng Jie MA ; Wei Qiang MA ; Miao Yanwei MD**

## PURPOSE

## METHOD AND MATERIALS

## RESULTS

## CONCLUSION

DKI will detect early the subtle injury before abnormal changes occurs in routine MRI examination in MS patients.

## CLINICAL RELEVANCE/APPLICATION

DKI may be a new sensitive tool to detect NAWM damage in MS patients.

## SSG12-07 • Fast Whole-brain Macromolecular Proton Fraction (MPF) Mapping for Quantitative Imaging of White and Gray Matter Demyelination in Multiple Sclerosis

**Vasily L Yarnykh PhD (Presenter) ; James D Bowen MD ; Alexey A Samsonov PhD ; Pavle Repovic MD ; Kenneth R Maravilla MD \* ; Lily K Junghenson MD ; Angeli Mayadev MD ; Beena Gangadharan PhD ; Hunter R Underhill MD, PhD ; Bart P Keogh MD, PhD**

## PURPOSE

MPF is a key parameter determining the magnetization transfer (MT) effect in MRI. Earlier animal studies suggest that MPF can be used as a potential quantitative biomarker of myelin. A new clinically targeted fast MPF mapping method based on single MT-weighted acquisition was recently published. Our purpose was to investigate clinical relevance of MPF changes measured by this method in multiple sclerosis (MS).

## METHOD AND MATERIALS

Images were acquired on a 3T MRI scanner from 14 healthy controls (HC), 19 relapsing-remitting (RRMS), and 11 secondary progressive (SPMS) MS patients. Neurological status was reported as Expanded Disability Status Scale (EDSS) and Multiple Sclerosis Functional Composite (MSFC). MPF mapping protocol comprised gradient-echo sequences with and without off-resonance saturation (offset frequency 4 kHz), 3-point variable flip angle T<sub>1</sub> mapping, and fast B<sub>0</sub> and B<sub>1</sub> mapping sequences. Whole-brain 3D MPF maps were obtained with  $1.5 \times 1.5 \times 4 \text{ mm}^3$  resolution and 15 min acquisition time. Brain tissues were segmented into normal appearing white matter (NAWM), gray matter (NAGM), and lesions. Mean MPF in tissues were compared between subject groups by independent two-tailed t-test. Pearson correlation coefficient ( $r$ ) was used to test associations between MPF and clinical scales.

## RESULTS

MS patients had significantly reduced ( $Pr = -0.70$  for EDSS,  $r = 0.81$  for MSFC,  $Pr = -0.56$ ,  $Pr = 0.72$ ,  $Pr = -0.42$ ,  $Pr = 0.50$ ,  $Pr = 0.42$ ,  $Pr = -0.57$ ,  $P$

#### CONCLUSION

MPF mapping allows quantitative assessment of microscopic demyelination in both NAWM and NAGM. NAWM and NAGM MPF abnormalities appear more clinically relevant than lesion pathology. Our results suggest a critical role of NAGM demyelination for disability progression in MS.

#### CLINICAL RELEVANCE/APPLICATION

Fast whole-brain MPF mapping detects demyelination in both white and gray matter and provides a promising approach for quantitative monitoring of myelin damage and repair in MS clinical studies.

### **SSG12-08 • Extra Cranial Venous Abnormality in MS Patients with Regard to Chronic Cerebrovascular Venous Insufficiency (CCSVI): A True Pathological Finding or an Anatomical Variant?**

**Satya N Patro MD (Presenter) ; Carlos H Torres MD ; Cheemun Lum MD ; Santanu Chakraborty FRCR ; Thanh Nguyen MD \* ; Miguel Bussiere ; Matthew Hogan MD**

#### PURPOSE

To evaluate the extra cranial venous anatomy with contrast enhanced MR Venogram (CE-MRV) in patients without MS. To assess the prevalence of various venous anomalies such as asymmetry and stenosis in this population.

#### METHOD AND MATERIALS

The study was approved by our local REB and all participants gave informed consent. We recruited 100 patients without MS referred for a contrast enhanced MRI, who underwent additional CEMRV from the skull base to the mediastinum on a 3T scanner. The study started in Feb 2012 and completed in Jul 2010. We included patients between 18 and 60 years old with a male: female ratio of 1:1. Exclusion criteria included prior neck radiation, neck surgery, neck or mediastinal masses or significant cardiac or pulmonary disease. Two neuroradiologists independently evaluated the studies to document the presence of asymmetry and stenosis in the jugular, vertebral and azygous veins.

#### RESULTS

Asymmetry of the IJVs was found in 70% of patients. 91% of patients had a focal stenosis in the right IJV and 82% in the left IJV. The stenoses were found in the upper third of the vein in 95% of the cases. Stenosis of the azygous vein was found in 21% of patients. There was prominence of the external jugular veins in 39% of cases, of the anterior jugular veins in 27% and of the deep cervical veins in 22.4%.

#### CONCLUSION

The venous anatomy of non MS patients demonstrates multiple variants including asymmetry and stenoses of the IJVs. We believe the stenoses in the upper third of the IJVs are secondary to indentation of the vessel between the posterior belly of the digastric muscle and the occipital bone. This study will be used as a comparative data to the MS population.

#### CLINICAL RELEVANCE/APPLICATION

It is recommended to keep in mind the various normal variants of extra cranial venous system while evaluating MS patients with suspected CCSVI.

### **SSG12-09 • Quantitative Rapid Assessment of Leukoaraiosis: Fully Automated CT-based Quantification of Microangiopathic Density Reduction in White Matter in Comparison to Gold Standard MRI**

**Uta Hanning (Presenter) ; Georg Homann ; Ludger Feyen ; Thomas Niederstadt MD ; Volker Hesselmann MD ; Walter L Heindel MD ; Andre Kemmling MD**

#### PURPOSE

Assessment of white matter lesions is primarily a domain of magnetic resonance imaging (MRI), however, computed tomography (CT) is the more frequently used diagnostic procedure. Particularly in stroke, a rapid objective CT based quantification of microangiopathic WM changes may prove useful to estimate risk of thrombolytic hemorrhage. We present a new CT-based fully automated rater-independent method for quantification of microangiopathic white matter changes.

#### METHOD AND MATERIALS

Tissue segmentation was performed in 600 normal brains MRI (3.0 Tesla, T1-3D-Turbo-Field-Echo) of two large population studies (BiDirect and SEARCH-Health Study) to obtain a probabilistic WM-tissue-map in standard MNI-152 space as published. A total of 103 patients with varying degree of leukoaraiosis excluding other lesions were retrospectively selected based on availability of CT and MR within 1 month. The tissue-specific density (Hounsfield Unit, HU) within WM-space was determined by the mean of all voxel densities weighted by WM content:  $S(HU_{xyz} \times P_{xyz}(WM)) / S(P_{xyz}(WM))$ ; ( $HU_{xyz}$  = density of voxel $_{xyz}$ ;  $P_{xyz}$  = partial WM content at voxel $_{xyz}$ ). The reduction of HU over WM-space in CT images was correlated with gold standard MR-based WM lesion volume measurements. Results were compared with rater-based Fazekas scores for severity of WM disease.

#### RESULTS

The process of CT-based tissue-specific segmentation involving automated segmentation of probabilistic white matter space with quantification of WM density was reliable in 103 cases with no algorithm failures. Mean time of processing was 153 second. In comparison with MRI FLAIR-based WM-lesion volume, the CT-based HU-weighted reduction of the white matter density showed a significant correlation coefficient (0.87). Spearman rank correlations between MR or CT based WM lesion quantification did not differ significantly in comparison to visual Fazekas scores, respectively.

#### CONCLUSION

The presented method allows fully automated observer-independent quantification of microangiopathic HU-induced reduction of the white matter in CT with high correlation to gold standard MRI.

#### CLINICAL RELEVANCE/APPLICATION

The algorithm targets the need for a rapid objective CT based assessment of WM lesion load which may be used as a risk score of hemorrhage in the setting of thrombolytic stroke therapy.

## **Physics (Quantitative Imaging I)**

**Tuesday, 10:30 AM - 12:00 PM • S403A**

**PH** **CT** **BQ**

[Back to Top](#)

**SSG13 • AMA PRA Category 1 Credit™:1.5**

**Moderator**

**Robert M Nishikawa**, PhD \*

**Moderator**

**Marc Kachelriess**, PhD

**SSG13-01 • Characterization of Carotid Atherosclerotic Plaque Components Based on Quantitative Phase-contrast Hounsfield Units**

**Tobias Saam MD (Presenter) \* ; Marian Willner ; Sandra Fill ; Julia Herzen ; Ulrich Schueller ; Holger Hetterich MD ; Alexander C Hipp ; Maximilian F Reiser MD ; Franz Pfeiffer ; Fabian Bamberg MD, MPH \***

## PURPOSE

Conventional CT can distinguish between soft, mixed and calcified plaques but has difficulties to further differentiate soft plaques due to an overlap in Hounsfield units (HU) of fibrous and lipid tissue. Phase-contrast imaging is a novel X-ray based imaging technique that relies on the X-ray phase-shift rather than its absorption, yielding a higher contrast in biological soft tissue. The purpose of our study was to evaluate whether plaque components can be differentiated based on their phase-contrast HU (HU-P), which can be calculated in analogy to absorption-contrast HU.

## METHOD AND MATERIALS

Four ex-vivo human carotid arteries were imaged at a laboratory-based set-up using a conventional X-ray tube (35kV) and grating-interferometer. Tomographic images were reconstructed with an effective pixel size of 100  $\mu$ m and correlated with histopathology sections. Regions corresponding to fibrous, lipid or calcified tissue based on histopathology were manually traced. Mean HU-P were calculated for all analyzed regions.

## RESULTS

A total number of 80 cross-sections with 72 fibrous, 19 lipid and 24 calcified tissue containing regions were assessed. Fibrous, lipid and calcified tissues were associated with significant different mean HU-P ( $52.6 \pm 7.0$ ,  $21.0 \pm 9.8$  and  $371.5 \pm 158.0$ , p no overlap of HU-P between fibrous (range 44.9  $\diamond$  63.3) and lipid tissue (3.1-30.1). Similarly, no overlap of HU-P was observed between calcified tissue (range 174.4  $\diamond$  593.7) and the other tissue components. Figure 1 demonstrates axial phase contrast CT images (A) and corresponding histology sections (B, C, Fib=fibrous, Lip=lipid and Cal=calcified tissue; length of the scale bar = 2 mm).

## CONCLUSION

In an ex-vivo experimental set-up grating-based phase contrast CT can reliably differentiate between calcified, fibrous and fatty tissue based on quantitative HU-P, indicating its high potential for improved assessment of carotid atherosclerotic disease.

## CLINICAL RELEVANCE/APPLICATION

Phase-contrast computed tomography might improve characterization of carotid atherosclerotic plaque morphology compared to conventional absorption CT.

## SSG13-02 • Quantitative Image Analysis of MRI for Treatment Response Assessment of Multiple Myeloma

**Chuan Zhou** PhD (Presenter) ; **Qian Dong** MD ; **Daniel R Couriel** ; **Heang-Ping Chan** PhD ; **Lubomir M Hadjiiski** PhD ; **Jun Wei** PhD

## PURPOSE

It is challenging for radiologists to visualize early changes in multiple myeloma (MM) within 3-6 months after autologous bone marrow transplant (BMT) due to small amount of marrow infiltration evident on MR images. This pilot study investigated the feasibility of using quantitative image analysis to evaluate early changes of BM in MRI for assessing treatment response.

## METHOD AND MATERIALS

With IRB approval, 29 cases with MM requiring BMT were evaluated retrospectively. 31 pairs of spine MRI scans performed pre- and post-BMT (3-6 months), including 2 patients underwent second BMT after 4 and 6 months of the first BMT, respectively, were collected. The vertebral body volumes in sagittal views of T1-weighted sequence were manually outlined and their adjacent disc volumes were automatically extracted using morphological operations. A 3D dynamic intensity energy transformation (DIET) method was developed to characterize BM infiltration after BMT. DIET transformed the voxel intensity of a vertebral body to an energy enhancement value (EEV), defined as the ratio of the intensity entropy at the voxel to the median intensity entropy in the adjacent discs. Treatment response was quantified by an EEV response index (EEV-RI) calculated as the percentage of vertebrae with an increase in the mean EEV over the vertebral body in the post-BMT scan. In addition, the EEV heat map accentuated the intensity distribution pattern of the vertebral body and facilitated radiologist's visual assessment of the pre-to-post changes of BM infiltration.

## RESULTS

Of the 31 follow up MRI scans, 25 were clinically diagnosed as good responders to BMT. The DIET method correctly identified 22 good responders using a decision threshold of  $> 40\%$  for the EEV-RI. The agreement reached  $0.903 \pm 0.14$  with a kappa value of 0.74. The mean EEV increased by an average of  $35.4 \pm 36.7\%$  for the 22 good responders and decreased by  $14.6 \pm 10.0\%$  for the 6 non-responders. The mean EEV decreased by  $19.0 \pm 20.5\%$  for the 3 cases that were mistakenly identified as no response.

## CONCLUSION

The substantial agreement between computer and clinical outcomes demonstrated the feasibility of using the quantitative image metric (EEV) for assessing treatment response for MM.

## CLINICAL RELEVANCE/APPLICATION

Quantitative image-based biomarker may improve the accuracy and efficacy for staging and assessing treatment response for MM, allowing clinicians to optimize therapy of individual patients.

## SSG13-03 • Use of a Dedicated Extremity Cone-beam CT Scanner for Evaluation of the Weight-bearing and Non-weight-Bearing Knee

**Gaurav K Thawait** MD (Presenter) ; **Abdullah Muhit** PhD ; **Wojciech Zbijewski** PhD \* ; **Joseph W Stayman** PhD \* ; **John Yorkston** PhD \* ; **Shadpour Demehri** MD ; **John A Carrino** MD, MPH \* ; **Jeffrey H Siewerdsen** PhD \*

## PURPOSE

To prospectively compare cone-beam CT (CBCT) examination of the knee in sitting (non-weight-bearing, NWB) position versus upright (weight-bearing, WB) position as a potential indicator of osteoarthritis (OA).

## METHOD AND MATERIALS

A prototype CBCT scanner dedicated to extremity imaging was previously reported and assessed in terms of spatial resolution, contrast resolution, radiation dose, and optimal imaging protocols. An IRB approved study was performed in which 13 patients (8 females, 5 males; 31-78 yo, mean 56 yo) were prospectively enrolled for CBCT exams in NWB and WB positions using the prototype scanner. 11 were previously diagnosed with knee OA. 2 musculoskeletal radiologists measured the medial tibiofemoral (TF) joint space width and meniscal protrusion (MP) in coronal plane in consensus. Differences in such morphology were analyzed between NWB and WB images using paired Wilcoxon signed-rank test.

## RESULTS

The scanner exhibited spatial resolution of  $\sim 15$ -17 lp/cm, depending on reconstruction technique, with high-contrast bone detail judged comparable or superior to conventional CT. Optimal scan protocol was 80 kVp, 120 mAs, imparting 9.0 mGy (dose at the center of a CTDI phantom). Isotropic sub-mm spatial resolution facilitated precise measurement of joint space morphology. For the 2 non-OA patients, the change in joint space between NWB vs WB exams appeared minor (2.67 mm vs 2.41 mm, respectively), and there was no evidence of meniscal protrusion. A greater difference in medial TF joint space was observed in OA patients:  $1.91 \pm 0.85$  mm for the NWB setup versus  $1.23 \pm 0.8$  mm for the WB setup, and the results were statistically significant ( $p=0.003$ ). 4 of the OA patients exhibited no MP, 4 exhibited MP in both the NWB and WB exams, and 3 exhibited MP only in the WB exam ( $MP_{NWB} = 2.09 \pm 2.26$  mm,  $MP_{WB} = 5.16 \pm 1.46$  mm,  $p=0.016$ ).

#### CONCLUSION

The TF joint space width and MP in OA patients was found to change significantly in sitting (NWB) versus upright (WB) exams. The ability to conduct NWB and WB exams in CBCT with a favorable dose profile and image quality sufficient for such morphological analysis could provide a valuable tool for OA diagnosis and treatment assessment.

#### CLINICAL RELEVANCE/APPLICATION

Weight-bearing CBCT of the knee can provide functional information and precise morphological analysis in cross sectional imaging not achieved by projection radiographs.

### **SSG13-04 • Comparison of Estimation of Patient Size Specific Dose Estimates (SSDE) Using Attenuation-based Estimation of Patient Size versus Geometrical Diameter for CT Examination of Thorax**

**Shima Aran MD (Presenter) ; Laleh Daftaribesheli MD ; Bob Liu PhD ; Hani H Abujudeh MD, MBA \***

#### PURPOSE

The attenuation-based estimation of patient size and geometrical diameters are 2 methods introduced for the purpose of converting displayed CTDI volume to patient Size Specific Dose Estimates (SSDE). We assessed feasibility of applying the AAPM TG 204 for estimating patient SSDE using water equivalent diameter (Dw) and anteroposterior (DAP), lateral (DL), Sum (DSum= DAP +DL) and effective (DEff) diameters for chest CT.

#### METHOD AND MATERIALS

In an IRB-approved study, we evaluated 100 consecutive adult chest CT exams (M:F 60:40, mean age 61.5±12.8 years). Patients were classified into 2 groups of

#### RESULTS

Complete skin to skin measurements were possible in 6% the patients. Geometrical diameters (DLat, DSum and DEff) were significantly different and larger compared with Dw except for DAP (p0.92). However, SSDE values were significantly lower (p

#### CONCLUSION

The attenuation values measured from axial CT can be feasibly used to estimate SSDE. These values are significantly larger compared with Geometrical diameters derived SSDE for chest CT. The lack of specific levels of measurement (along the z axis) of attenuation or geometrical diameters has profound effect on SSDE variability.

#### CLINICAL RELEVANCE/APPLICATION

SSDE estimations are different using attenuation-based vs. geometrical diameters for chest CT. An optimal level of measurements should be defined for best use of SSDE estimations from CTDIvol.

### **SSG13-05 • Evaluating Proximal Femur Bone Strength Prediction by Advanced Characterization of Trabecular Microarchitecture Using Scaling Index Computation and Support Vector Regression**

**Chien-Chun Yang (Presenter) ; Mahesh Nagarajan ; Markus B Huber PhD ; Felix Eckstein MD \* ; Thomas M Link MD, PhD \* ; Axel Wismueller MD, PhD ; Julio Carballido-Gamio PhD ; Thomas Baum MD ; Sharmila Majumdar PhD \* ; Jan S Bauer MD ; Eva-Maria Lochmueller MD**

#### PURPOSE

Biomechanical bone strength prediction in proximal femur is important for osteoporosis diagnosis and fracture risk estimation. Our study proposes using advanced geometrical scaling index bone structure characterization in combination with statistical bone mineral density (BMD) features extracted from multi-detector computed tomography (MDCT) images of proximal femur specimens, with subsequent prediction of bone strength through support vector regression (SVR). The performance of this system is compared with a standard approach that uses mean BMD and multi-regression models.

#### METHOD AND MATERIALS

Axial MDCT images were acquired from 146 proximal femur specimens using a 16-row scanner and a calibration phantom. Adaptive spherical volumes of interest (VOI) were positioned in the femoral head (Huber et al., Radiology 2008) for BMD conversion and image analysis. VOIs of these BMD images were characterized through statistical moments as well as advanced geometrical features extracted with the Scaling Index Method (SIM) (Huber et al., IEEE-TBME 2011). The specimens were then biomechanically tested through a lateral fall on the greater trochanter, and failure load was recorded. All features were analyzed by multi-regression and SVR for predicting bone strength. The performance for different combinations of feature groups was compared using root-mean-square error (RMSE) and coefficient of determination ( $R^2$ ). A Wilcoxon signed-rank test was used to compare two RMSE distributions and test for statistically significant differences in performance.

#### RESULTS

Combination of SIM features and mean BMD, when used in conjunction with SVR, exhibited the best prediction performance (RMSE =  $0.95 \pm 0.13$ ;  $R^2 = 0.62$ ). This was significantly better than the standard approach of using BMD and multi-regression (RMSE =  $1.11 \pm 0.141$ ;  $R^2 = 0.490$ ).

#### CONCLUSION

Our results show that the performance of predicting biomechanical strength in proximal femurs can be significantly improved by including SIM-derived geometrical features in addition to mean BMD, and through the use of support vector regression.

#### CLINICAL RELEVANCE/APPLICATION

Complementing BMD characterization on MDCT images with advanced geometrical features and machine learning can contribute to improved osteoporosis diagnosis and disease progression monitoring.

### **SSG13-06 • A New Method for Automated Anatomic Landmark Detection to Aid Automated Patient-specific Radiation Dosimetry in Tube-current Modulated CT Scans**

**Tim O'Connell MD, MEng (Presenter) \* ; Maryam Khatonabadi \* ; Michael F McNitt-Gray PhD \* ; Aaron D Sodickson MD, PhD**

#### PURPOSE

To develop an automated method of body part determination and body landmark detection for the purpose of characterizing regional variations in X-ray tube output and enabling regional radiation dose estimation.

#### METHOD AND MATERIALS

Software was created that extracts the image data from CT scans, detects the body contours, and performs thresholding to determine image tissue characteristics. The software then performs analysis on the tissue-specific attenuation curves along the Z-axis to determine body part scanned and anatomic landmarks. If the images are from a chest CT, the software computes the position (image number) of the lung apices, and the start of the right and left hemidiaphragms. If the images are from an abdomen/pelvis CT, the software computes the position of the start of the right and left hemidiaphragms, and the position of the iliac crests. Transaxial images from 100 CT scans (50 chest, 50 abdomen/pelvis) were retrieved from PACS for automated body part determination and landmark detection. These scans were also evaluated by a radiologist and the position of the relevant landmarks was recorded manually for comparison with the computed values.

#### RESULTS

100% of scans were correctly identified as being either chest (50/50) or abdomen/pelvis (50/50). In the chest CT group, there was no significant difference between the measured and computed location of the lung apices, right, and left diaphragm (t-test p = 0.42, 0.93, and 0.19 respectively); the mean difference between measured and computed position of the lung apices was 0.14 +/- 1.02cm, the right diaphragm was 0.05 +/- 2.60cm and the left diaphragm was 0.40 +/- 2.06cm. In the abdomen/pelvis CT group, there was no significant difference between the measured and computed location of the right diaphragm (p = 0.051) or the iliac crests (p = 0.19), but there was

a significant difference in left diaphragm detection ( $p = 0.03$ ). In this group, the mean difference between measured and computed position of the right diaphragm was  $-0.13 \pm 0.51\text{cm}$ , the left diaphragm was  $-0.24 \pm 0.62\text{cm}$ , and the iliac crests were  $-0.06 \pm 0.98\text{cm}$ .

#### CONCLUSION

This study demonstrates a new method of body part determination and body landmark detection that has high reliability and can provide crucial information needed for automated CT radiation dosimetry calculations.

#### CLINICAL RELEVANCE/APPLICATION

Relevant for improving radiation dosimetry through automated image analysis.

### SSG13-07 • Fully-automated Segmentation of Cartilage from the MR Images of Knee Using a Multi-atlas and Local Structural Analysis Method

**June-Goo Lee** PhD (Presenter) ; **Serter Gumus** MD ; **Chan Hong Moon** PhD ; **Cheng Tao** MD ; **Sonu K Bae** ; **Kyongtae T Bae** MD, PhD \*

#### PURPOSE

To develop a fully-automated method to segment cartilage from the magnetic resonance (MR) images of knee and to evaluate the performance of the method on a public open dataset.

#### METHOD AND MATERIALS

For the development and testing of a fully-automated program for cartilage segmentation, we used 100 cases of knee MR images from a public open dataset (available at [www.ski10.org](http://www.ski10.org)). MR images were acquired in the sagittal plane with gradient-echo T1-weighting sequence and fat suppression at  $0.4 \times 0.4\text{mm}$  in-plane and  $1\text{mm}$  slice-thickness resolution. The dataset also includes the segmentation result by experts to label and delineate the bone and cartilage of the femur and tibia. We randomly divided the 100 cases into the training set (60 cases) and the test set (40 cases).

The segmentation process was carried out in two steps, atlas-building and local-adjustment. In the atlas-building step, all training cases were registered to a test case via a non-rigid registration scheme. The final metric values from each registration were recorded for sorting. Nine best matched results were selected and merged to generate the atlas-based segmentation mask by majority voting. In the local-adjustment step, the statistical information of bone, cartilage and surrounding regions was computed from the atlas-based segmentation result. This information was used to determine seed points for a graph-cut algorithm to segment bone regions. Structurally similar points from the registered multiple atlases were identified via a Hessian analysis. Finally, a locally-weighted voting process was applied for a local adjustment. The performance of the segmentation program was evaluated in terms of dice similarity coefficient (DSC), sensitivity and specificity of segmented femoral and tibial cartilages against the reference cartilage segmentation of the test cases from the dataset.

#### RESULTS

The cartilages were segmented successfully in all test cases. The DSC was  $0.67 \pm 0.07$  for femoral and  $0.53 \pm 0.08$  for tibial cartilage. The segmentation performance was according to (sensitivity, specificity): ( $57.5 \pm 9.6\%$ ,  $99.9 \pm 0.04\%$ ) for femoral and ( $53.0 \pm 8.4\%$ ,  $99.9 \pm 0.02\%$ ) for tibial cartilage.

#### CONCLUSION

We have developed a fully-automated segmentation program for knee cartilage from MR images. The performance of the program on 40 test cases was highly promising.

#### CLINICAL RELEVANCE/APPLICATION

The fully-automated segmentation method will facilitate the quantification of cartilage.

### SSG13-08 • Iodine-density Analysis Using Spectral CT Imaging in Differentiating Benign and Malignant Serous Cavity Effusion

**Ye Ju** (Presenter) ; **Ailian Liu** MD ; **He Qing Wang** MSc ; **Yijun Liu** ; **Renwang Pu** MBBCh, FRCPC ; **Wenjun Cui**

#### PURPOSE

To assess the value of quantitatively iodine concentration measurement of enhanced spectral CT imaging in the differential diagnosis of malignant and benign serous cavity effusion.

#### METHOD AND MATERIALS

Approval for this retrospective HIPAA compliant study was obtained from the institutional review board, and informed consent was waived. From August 2012 to February 2013, totally 45 patients, including 13 cases of benign serous effusion and 32 cases of malignant serous effusion proven by histopathological diagnosis or laboratorial examination, underwent plain and three-phase enhanced spectral CT imaging through fast kVp-switching technique. 140 kVp polychromatic images and iodine-based material density images were reconstructed. The mean CT value (M-CT) was measured at plain and three-phase enhanced 140 kVp images, and the difference of CT values (D-CT) was calculated. The iodine concentration (M-I) was also quantitatively measured at iodine-based material density images and the difference (D-I) was calculated. The difference of these parameters was evaluated statistically by independent-samples t test.

#### RESULTS

#### CONCLUSION

The nature of the serous cavity effusion was difficult to be identified only by the CT values on conventional enhancement scanning. The iodine-density images of spectral CT imaging at venous phase and delayed phase play an important role in identifying malignant and benign effusion.

#### CLINICAL RELEVANCE/APPLICATION

The iodine-density images of enhanced spectral CT scanning provides a sensitive approach for identifying benign and malignant serous cavity effusion.

### SSG13-09 • Quantitative Measures of Normal Lung Texture Change during Respiration: Analysis of Variation Using 4-dimensional CT

**Shane P Krafft** MS, BS (Presenter)

#### PURPOSE

While image quality is often considered the main barrier to achieving valid, reproducible quantitative image biomarkers, anatomic motion during CT acquisition presents another unique challenge. The implementation of 4-dimensional CT allows us to reconstruct the lung volume at equally spaced phases of the breathing cycle and, as a result, we can estimate the impact of anatomic variability on quantitative analysis of lung parenchyma. The purpose of this study was to demonstrate the variation of lung texture features with the phase of the respiratory cycle.

#### METHOD AND MATERIALS

4DCT scans were acquired for 10 patients with non-small-cell lung cancer prior to radiotherapy. Normal lung volumes were segmented with a semi-automatic 3D region-growing algorithm on each of the 10 binned phase reconstructions (0-90%). The original 12-bit CT images were reduced to a bit depth of 8 and gray-level co-occurrence and run length matrices were used to extract 17 non-directional 2D texture features from the segmented total lung volume. The extracted features were evaluated for phase dependence relative to the end exhalation phase (50%). For each patient, Spearman's rank correlation ( $R_s$ ) was used to determine the relationship between feature and the calculated lung volume from each phase image set.

## RESULTS

Within an individual 4DCT scan, change in texture relative to the end exhale phase varied up to 75.3%. Over the entire patient population, 8 of the 17 metrics showed an average change due to respiratory phase of less than 5%; however, the range of measured changes was 0.9-31.2% over all of the considered texture features. 5 of 17 features were highly correlated ( $|R_s| > 0.7$ ) to lung volume.

## CONCLUSION

Using 4DCT the phase dependence of texture measures was demonstrated. While some of the extracted texture features may be reasonably independent of respiratory phase, large differences were observed for others. The correlation of features to the lung volume highlights the periodic phase dependence of some of the considered texture metrics.

## CLINICAL RELEVANCE/APPLICATION

As the respiratory phase influences extracted texture measures of lung parenchyma, anatomic variability must be considered in attempts to standardize quantitative imaging biomarkers.

## Gastrointestinal: Tumor Response Assessment

Tuesday, 04:30 PM - 06:00 PM • E350

[OI](#) [MR](#) [BQ](#) [GI](#)

[Back to Top](#)

**RC409** • AMA PRA Category 1 Credit™:1.5 • ARRT Category A+ Credit:1.5

### RC409A • RECIST and Other Criteria

**Vahid Yaghmai MD** (Presenter)

#### LEARNING OBJECTIVES

1) To review the concepts behind development of anatomic imaging biomarkers. 2) To learn the strengths and weaknesses of RECIST and other anatomic imaging biomarkers. 3) New criteria for evaluation of gastrointestinal tumor response assessment.

#### ABSTRACT

Improvements in imaging technology and therapeutic options for the management of gastrointestinal tumors have revolutionized the way tumor response to therapy is assessed. Cytotoxic therapies result in tumor shrinkage and their efficacy is commonly assessed by evaluating tumor size based on strict guidelines such as the Response Evaluation Criteria in Solid Tumors (RECIST). This review will familiarize radiologists with the steps that have led to the development and modifications of the RECIST. New cytostatic and locoregional therapies may not change tumor size and have exposed many weaknesses of the RECIST. As a result, tumor and therapy specific response assessment criteria have been developed. These new criteria, including Choi, EASL, mRECIST and irRC will also be discussed.

### RC409B • CT and MR Perfusion Imaging

**Dushyant V Sahani MD** (Presenter)

#### LEARNING OBJECTIVES

1) Understand newer concepts in oncology including tumor angiogenesis and the evolving role of imaging biomarkers in drug trials. 2) Discuss the basic principles of CT-MR perfusion and limitations of each method. 3) Develop basic knowledge and skills for acquisition and interpretation of perfusion imaging in the abdomen and pelvis. 4) Assess the potential of perfusion imaging in the oncology trials and in non-oncologic clinical settings.

### RC409C • Diffusion-Weighted Imaging

**Ihab R Kamel MD, PhD** (Presenter) \*

#### LEARNING OBJECTIVES

1) Discuss the basic concepts for DWI in body applications. 2) Describe the emerging role of DWI in assessing response in cancer. 3) Discuss the application of DWI in whole body imaging.

#### ABSTRACT

Diffusion-weighted magnetic resonance imaging (DWI) can provide functional information at a cellular level by measuring water diffusion values. DWI is sensitive to changes in the micro diffusion of water and the apparent diffusion coefficient (ADC) is an indicator of the movement of water within the tissue. In abdominal oncology, DWI has been successfully used in assessing treatment response of liver tumors. In addition, ADC values have been shown to predict tumor response to treatment. In some instances low tumor ADC before treatment can be predictive of better outcome. Assessing response of in the entire tumor volume may be more valuable than a single ROI measurement. Moreover, multiparametric response maps that include changes in both ADC and enhancement after therapy are more predictive of response and patient survival compared to ADC or enhancement alone. We will review the different response criteria for various liver tumors treated with intra arterial therapy. New application of DWI including whole body applications will also be discussed.

### RC409D • PET-MR-What Do We Know in 2013

**Raj M Paspulati MD** (Presenter)

#### LEARNING OBJECTIVES

1) To understand the PET-MR technology, types of current PET-MR scanners and challenges. 2) To understand the clinical application, comparison with PET-CT, protocols and optimizing work flow. 3) To understand the pitfalls, artifacts and future of PET-MR.

#### ABSTRACT

Introduction of PET-CT had substantial influence on cancer staging and has become a standard practice of care in certain types of cancer staging, restaging and document tumor response to treatment. The low soft tissue contrast of the CT, especially the low dose non contrast CT is the main limitation of hybrid PET-CT imaging. MR imaging proved to be superior to even contrast enhanced CT certain anatomical regions such as pelvis, head and neck due to its excellent soft tissue contrast resolution. There has been a quest for combined PET ;MRI system to provide anatomical, physiological and molecular information with single integrated imaging. The main hurdle has been the sensitivity of PET photomultiplier tubes to magnetic field. This is overcome and integrated PET-MR systems are now available for clinical practice. There are currently two types of integrated PET-MR systems available from two different vendors. In the sequential type the photomultiplier tubes of PET are shielded from magnetic field by separating the PET and MR gantries. In the simultaneous type Photomultiplier tubes and MR coils are integrated in one system by using magnetically insensitive avalanche photo diodes. Both these systems have some advantages and disadvantages, but have common challenges. MR attenuation correction is the major challenge faced by both type of systems. World wide, there is limited literature available on the utility and clinical application of the PET-MR system. There has been lot of enthusiasm as well as anxiety in incorporating this integrated system into clinical practice by radiologists as well as physicians involved in managing cancer patients. This refresher course addresses these issues of clinical PET ;MR system, key areas where they have impact on patient care and management. At the end of the course the attendees of the course will be familiar with current types of PET-MR systems, clinical applications in oncology, advantages, limitations, pit falls and challenges.

## Quantitative CT and MR Perfusion Imaging

Tuesday, 04:30 PM - 06:00 PM • S504CD

**RC417** • AMA PRA Category 1 Credit™:1.5 • ARRT Category A+ Credit:1.5**Moderator****Sandip Biswal**, MD \***LEARNING OBJECTIVES**

1) To understand the principles of CT perfusion analysis for tumor assessment. 2) To understand the pathophysiological basis of CT perfusion parameters for tumors. 3) To understand unique CT perfusion analysis of the liver due to its characteristic dual blood supply. 4) To describe the potential clinical applications, with a focus on hepatic and extrahepatic applications and clinical trials. 5) To discuss several recent challenging issues regarding CT perfusion. 6) To discuss areas for further development including assessment of tumor heterogeneity.

**ABSTRACT**

With the emergence of novel targeted therapies for cancer, imaging techniques that assess tumor vascular support have gained credence for response assessment alongside standard response criteria. CT perfusion techniques that quantify regional tumour blood flow, blood volume, flow-extraction product, and permeability-surface area product through standard kinetic models, are attractive in this scenario by providing evidence of a vascular response or non-response. Additionally, these techniques may provide prognostic and predictive information to the clinician. Their increasing acceptance in oncological practice in recent years has been related to the combination of clinical need and technological improvements in CT, including faster tube rotation speeds, higher temporal sampling rates, the development of dynamic 3D acquisitions and development of commercial software programmes embedded within the clinical workflow. Recently published consensus guidelines provide a way forward to performing studies in a more standardized manner. To date single centre studies have provided evidence of clinical utility. Future studies that include good quality prospective validation correlating perfusion CT to outcome endpoints in the trial setting are now needed to take CT perfusion forward as a biomarker in oncology. These presentations will cover the principles of CT perfusion analysis for tumor assessment and its pathophysiological basis. Clinical applications will be discussed focusing on hepatic and extrahepatic applications and clinical trials. Areas for further development including assessment of tumor heterogeneity will also be discussed.

**RC417A • CT Perfusion in Oncology: Hepatic Imaging****Se Hyung Kim** (Presenter)**LEARNING OBJECTIVES**

1) To understand unique CT perfusion analysis of the liver due to its characteristic dual blood supply. 2) To describe the potential clinical applications, with a focus on hepatic applications. 3) To discuss several recent challenging issues regarding CT perfusion.

**RC417B • CT Perfusion in Oncology: Extrahepatic Imaging****Vicky J Goh** MBBCh (Presenter) \***LEARNING OBJECTIVES**

1) To understand the principles of CT perfusion analysis for tumor assessment. 2) To understand the pathophysiological basis of CT perfusion parameters for tumors. 3) To describe the potential clinical applications, with a focus on extrahepatic applications and clinical trials. 4) To discuss areas for further development including assessment of tumor heterogeneity.

**ABSTRACT**

With the emergence of novel targeted therapies for cancer, imaging techniques that assess tumor vascular support have gained credence for response assessment alongside standard response criteria. CT perfusion techniques that quantify regional tumour blood flow, blood volume, flow-extraction product, and permeability-surface area product through standard kinetic models, are attractive in this scenario by providing evidence of a vascular response or non-response. Additionally, these techniques may provide prognostic and predictive information to the clinician. Their increasing acceptance in oncological practice in recent years has been related to the combination of clinical need and technological improvements in CT, including faster tube rotation speeds, higher temporal sampling rates, the development of dynamic 3D acquisitions and development of commercial software programmes embedded within the clinical workflow. Recently published consensus guidelines provide a way forward to performing studies in a more standardized manner. To date single centre studies have provided evidence of clinical utility. Future studies that include good quality prospective validation correlating perfusion CT to outcome endpoints in the trial setting are now needed to take CT perfusion forward as a biomarker in oncology. This presentation will cover the principles of CT perfusion analysis for tumor assessment and its pathophysiological basis. Clinical applications will be discussed focusing on extrahepatic applications and clinical trials. Areas for further development including assessment of tumor heterogeneity will also be discussed.

**RC417C • Technical Considerations for Perfusion Imaging: CTP, DSC, and ASL****Roland Bammer** PhD (Presenter) \***LEARNING OBJECTIVES**

1) Understand the key technical principles of Dynamic Susceptibility Contrast, Arterial Spin Label, and CT Perfusion Imaging. 2) Know the basic MR pulse sequences and CT acquisition schemes for perfusion imaging. 3) Appreciate the strengths and weaknesses between CT and MR Perfusion imaging methods. 4) Understand the Central Volume Principle, Diffusible Tracer, and Deconvolution Methods.

**RC417D • Quantitative MR Perfusion Imaging of the Brain****Greg Zaharchuk** MD, PhD (Presenter) \***LEARNING OBJECTIVES**

1) Understand the difference between quantitative and qualitative perfusion measurements. 2) Distinguish several approaches for obtaining quantitative perfusion maps in the brain. 3) Appreciate the strengths and weaknesses between the two major techniques, arterial spin labeling and bolus contrast dynamic susceptibility imaging.

**Quantitative Imaging: Dynamic Contrast Enhanced MRI (DCE-MRI)****Tuesday, 04:30 PM - 06:00 PM • S404AB****RC425** • AMA PRA Category 1 Credit™:1.5 • ARRT Category A+ Credit:1.5**Director****Michael F McNitt-Gray**, PhD \***RC425A • The Physical Principles and Challenges of Dynamic Contrast Enhanced MRI Applications****Edward F Jackson** PhD (Presenter)**LEARNING OBJECTIVES**

1) Understand selected applications of quantitative MR imaging biomarkers, particularly DCE-MRI applications. 2) Understand the factors

that currently limit widespread acceptance and use of such quantitative MR imaging biomarkers, including sources of bias and variance. 3) Understand some of the current initiatives focused on the standardization, qualification, and validation of selected quantitative MR imaging biomarkers.

#### ABSTRACT

Clinical and clinical research applications of quantitative anatomical and functional MR imaging biomarkers, including those focused on treatment assessment, have continued to dramatically expand. Studies at single centers have clearly demonstrated the potential of such applications. However, sources of bias and variance of quantitative MR imaging biomarkers have not previously been adequately investigated, thus limiting the implementation of robust methods to mitigate their effects. Therefore, when it comes to applications of such techniques across vendor platforms, centers, and time, challenges arise due to lack of standards, appropriate phantoms, and protocols. During the past few years, several quantitative MR imaging initiatives have been instigated. This symposium presentation will review selected applications of quantitative MR imaging biomarkers, illustrate some of the current challenges in broadening the use of such biomarkers, and discuss some of the current initiatives of various scientific and federal organizations that are focused on the standardization, qualification, and validation of MR quantitative imaging biomarkers. Specific examples of DCE-MRI applications and standardization efforts will be provided.

URL's

web.me.com/efjackson

### RC425B • Clinical Applications of Quantitative DCE-MRI

**Michael V Knopp** MD, PhD (Presenter)

#### LEARNING OBJECTIVES

1) To apply the concepts and pathophysiology of quantitative DCE MRI in clinical applications. 2) To review technical and procedure considerations for clinical applications. 3) To familiarize with current and evolving clinical applications of qDCE-MRI. 4) To utilize qDCE-MRI in and interpret clinical applications.

#### ABSTRACT

Dynamic contrast enhanced MRI has evolved over the last two decades into a readily available MRI add-on procedure that enables a spatial and time resolved insight into the microcirculation of tissues, both neoplastic as well as benign. While the cinematic display of the temporal contrast enhancement as well as the visual inspection of a signal intensity curve placed over a region of interest enables a ready visual perception of the characteristics of contrast enhancement, a methodological data reduction to a quantitative readout has been more challenging to validate, implement and interpret. Today, the fundamental pathophysiology, appropriate MRI acquisition and post-processing approach are well understood. Quantification is a key enabler to use imaging more as a disease (bio) marker especially for monitoring disease response or progression, as well as putting a more structured interpretation of the dynamic imaging findings into the patient care process. The clinical applications that benefits the most are those where the extent and/or intensity of tissue microcirculation can serve as a marker of biologic characteristics, guide the further diagnostics (tissue biopsies) and/or therapy management. The most common use of applying the fundamental methodologies of DCE-MRI is MR Mammography which is further evolving from a purely morphologic to a semi-quantitative or quantitative imaging procedure. Characterizing malignant tissues, inflammation or angiogenic processes with quantitative approaches is expanding our radiologic toolbox and ability to provide outcome impacting information. Quantitative DCE MRI is evolving to be an increasingly meaningful, clinically relevant and obtainable functional readout of the underlying tissue microcirculation and it will depend on our expansion of radiologic disease insight to truly capitalize on its capabilities.

### RC425C • Oncologic Applications of Quantitative DCE-MRI

**Anwar R Padhani** MD (Presenter) \*

#### LEARNING OBJECTIVES

1) To show that DCE-MRI can be analyzed using qualitative to quantitative methods. 2) To illustrate that routine clinical use of DCE-MRI makes use of qualitative assessments. 3) To indicate that early drug development requires quantification including reproducibility assessments. 4) To realise that complex DCE analysis has roles in validation, drug development, and is needed for multiparametric assessments.

#### ABSTRACT

Using DCE-MRI in oncologic clinical practice should not be delayed/hindered by the complexities of the technique. The last 20 years of validation work allows us to be confident that DCE-MRI (morphology, subtraction maps, curve shapes and semi-quantitative methods) work in the clinic. Complex quantitative DCE analysis has roles in validation, drug development, and is needed for multiparametric assessments. Future work should now focus on incorporating mpMRI imaging for directing personalized medicine.

## Quantitative Imaging: Quantitative Imaging in FDG-PET

Wednesday, 08:30 AM - 10:00 AM • S102AB

PH NM BQ

[Back to Top](#)

RC525 • AMA PRA Category 1 Credit™:1.5 • ARRT Category A+ Credit:1.5

Director

**Michael F McNitt-Gray**, PhD \*

### RC525A • Lessons Learned from Drug Development Trials Using Molecular Imaging

**Jeffrey L Evelhoch** PhD (Presenter) \*

#### LEARNING OBJECTIVES

1) Understand how pharma uses the information provided by FDG-PET. 2) Become familiar with site qualification and quality control methods used in clinical trial of an investigational therapeutic agent. 3) Understand why specific clinical trial imaging protocols may differ from clinical practice and importance of adhering to the clinical trial imaging protocol. 4) Realize which issues confound attempts to achieve more quantitative FDG-PET in the context of a clinical trial of an investigational therapeutic agent.

### RC525B • Examples of Multi-Center Molecular Imaging Trials: Trial Design and Quantitative Approaches

**David A Mankoff** MD, PhD (Presenter)

#### LEARNING OBJECTIVES

1) Describe applications of molecular imaging as a biomarker for cancer drug therapy. 2) Discuss elements of clinical study design for molecular imaging. 3) Contrast molecular imaging versus conventional imaging and therapy trials.

### RC525C • Understanding and Controlling Sources of Variability in Multi-Center PET Imaging

**Paul E Kinahan** PhD (Presenter) \*

#### LEARNING OBJECTIVES

1) Identify the importance of quantitative imaging principles in the setting of clinical trials. 2) Identify the role of standards, including



## Musculoskeletal (Tumor II)

Wednesday, 10:30 AM - 12:00 PM • E451A

[Back to Top](#)

[MR](#) [CT](#) [BQ](#) [MK](#)

**SSK14** • *AMA PRA Category 1 Credit*™:1.5 • ARRT Category A+ Credit:1.5

**Moderator**  
**Kambiz Motamedi**, MD  
**Moderator**  
**Mark J Kransdorf**, MD

### **SSK14-01 • Diagnostic Performance of Tomosynthesis for Evaluation of Suspicious Bone Tumors: Comparison with Radiography and CT**

**Jihyun Bae MD (Presenter)** ; **In Sook Lee** ; **You Seon Song** ; **Jeung Il Kim MD, PhD** ; **Jong Woon Song**

#### **PURPOSE**

To compare tomosynthesis with radiography for evaluation of suspicious bone tumors, using multidetector computed tomography (CT) as the reference method.

#### **METHOD AND MATERIALS**

The study was approved by the institutional review board of our institution and written consent was obtained from all patients. From January 2012 to March 2013, 24 consecutive patients with suspicious bone tumors underwent radiography, tomosynthesis, and CT within 3 days. Two radiologists analyzed about the presence or absence of periosteal reaction, space occupying lesion (SOL), mineralization and fracture on each three imaging modality.

#### **RESULTS**

Fourteen patients had benign bone tumors, nine had malignant bone tumors and one had only cortical fracture. The overall sensitivity, specificity, and accuracy of tomosynthesis were, respectively, 88.9%, 100%, and 95.8% about the periosteal reaction, all 100% about the SOL and mineralization, and 87.5%, 100% and 91.7% about the fracture. Those of radiography were, respectively, 88.9%, 100%, and 95.8% about the periosteal reaction, 81.8%, 100% and 83.3% about the SOL, 83.3%, 100%, and 95.8% about the mineralization, and 43.7%, 100%, and 62.5% about the fracture. The degrees of agreement between CT and tomosynthesis were 0.909 about periosteal reaction, 1 about the SOL and mineralization and 0.824 about the fracture ( $p < 0.05$ ). Those between CT and radiography were respectively 0.909, 0.429, 0.882, and 0.341 ( $p < 0.05$ ).

#### **CONCLUSION**

The diagnostic performance of tomosynthesis for evaluation of suspicious bone tumors was significantly greater than radiography and comparable to CT.

#### **CLINICAL RELEVANCE/APPLICATION**

The imaging qualities of tomosynthesis in the cases of suspicious bone tumors may comparable to those of CT images, with relatively lower radiation dose.

### **SSK14-02 • Treatment Response Evaluation of Patients with Malignant Bone Tumors; Correlation of ADC from 3.0T MR Imaging and SUV from FDG PET/CT**

**So-Yeon Lee MD (Presenter)** ; **Won-Hee Jee MD** ; **Joon-Yong Jung MD** ; **Jin-Kyeong Sung MD** ; **Soo Ah Im** ; **Jin Hyoung Kang** ; **Ie Ryung Yoo**

#### **PURPOSE**

To retrospectively determine whether the apparent diffusion coefficients (ADC) at 3T diffusion-weighted MR imaging (DWI) correlate with the standardized uptake values (SUV) at positron emission tomography (PET)/computed tomography (CT) for evaluating treatment response in malignant bone tumors.

#### **METHOD AND MATERIALS**

The institutional review board approved this HIPAA-compliant study and informed consent was waived. Twenty-two patients with 27 malignant bone tumors underwent 3T MR imaging including DWI with b value of 0, 800 sec/mm<sup>2</sup> and whole-body fluorine 18 fluorodeoxyglucose PET/CT before and after treatment. Minimum ADC (ADC<sub>min</sub>) of the tumor was measured by two independent musculoskeletal radiologists and correlated the maximum SUV (SUV<sub>max</sub>) of the tumor. The percentage changes of ADC<sub>min</sub> and SUV<sub>max</sub> were calculated by the difference between the initial and follow-up values divided by the initial value. The change ratios of ADC<sub>min</sub> and SUV<sub>max</sub> were defined as the ratio of the follow-up value to the initial value. The Spearman rank correlation were obtained for statistical analysis.

#### **RESULTS**

There was significant correlation between the differences between the initial and follow-up values of ADC<sub>min</sub> and SUV<sub>max</sub> ( $r = 0.573$  for reviewer 1 and  $r = 0.597$  for reviewer 2,  $P < .005$ ), the change ratios of ADC<sub>min</sub> and SUV<sub>max</sub> ( $r = 0.457$ ,  $r = 0.491$ ,  $P < .05$ ), and percentage changes of ADC<sub>min</sub> and SUV<sub>max</sub> ( $r = 0.457$ ,  $r = 0.491$ ,  $P < .05$ ). DWI and PET CT showed treatment response in 18 lesions: the ADC was increased by 105% (interquartile range, 61-166) and SUV<sub>max</sub> was decreased by 56% (37-83). The ADCs of two responded lesions returned to the range of normal bone marrow and resulted in a decrease of the ADC<sub>min</sub> (65% and 32%, respectively) and decrease of SUV<sub>max</sub> (71% and 87%, respectively). There was no response in six lesions: the ADC was decreased by 23% (13-30) and SUV<sub>max</sub> was increased by 55% (26-90). There was one lesion with a discrepancy in changes of ADC<sub>min</sub> (decreased by 29%) and SUV<sub>max</sub> (decreased by 13%).

#### **CONCLUSION**

There was significant correlation between the ADC and SUV for evaluating treatment response in malignant bone tumors.

#### **CLINICAL RELEVANCE/APPLICATION**

Quantitative DWI is comparable to PET/CT for evaluating treatment response in malignant bone tumors.

### **SSK14-03 • Negative Relationship between CT Attenuation Values and ADC Values in Densely Sclerotic Bone Metastases from Prostate Cancer**

**Usman Bashir MBBS (Presenter)** ; **Nina Tunariu MD** ; **David J Collins BSC, BA** ; **Diletta Bianchini** ; **Andrea Zivi** ; **Dow-Mu Koh MD, FRCS**

#### **PURPOSE**

To investigate relationship between CT attenuation and ADC value of skeletal metastasis in prostate cancer.

#### **METHOD AND MATERIALS**

26 patients of prostate cancer with bone metastases, who underwent contemporaneous whole body diffusion-weighted MRI (WB-DWI) and CT were retrospectively reviewed. WB-DWI was performed on a 1.5T system using b-values 50, 900 s/mm<sup>2</sup>. CT of chest, abdomen and

pelvis was acquired at 65s post-contrast. Slice-by-slice synchronization was obtained between CT and MRI data-sets by careful use of anatomic landmarks. A lucent and a sclerotic metastasis were chosen on CT, when present, at each of the following skeletal sites: thoracic spine, lumbar spine, sacrum, right pelvis and left pelvis. A maximum of 10 lesions were evaluated per patient. Lesion signal intensity on b900 image was recorded as hyperintense or iso/hypointense to skeletal muscle. A region of interest (ROI) was drawn on CT around each lesion to record the mean CT value (HU) and copied on the matching b900 image to derive lesion's mean ADC value ( $\times 10^{-3} \text{ mm}^2/\text{s}$ ). The relationship between lesion CT HU and ADC values was evaluated by Spearman's correlation. The mean CT HU and ADC values of hyperintense versus iso/hypointense lesions were compared using t-test. A p-value of

#### RESULTS

212 lesions were evaluated. The mean CT HU was 481 (33-1152); the mean ADC value was 0.91 (0.18-2.13). 140/212 (66%) lesions appeared hyperintense; 73/212 (34%) were iso/hypointense on DWI. The mean CT HU of hyperintense metastases was significantly lower than iso/hypointense lesions (371 vs 681,  $p = 650\text{HU}$ ;  $n=57$ ), a highly significant negative correlation was observed between CT HU and ADC ( $r = -0.60$ ,  $p$

#### CONCLUSION

Densely sclerotic prostate cancer bone metastases (CT HU  $\geq 650$ ) showed a strong negative correlation between CT HU and ADC values, but this was not observed for less sclerotic/lytic disease.

#### CLINICAL RELEVANCE/APPLICATION

Understanding the interplay of DWI signal intensity, ADC, marrow fat fraction and CT attenuation value of prostate bone metastases can help characterize lesions for response evaluation to treatment

### **SSK14-04 • Differentiation of Osteogenic Bone Metastases and Bone Islands Using Conventional Single-energy CT Value and Monochromatic CT Value from Spectral CT in Patients with Bronchogenic Carcinoma**

**Yue Dong** (Presenter) ; **Shaowei Zheng** ; **Bing Wang** ; **Ruxin Wang** ; **Lifei Sun**

#### PURPOSE

To evaluate the diagnostic efficacy of single-energy CT and single-source Dual-energy CT in the identification of osteogenic bone metastases and bone islands in patients with bronchogenic carcinoma.

#### METHOD AND MATERIALS

45 cases of osteogenic metastases in patients with pathologically proven bronchogenic carcinoma and 43 cases of bone islands were confirmed via MRI, single-photon emission computed tomography (SPECT) and one year follow-up. All subjects underwent dual-energy spectral CT imaging using a high definition CT (Discovery CT750 HD, GE). The means, standard deviation (SD) and coefficient variation (CV) of 140kVp-quality check (QC) CT values and virtual monochromatic (40-140 keV) CT values of osteogenic metastases and bone islands were measured and compared with independent-samples t-test. The lesion center was selected as ROI (20-30mm<sup>2</sup>). ROC curves were used to compare the diagnostic efficacies of conventional single-energy CT and monochromatic CT in the identification of osteogenic bone metastases and bone islands.

#### RESULTS

The mean mono-energy CT values (40-140 keV) and QC CT value of osteogenic bone metastases were all significantly lower than that of bone islands ( $p$

#### CONCLUSION

Both conventional single-energy CT and monochromatic CT were reliable for differential diagnosis of osteogenic bone metastases and bone islands. SD of monochromatic CT value at higher keV has better diagnostic efficacies.

#### CLINICAL RELEVANCE/APPLICATION

SD of monochromatic CT value at higher keV has better dSD of monochromatic CT value at higher keV has better diagnostic efficacies for differentiation of osteogenic bone metastases and bone islands.

### **SSK14-05 • Can IDEAL-MR Imaging of Multiple Myeloma Be Used as a Biomarker for Predicting Symptomatic Myeloma?**

**Miyuki Takasu** MD (Presenter) ; **Yoko Kaichi** ; **Miho Ishikawa** MD ; **Shuji Date** ; **Yuji Akiyama** ; **Kazuo Awai** MD \* ; **Yoshiaki Kuroda** ; **Akira Sakai**

#### PURPOSE

Asymptomatic multiple myeloma is an asymptomatic plasma-cell proliferative disorder associated with a high risk of progression to symptomatic multiple myeloma. Predictive factors for the progression of this disease are unclear. This study was performed to evaluate the effectiveness of the iterative decomposition of water and fat with echo asymmetric and least-squares estimation (IDEAL) MRI to predict symptomatic myeloma in patients without visible focal lesions.

#### METHOD AND MATERIALS

The lumbar spine was examined with 3T-MRI in 47 patients with multiple myeloma (asymptomatic myeloma, 23; symptomatic myeloma, 24). The fat-signal fraction (FSF) obtained by IDEAL sequence was calculated as the mean value from three vertebral bodies. We evaluated factors predictive of symptomatic myeloma. They included sex, age, FSF, MR signal intensity pattern (MR pattern), bone marrow plasma cell percentage (BMPC%) obtained from a biopsy specimens, presence of IgA monoclonal protein, serum monoclonal protein level (M protein), serum albumin level, serum  $\beta_2$ -microglobulin ( $\beta_2\text{m}$ ) level, the  $\beta_2\text{m}/\text{albumin}$  ratio, reductions in levels of uninvolved immunoglobulins, and the kappa/lambda ratio. For data analysis, univariate and multivariate logistic regression analyses, as well as receiver operating characteristic curves, were used. A difference with  $P < .05$  was considered significant.

#### RESULTS

Univariate analysis demonstrated that MR pattern, FSF, BMPC%, M protein, the reduction in uninvolved immunoglobulins,  $\beta_2\text{m}$ , and the  $\beta_2\text{m}/\text{albumin}$  ratio were significantly associated with symptomatic myeloma. Results of multivariate analysis demonstrated that  $\beta_2\text{m}$ , FSF, and the reduction in uninvolved immunoglobulins had significant effects in differentiation between asymptomatic and symptomatic myeloma. The area under the curve was 0.805 for FSF, 0.844 for  $\beta_2\text{m}$ , and 0.793 for BMPC%.

#### CONCLUSION

Fat quantification results using the IDEAL sequence in MRI were significantly different in patients with symptomatic- and asymptomatic myeloma. The FSF and  $\beta_2\text{m}$  facilitated the discrimination of symptomatic- from asymptomatic myeloma.

#### CLINICAL RELEVANCE/APPLICATION

Predictive factors for the progression to symptomatic myeloma included FSF and  $\beta_2\text{m}$ . The discriminative performance of FSF is comparable to that of BMPC% obtained from biopsy specimen.

### **SSK14-06 • Magnetic Resonance Imaging Differentiation between Malignant Marrow Replacing Lesion and Benign Red Marrow Deposition of Vertebra Using T2\*-corrected Fat Fraction Map Imaging Based on Three-point Dixon-VIBE Sequence**

**Yong Pyo Kim** (Presenter) ; **Sungjun Kim** MD ; **Tae Sub Chung** ; **Yaena Kim** MD ; **Munyoung Paek** ; **Choon Sik Yoon** MD ; **Young Han Lee** MD ; **Ho-Taek Song** MD ; **Jin-Suck Suh** MD

#### PURPOSE

To assess feasibility of T2\*-corrected fat fraction map using three-point Dixon-VIBE sequence as a tool for differentiation between malignant marrow replacing lesion and benign red marrow deposition of vertebra.

#### METHOD AND MATERIALS

From Mar. 2012 to Feb. 2013, magnetic resonance imaging was performed for consecutive 33 patients who were referred for vertebral marrow abnormality assessment. Twenty two pathologically confirmed malignant marrow replacing lesions and 11 benign red marrow lesions from the patients were subjects of this study. Three sequences were applied using a 1.5-T MR imaging scanner like follows:

three-point Dixon-volumes interpolated breath-hold GRE sequence (VIBE) for fat fraction (FF) measurement; conventional T1 weighted imaging (T1WI); pre- and post-contrast enhanced fat-suppressed T1WI (CE). To measure fat fraction or signal intensity (SI), region of interest (ROI) was placed at the target lesions. Average measurements from consecutive three slices of the target lesions were used for data analysis. Three parameters from the measurements were obtained like follows for each lesion: FF from VIBE; LDR (lesion-disc ratio; [SI of marrow lesion / SI of disc]\*100) for T1WI; CER (contrast enhancement ratio; [LDR of post-contrast T1WI-LDR of pre-contrast T1WI]\*100 / LDR of pre-contrast T1WI) for CE. To evaluate diagnostic performance of the three parameters, receiver operating characteristic (ROC) curves were obtained and areas under curves (AUCs) of the parameters were compared to each other. The sensitivity and specificity at the most ideal cut off values for the parameters were obtained.

#### RESULTS

AUCs of FF, LDR, CER were 0.96, 0.83, 0.74. FF showed superior AUC than CER with statistical significance. The optimal cut-off value and the corresponding sensitivity/specificity in percentage were like follows: 16, 0.81/1 in FF; 116.2, 1/63.6 in LDR; 93.4, 0.68/0.81 in CER.

#### CONCLUSION

T2\*-corrected fat fraction measurement using a three-point Dixon-VIBE sequence showed superior diagnostic performance than contrast enhanced T1WI, and it showed excellent specificity in differentiation between malignant marrow replacing lesion and benign red marrow deposition of vertebra.

#### CLINICAL RELEVANCE/APPLICATION

T2\*-corrected fat fraction measurement using a three-point Dixon-VIBE sequence is expected to play an important role to differentiate benign red marrow from malignant marrow lesion.

### **SSK14-07 • Diagnostic Efficacy of Whole-body Ultra Low Dose CT (WBULDCT) in Comparison with Spinal Magnetic Resonance Imaging (SMRI) in the Assessment of Disease in Patients with Multiple Myeloma (MM)**

**Valeria Besotri MD (Presenter) ; Davide Ippolito MD ; Pietro A Bonaffini MD ; Valentina Bartolo ; Alessandra Cuccia ; Sandro Sironi MD**

#### PURPOSE

To compare the diagnostic value of Whole-Body Ultra Low-Dose CT (WBULDCT) with dedicated Spinal Magnetic Resonance Imaging (SMRI) in the identification of bone marrow involvement of patients with Multiple Myeloma (MM).

#### METHOD AND MATERIALS

A total of 30 patients (17 males and 13 females; mean age 68 years, range 52-83 years), with histologically proven MM, undergoing WBULDCT and a dedicated SMRI (9/30 for staging, 21/30 during follow-up), were evaluated in our study. Unenhanced WBULDCT was performed on a 256-slice scanner (iCT, Philips), with the following parameters: tube voltage 120 kV, tube current time product 40 mAs, collimation 128x0.65. Spine MRI was performed on a 1.5T magnet (Achieva, Philips), with the following protocol: T1 TSE and T2 STIR acquired on sagittal plane. WBULDCT was compared to spine MRI in terms of lesion detection, pattern of bone marrow involvement and risk fractures.

#### RESULTS

In 21/30 patients (70%), WBULDCT and SMRI were concordant, detecting (14/21) or excluding (7/21) involvement of the axial skeleton. In 9/30 patients (30%) WBULDCT and SMRI were discordant in terms of axial skeleton involvement: in 2/9 patients SMRI was positive and WBULDCT was negative, while in 7/9 patients only WBULDCT was positive. The corresponding sensitivity for lesion detection in the spine was 73% for WBULDCT and 53% for SMRI, respectively. Only one patient with a negative WBULDCT scan showed multifocal lesions on SMRI. Moreover, in 22/30 of cases (73%) WBULDCT detected additional osteolytic lesions in other extra-axial districts (skull, sternum and ribs, pelvis, upper and lower limbs).

#### CONCLUSION

WBULDCT demonstrated superior capability as compared to SMRI, for the detection of disease in the axial skeleton and also offers detailed information about extra-axial involvement, which could be potentially missed with dedicated SMRI alone.

#### CLINICAL RELEVANCE/APPLICATION

WBULDCT imaging appears to be helpful in detecting spinal involvement in patients with MM, reserving SMRI in case of negative results in symptomatic patients.

### **SSK14-08 • Appearance of Monoclonal Plasma Cell Diseases in Whole-body MRI and Correlation with Parameters of Disease Activity**

**Jost Kloth (Presenter) ; Jens Hillengass MD ; Karin Listl MD ; Stefan Delorme MD ; Hans-Ulrich Kauczor MD \* ; Marc-Andre Weber MD \* ; Hartmut Goldschmidt MD**

#### PURPOSE

To examine a possible association of the presence of focal lesions (FL) or a diffuse infiltration pattern of bone marrow in whole-body MRI (WB-MRI) with the disease stage and established markers of disease activity in patients with monoclonal plasma cell disease.

#### METHOD AND MATERIALS

Institutional review board approval was obtained. We examined the WB-MRI scans in 547 consecutive, unselected and untreated patients with monoclonal gammopathy of undetermined significance (MGUS, n=138), smoldering multiple myeloma (SMM, n=157) and multiple myeloma (MM, n=252) on two identical 1.5 Tesla MRI-scanners with body array coils. Assessment was done by two experienced radiologists blinded to the diagnosis of the patients in consensus.

#### RESULTS

We found focal lesions in 23.9% (MGUS), 34.4% (SMM) and 81.3% (MM), respectively. A diffuse infiltration pattern was detected in 38.4%, 45.9%, and 71% of the corresponding patients. Infiltration patterns were significant (p

#### CONCLUSION

The frequency of focal or diffuse bone marrow abnormalities as well as the severity of diffuse signal changes in bone marrow are significantly associated with the stage of plasma cell disease as well as established markers of disease activity.

#### CLINICAL RELEVANCE/APPLICATION

Considering nearly riskless application and non-invasiveness of wb-MRI its future application in the prognostic evaluation of MM and its asymptomatic precursors MGUS and SMM is promising.

### **SSK14-09 • Whole-body MRI for Diagnosing Multiple Myeloma and Evaluating Treatment Efficacy**

**Min Zong MD, PhD (Presenter) ; Dehang Wang MD ; Si-Guang Zhu MD ; Li-Juan Chen**

#### PURPOSE

To investigate the initial diagnostic value and treatment efficacy of the whole-body MRI for Multiple Myeloma.

#### METHOD AND MATERIALS

Forty-seven Multiple Myeloma patients confirmed with histopathology were enrolled in the study. All patients underwent whole-body MRI before chemotherapy, and follow up scan at 3 and 6 months after the first and second rounds of chemotherapy treatment, respectively. The lesions found by whole-body MRI of each patient were counted at different time points and compared by one-way ANOVA statistic analysis

#### RESULTS

Five imaging patterns were identified on whole-body MRI, which were smoldering type (5 patients), diffuse type (7 patients), focal type (25 patients), mixed type (3 patients), and salt-and-pepper type (7 patients). Out of the 47 patients, there were 42 patients with visible lesions on follow up whole-body MRI scans during chemotherapy. The mean number of lesions was  $113.90 \pm 45.71$  on whole-body MRI before chemotherapy and decreased to  $28.00 \pm 22.49$  and  $10.04 \pm 9.02$  at the third and sixth month on follow-up whole-body MRI. Statistically significant differences were confirmed between either two of the three groups (P

#### CONCLUSION

Whole-body MRI is a valuable tool for initial Multiple Myeloma diagnosis and monitoring treatment efficacy after chemotherapy.

#### CLINICAL RELEVANCE/APPLICATION

Whole-body MRI is a valuable tool for initial Multiple Myeloma diagnosis and monitoring treatment efficacy after chemotherapy

## Neuroradiology (Advanced Neuroimaging of Alzheimer's Disease)

Wednesday, 10:30 AM - 12:00 PM • N230

[MR](#) [BQ](#) [NR](#)

[Back to Top](#)

**SSK16** • AMA PRA Category 1 Credit™:1.5 • ARRT Category A+ Credit:1.5

#### Moderator

**Jeffrey R Petrella**, MD \*

#### Moderator

**Gloria C Chiang**, MD

**SSK16-01 • Prediction of Conversion from MCI to AD: Integration and Relative Values of Brain Atrophy Patterns, Clinical Scores, CSF Biomarkers, and APOE Genotype**

**Xiao Da** (Presenter); **Jon B Toledo** MD; **Jarcy Zee**; **David A Wolk** MD; **Sharon X Xie**; **Yangming Ou** PhD; **Amanda Shacklett** MS; **Paraskevi Parmpi** MS; **Leslie Shaw** PhD; **John Trojanowski**; **Christos Davatzikos**

#### PURPOSE

We evaluate the individual, as well as relative and joint values of indices obtained from MRI patterns of atrophy, cerebrospinal fluid (CSF) biomarkers, APOE genotype, and cognitive performance for prediction of clinical progression of MCI patients, on an individual person basis.

#### METHOD AND MATERIALS

The SPARE-AD index, a previously characterized imaging biomarker capturing spatial patterns of brain atrophy, was first tested for sensitivity and specificity as a biomarker of Alzheimer's disease (AD), in a training set of 411 participants. SPARE-AD, and a related mild cognitive impairment (MCI)-specific index called SPARE-MCI, were then evaluated at baseline in 212 MCI patients who either converted to AD within 18 months or remained stable for at least 3 years. Baseline predictive value of SPARE-AD, SPARE-MCI, CSF biomarkers (total and phosphorylated tau and A $\beta$ ), MMSE, ADAS-Cog, and APOE genotype were then evaluated using a support vector machine classifier.

#### RESULTS

SPARE-AD offered excellent diagnostic accuracy of AD (AUC between 0.96-0.98). Excluding CSF biomarkers, MRI-derived SPARE scores offered the highest predictive power for MCI conversion to AD (AUC=0.76); followed by ADAS-Cog (AUC=0.74). Their combination offered the best accuracy (AUC=0.76). Other cognitive and APOE4 markers did not add any predictive power beyond them. In a subset (112 MCI patients) who also had CSF biomarkers, SPARE had the best predictive power (AUC=0.73), being enhanced by CSF biomarkers (AUC=0.76), which by themselves were relatively poorer predictors (AUC=0.68). In amyloid-negative MCI patients, SPARE-AD had high predictive power.

#### CONCLUSION

MRI patterns of atrophy, quantified via advanced pattern analysis methods, offer the highest predictive power of conversion from MCI to AD, but are slightly better than ADAS-Cog. Combination of MRI and CSF biomarkers improves predictive power. High predictive value of SPARE in negative amyloid MCI is not expected under the amyloid hypothesis and merits further investigation.

#### CLINICAL RELEVANCE/APPLICATION

A highly sensitive and specific imaging biomarker of AD is evaluated as an earlier predictor of clinical progression from MCI to AD, which can become an AD-specific marker for diagnosis and treatment.

**SSK16-02 • MR Elastography of Alzheimer's Disease and Frontotemporal Dementia**

**John Huston** MD (Presenter); **Matthew C Murphy** PhD; **Kevin J Glaser** \*; **Clifford R Jack** MD \*; **Richard L Ehman** MD \*

#### PURPOSE

Several MR imaging biomarkers exist to measure various MR disease processes associated with Alzheimer's disease (AD) and frontotemporal dementia (FTD). Patterns of hippocampal and whole brain atrophy, MR spectroscopy, perfusion, diffusion and functional MRI have been reported. Magnetic resonance elastography (MRE) is a noninvasive technique to measure tissue stiffness, akin to manual palpation. Our purpose was to investigate the effect of AD and FTD on brain stiffness.

#### METHOD AND MATERIALS

We examined 59 subjects with brain MRE including 39 age and gender matched cognitively normal controls (NC), 15 subjects with AD and 5 subjects with behavioral variant FTD. MRE data were collected with a modified spin-echo EPI pulse sequence on a 3.0T MR imager including full head coverage in just less than 7 minutes. Shear waves were introduced with a soft pillow-like vibration source operating at 60 Hz using a pneumatic actuator. The wave data underwent a curl operation to remove contributions of the longitudinal waves and a 3D direct inversion algorithm calculated the elastogram. In subjects with 3 mm isotropic sampling we measured age adjusted global brain stiffness (entire brain excluding cerebellum), in 8 regions.

#### RESULTS

Global stiffness was decreased in AD subjects (2.20 kPa) compared to NC (2.37 kPa). Group-wise differences in stiffness were demonstrated within the lobes of the brain that contain association cortices (p

#### CONCLUSION

We have demonstrated that AD and FTD alter the mechanical properties of the brain in a way that can be measured in vivo by MRE, following the known topography of the diseases. Measures of brain elasticity have the potential to offer insights into the ultrastructural alternations of brain tissue that occur with AD and FTD, how these change with time and the clinical expression of the diseases.

#### CLINICAL RELEVANCE/APPLICATION

MR Elastography demonstrates Alzheimer's disease and frontotemporal dementia alter the mechanical properties of the brain by decreasing brain stiffness, following the known topography of the diseases.

**SSK16-03 • Different Post Label Delay Cerebral Blood Flow Measurements in Patients with Alzheimer's Disease Using 3D Arterial Spin Labeling**

**Ying Liu** MD (Presenter); **Huishu Yuan** MD; **Xiangzhu Zeng** MD; **Zheng Wang** MS

#### PURPOSE

To evaluate cerebral blood flow (CBF) and find out differences in patients with Alzheimer's disease (AD) and healthy control group (HC)

using 3D Arterial Spin Labeling (ASL) on 3.0T MR. Changing the label time in 3D ASL in order to obtain two CBF maps. To observe the analysis of different label time for CBF map result and explore the 3D ASL in the display of brain perfusion factor and its clinical significance

#### METHOD AND MATERIALS

Thirteen AD patients (5 men and 8 women; age range, 58-88 years, mean age  $75.00 \pm 7.36$  years) and fifteen healthy control subjects (4 men and 11 women; age range, 56-84 years, mean age  $71.20 \pm 7.89$  years) were recruited. All MRI examinations were performed using a 3.0T scanner, pseudo-continuous ASL scanning was conducted with 36 label/control images acquired on a GE750 3T scanner. The acquisition parameters were: TR/TE = 4632/10.5ms, voxel size =  $2 \times 2 \times 4 \text{mm}^3$ . High-resolution T1SPGR images were acquired as well. ASL sequence was obtained twice with different post label delay (PLD) which were 1.5s and 2.5s. Comparing CBFAD1.5 with CBFHC1.5 and CBFAD2.5 with CBFHC2.5, and CBFAD1.5 with CBFAD2.5. ASL and structural images were coregistered using SPM8

#### RESULTS

1. SPM analyses revealed focal hypoperfusion in areas over the bilateral parietal lobe, temporal lobe and posterior cingulate gyrus in AD patients in comparison with control subjects with PLD1.5(p

#### CONCLUSION

1. revealed patterns of regional hemodynamic impairment typical of mild AD. Certain hypoperfusion areas in AD patients in comparison with control subjects with PLD1.5. 2. When the labeling time was set with 2.5s, the areas of CBF map were reduced significantly to nearly zero. Therefore, short labeling time could discover perfusion abnormal earlier

#### CLINICAL RELEVANCE/APPLICATION

3D ASL is a useful noninvasive MRI sequence to identify the Alzheimer's disease and the PLD of 1.5s was probably better than that of 2.5s

### SSK16-04 • The Correlation of Hippocampal T2-mapping with Neuropsychology Test in Patients with Alzheimer's Disease

Zhu-Ren Luo (Presenter) ; Xiong-Jie Zhuang

#### PURPOSE

1) To deduce  $T_2$ , the inverse of the transverse relaxation rate ( $R_2$ ), in the hippocampus of healthy adults; 2) to investigate the brain iron deposition in Alzheimer's disease (AD) patients and age-matched healthy controls using  $T_2$ -values.

#### METHOD AND MATERIALS

$T_2$ -weighted data from the bilateral-hippocampi of ten AD patients and sixty healthy controls were collected using multi-slice multi-echo turbo spin echo (MSME-TSE) imaging on a 3.0T MR-scanner, followed by the neuropsychological testing. The correlations between  $T_2$ -values and Mini-Mental-State-Examination (MMSE) score were investigated on group-wise basis (gender, age, side and healthy/AD).

#### RESULTS

There were no significant differences in hippocampal  $T_2$ -values on intra-gender and inter-gender basis ( $P > 0.05$ ). Hippocampal  $T_2$ -values of both sides were similar (right:  $85.17 \pm 2.44$  milliseconds; left:  $85.28 \pm 2.51$  milliseconds). The bilateral hippocampal  $T_2$  values correlated moderately with age (right:  $r = -0.59$ ; left:  $-0.58$ ;  $P < 0.001$ ). Mean hippocampal  $T_2$ -values from ten controls correlated strongly ( $r = -0.90$ ,  $P < 0.001$ ) with reference brain iron concentrations for healthy adults. The AD-group had significantly lowered  $T_2$ -values in the hippocampus when compared to normal controls ( $P < 0.001$ ) and had a strong positive correlation with the MMSE score ( $R^2 = 0.97$ ;  $P < 0.05$ ).

#### CONCLUSION

Patients with AD showed significantly iron depositions in the hippocampus resulting in the decreased  $T_2$  values. A positive correlation between  $T_2$ -values and cognition/ memory scores, suggests that quantitative  $T_2$  can be used in the early diagnosis of AD and monitoring of the treatment response.

#### CLINICAL RELEVANCE/APPLICATION

In vivo proton transverse relaxation rate imaging is capable of quantitatively measuring the iron deposition in the hippocampus in AD patients, consistent with incipient AD pathogenesis.

### SSK16-05 • GABA-edited Magnetic Resonance Spectroscopy in Alzheimer's Disease at 3T

Xue Bai BA (Presenter) ; Guangbin Wang MD

#### PURPOSE

Gamma-aminobutyric acid (GABA) is the essential inhibitory neurotransmitter in human brain. It is considered that reduced neuronal GABA concentration and neurotransmission results in cognitive impairments in Alzheimer's disease (AD). However, few in vivo studies have directly certified this hypothesis. In this study, we used magnetic resonance spectroscopy at high field to measure GABA levels, aiming to investigate whether there is a regional GABA level decline in AD.

#### METHOD AND MATERIALS

Twelve untreated AD patients (5 males and 7 female; range 56-79, mean =  $67.6 \pm 8.4$  years) and twelve age- and sex-matched healthy control subjects were recruited. AD patients were diagnosed according to National Institute of Neurological and Communicative Disorders and Stroke and the Alzheimer's Disease and Related Disorders Association. 1H-MRS was performed in a 3-tesla MR scanner (Philips Achieva TX, Best, The Netherlands). The voxel was set ( $3 \text{cm} \times 3 \text{cm} \times 3 \text{cm}$ ) in the frontal lobe and the parietal lobe (Fig 1), using high resolution T1-weighted three-dimensional TFE images as a localizer. The GABA concentration was measured using a MEGA-PRESS sequence (TR = 2000ms; TE = 68 ms; 320 averages; acquisition bandwidth = 1000 Hz; scan duration 11 minutes). All the metabolite quantitation was performed with time-domain fitting algorithm AMARES by jMRUI v.4.0. Each pixel in the brain images was segmented as to gray matter, white matter, or cerebrospinal fluid using the FSL package.

#### RESULTS

According to the result of segmentation result, there was no significant difference in the proportions of each part between AD patients and controls. Fig 2 shows the typical GABA-edited spectra from the MEGA-PRESS sequence in the frontal lobe of an AD patient. Significant differences of GABA/Cr ratio were found in parietal lobe between AD patients and Controls ( $t = -2.212$ ,  $p = 0.038$ ), but not found in frontal lobe ( $t = 0.799$ ,  $p > 0.05$ ).

#### CONCLUSION

In this study, GABA-edited MRS technique was successfully applied in AD patients to assess GABA level in vivo, and the brain GABA level in parietal lobe is decreased in AD. GABA may be a potential biomarker for early detection of AD, and could be used to assess the prognosis after treatment.

#### CLINICAL RELEVANCE/APPLICATION

GABA-edited MRS technique was useful to assess GABA level in vivo, GABA may be a potential biomarker for early detection of AD, and could be used to assess the prognosis after treatment.

### SSK16-06 • Relationships between the Structural Connectome and Amyloid Burden in Alzheimer's Dementia

Jeffrey W Prescott MD, PhD (Presenter) ; Arnaud Guidon PhD ; P. M Doraiswamy MD \* ; Chunlei Liu PhD ; Jeffrey R Petrella MD \*

#### PURPOSE

The hypothesis of the current study is that relationships between the structural connectome and cortical amyloid burden may provide complementary information about pathologic changes in Alzheimer's Disease (AD).

#### METHOD AND MATERIALS

Subjects were those newly enrolled in the ADNI2 study. Baseline data was used. T1 anatomical images were parcellated using FreeSurfer. DTI scans were registered to the T1 images using FSL. Structural connectomes were created using the Connectome Mapper Toolkit. Node degree, local efficiency, and clustering coefficient were calculated for the precuneus, posterior cingulate, inferior temporal, superior parietal, and superior frontal connectome nodes. The FreeSurfer parcellations were registered to the florbetapir PET scans. The global SUVR and four local SUVRs (frontal, cingulate, parietal, and temporal) were calculated. Clinical cognitive assessments included MMSE, ADAS-Cog, and Rey AVLT. Statistical analyses were performed between structural connection metrics, amyloid status, and clinical cognitive scores.

#### RESULTS

There were 102 ADNI2 subjects (64 males, 38 females) available at the time of the analysis. There were 37 normal control, 19 early mild cognitive impairment (MCI), 25 late MCI, and 21 AD subjects. All global and local AV45 amyloid burden measures were significantly associated with RAVLT, MMSE, and ADAS-Cog ( $p < 0.05$ ). The strongest associations between amyloid burden and structural connection metrics were in the posterior cingulate and precuneus (node degree;  $p < 0.05$ ). The strongest associations between structural connection metrics and clinical dementia scores were in the precuneus, superior parietal, and superior temporal regions (node degree vs. MMSE and ADAS-cog;  $p < 0.05$ ).

#### CONCLUSION

Brain amyloid burden has significant associations with clinical cognitive status in all regions analyzed, consistent with globally increased amyloid burden as an important condition for AD. The strongest associations between amyloid burden and structural connection metrics were in the posterior cingulate and precuneus (node degree;  $p < 0.05$ ), suggesting that these regions are most likely to have structural changes related to amyloid deposition in AD.

#### CLINICAL RELEVANCE/APPLICATION

The combination of quantitative amyloid PET and DTI tractography can provide information about global and local structural changes in AD, aiding in diagnosis and disease tracking.

### **SSK16-07 • Voxel-based Analysis of Quantitative Susceptibility Data Obtained from Subjects with AD and MCI**

**Hye Soo Koo MD (Presenter) ; Seong Jong Yun ; Kyung Mi Lee MD ; Eo Jin Hwang ; Heok Gi Kim ; Chang-Woo Ryu MD ; Hak Young Rhee ; Yi Wang PhD ; Tian Liu PhD ; Geon-Ho Jahng PhD**

#### PURPOSE

To investigate quantitative susceptibility in three groups of subjects with cognitive normal (CN), mild cognitive impairments (MCI) and Alzheimer's disease (AD). Because AD is expected to have the most iron plaques, we expected that the AD brains would produce the least signals in comparison to the CN and MCI brains.

#### METHOD AND MATERIALS

Subjects of 20 CN, 21 MCI, and 21 AD participated after informed consent. A fully first-order flow-compensated three-dimensional (3D) gradient echo sequence ran to obtain magnitude and phase images, which were later used to produce final quantitative susceptibility mapping (QSM). Furthermore, 3D T1-weighted images were acquired for the brain tissue segmentation, image registration, and masking-out of non-brain tissues, including CSF and vessels. The QSM images were produced by implementing the Morphology Enabled Dipole Inversion (MEDI) method. After the QSM images were smoothed using isotropic 4 mm Gaussian kernel, the differences of QSM data among the three groups were investigated by performing a voxel-based statistical analysis using a one-way analysis of variance (ANOVA) test with subject age and gender as covariates.

#### RESULTS

QSM values would decrease from CN to MCI and to AD. Compared with MCI subjects, QSM values in CN subjects were high in the left superior frontal gyrus and the left superior temporal gyrus. The lower signals were also found in the left superior frontal gyrus and the left superior temporal gyrus. Compared with the AD group, the QSM values in CN subjects were high in the left parahippocampal gyrus and the left inferior frontal gyrus, but low in the right cingulate gyrus. Compared with AD patients, QSM values in MCI subjects were high in the right superior temporal and the left superior temporal, but low in the left middle frontal gyrus.

#### CONCLUSION

We were able to identify the brain regions in which the susceptibility changes occurred among the different groups. More differences were found when CN and AD groups were compared than when CN and MCI groups were compared.

#### CLINICAL RELEVANCE/APPLICATION

The local variations in amyloid plaque can cause local magnetic susceptibility variations. Quantifying iron concentrations in vivo is instrumental for understanding the role of irons in MCI and AD.

### **SSK16-08 • Quantitative MRI Discrimination of Alzheimer's Dementia, Mild Cognitive Impairment, and Other Memory Disorders Using Volumetric MRI**

**Zachary T Berman BA (Presenter) ; Shamseldeen Y Mahmoud MD ; Alexander Rae-Grant MD ; Jennifer Bullen MSc ; Nancy A Obuchowski PhD ; Stephen E Jones MD, PhD**

#### PURPOSE

To investigate whether automated quantitative MRI may be useful in discriminating AD, MCI, and other memory disorders in a cognitive disorders clinic.

#### METHOD AND MATERIALS

The clinical records were reviewed of 669 consecutive patients at the Lou Ruvo Center for Brain Health who underwent quantitative MRI using NeuroQuant (Cortech Inc), which computes the brain volumes of 48 regions. These numbers were compared with the presence and type of dementia, whose gold standard was the clinical diagnosis made by neurologists, geriatricians, or general practitioners. Other clinical data collected included factors such as age, age of onset, and various test scores. These data were used to form a library to compare future patients whose dementia diagnosis is unknown. Specifically, a new patient's quantitative MRI is compared with the library of prior scans, and probabilities are provided associating the patient to either the presence of dementia or dementia type.

#### RESULTS

The 669 patients scanned with volumetric MRI were divided into three diagnoses: 328 were with Alzheimer's dementia, 262 with mild cognitive impairment, and 79 with age-related non-neurodegenerative memory loss. The attached figure shows the distribution of hippocampal volume for the three diagnoses. Using such data, including from other regions of the brain, probabilities are easily derived for any new patient with a quantitative volumetric MRI but without a diagnosis. These probabilistic maps may be useful in determining if a patient fits the profile for one of these three diagnostic categories given a specific set of MRI measures. We plan to apply this analysis prospectively to a cohort of patients seen in our cognitive disorders clinic to test the clinical utility of this procedure and analysis.

#### CONCLUSION

A center specific library of quantitative brain measures may be useful in categorizing patients with cognitive disorders. We review the initial results of our quantitative analysis and probabilistic maps generated during this analysis.

#### CLINICAL RELEVANCE/APPLICATION

Using institution specific libraries, quantitative volumetric MRI can be used to distinguish different cognitive disorders.

### **SSK16-09 • The Pattern of Metabolic Heterogeneity in the Hippocampus by 3T Multi-voxel Proton Spectroscopy in Alzheimer's Disease**

**Fei Chen** MS (Presenter) ; **Bing Zhang** PhD ; **Ming Li** ; **Xin Zhang** MD, MS ; **Yun Xu** ; **Bin Zhu** ; **Weibo Chen** MSc

#### PURPOSE

We explore the metabolic changes in the head, body and tail of hippocampal in Alzheimer's disease (AD) compared with normal control. We also investigate the distribution rules of metabolites concentration among different parts of the hippocampus for more accurate clinical diagnosis of AD.

#### METHOD AND MATERIALS

Thirty patients with AD and 30 cognitively normal person (CN) were scanned by a 3.0 T magnetic resonance (MR) by Multivoxel proton spectroscopy (Achieva, Philips Medical Systems, Netherlands). The 8channels-HEAD coil was employed. The data was processed by commercially available postprocessing workstation (Extended Workspace (EWS), Philips Medical Systems, Netherlands). The hippocampus was divided equally into three parts (head, body and tail). N-acetylaspartate (NAA)/creatine (Cr), myoinositol (MI)/Cr and MI/NAA ratio were calculated separately from each part. We compared with each metabolites concentration data of AD and CN groups and analyzed the anteroposterior metabolic profile in hippocampus.

#### RESULTS

The mean value of NAA/Cr is decreased and that of MI/Cr, MI/NAA are elevated in the bilateral hippocampi and hippocampal body and tail in AD group ( $p < 0.01$ ). MI/NAA in the head of left hippocampus is also increased statistically ( $p < 0.01$ ). Fig.1 shows NAA/Cr in the bilateral hippocampi from head to tail have the gradually rising trend ( $p < 0.01$ ) and MI/NAA gradually declines in CN group ( $p < 0.01$ ). MI/Cr in CN group and each metabolite concentration in AD group have no anteroposterior metabolic heterogeneity in bilateral hippocampil. (Fig.1).

#### CONCLUSION

The anteroposterior metabolic heterogeneity is dismissed in AD, which might be helpful on the early clinical diagnosis of AD.

#### CLINICAL RELEVANCE/APPLICATION

Application in the early diagnosis of AD.

## Physics (Quantitative Imaging II)

**Wednesday, 10:30 AM - 12:00 PM • S403B**

**PH** **CT** **BQ**

[Back to Top](#)

**SSK20 • AMA PRA Category 1 Credit**™:1.5 • **ARRT Category A+** Credit:1.5

#### Moderator

**John N Aarsvold** , PhD

#### Moderator

**Mats Danielsson** , PhD \*

### **SSK20-01 • Stability of Iodine Density Measurements with Spectral Detector CT in an Anthropomorphic Phantom of Varying Size: Comparison of Conventional and Virtual Mono-energy Images**

**Isaac Leichter** PhD (Presenter) ; **Tzvi Lipschuetz** ; **Zimam Romman** \* ; **Michal H Gabbai** MD ; **Jacob Sosna** MD \*

#### PURPOSE

Simultaneous dual-energy CT (DECT) data can be used to generate virtual mono-energy images at varying keV levels. These images include in-plane and object-size beam-hardening corrections. We aimed to evaluate the stability of iodine density measurements in virtual mono-energy images, using a phantom of two sizes.

#### METHOD AND MATERIALS

A customized water-equivalent anthropomorphic CT phantom (QRM, Moehrendorf, Germany) was scanned with and without a 2.5 cm extension ring to enable measurements at 2 phantom sizes (20x30 cm and 25x35 cm). The phantom included 8 tubes of 11.1 mm diameter, 2 tubes of 7.9 mm diameter, and 2 tubes of 6.4 mm diameter, all filled with 7 mg/ml iodine solution. The tubes were arranged 3.11 cm from the phantom center (Fig. 1). Conventional and 65 keV mono-energy images for both phantom sizes were obtained at 120 kVp and 500 mAs using a novel Spectral Detector CT (SDCT) prototype (Philips Healthcare, Cleveland, OH, USA). Variation between HU values of the iodine tubes was analyzed (paired T-test) for tube location, tube diameter, image type, and phantom size.

#### RESULTS

Mono-energy image HU values for the iodine tubes were independent of tube location, tube diameter, or phantom size. There was no significant difference ( $p=0.39$ ) in the standard deviation (SD) of HU values at different tube locations in the small-size phantom ( $SD=0.76\%$ ) vs. the large-size phantom ( $SD=0.88\%$ ). Variation of the HU values between tubes with different diameters was even smaller, 0.46% in the small-size and 0.64% and large-size phantom. Compared to mono-energy images, in the conventional images the variation of HU values at different tube locations was significantly higher ( $p$

#### CONCLUSION

The quality of virtual mono-energy images at 65 keV was superior to that of conventional images, with no beam-hardening effect. Mono-energy images demonstrated stable iodine density measurements, independent of phantom size, tube location, and tube diameter.

#### CLINICAL RELEVANCE/APPLICATION

Stable density measurements of contrast material, independent of patient size and ROI location, are important for integration of Spectral Detector CT into clinical practice.

### **SSK20-02 • The Size-based Emphysema Quantification Using Length Scale Analysis in 3D Volumetric Chest CT**

**Minho Lee** PhD (Presenter) ; **Namkug Kim** PhD ; **Joon Beom Seo** MD, PhD ; **Sang Young Oh** MD ; **Sang Min Lee** MD ; **Jae Seung Lee** ; **Yeon-Mok Oh** MD, PhD ; **Yongjun Chang**

#### PURPOSE

To propose a quantification method to classify emphysema clusters by size using length scale analysis in volumetric chest CT.

#### METHOD AND MATERIALS

Volumetric CT scans of twenty patients with chronic obstructive pulmonary disease (COPD) were performed by a 16-multi detector row CT scanner (Siemens Sensation 16) with in 0.75mm collimation. Using thresholding by -950 HU, emphysema index (EI) of low attenuation area (LAA) mask was evaluated. Based on these LAA masks, a length scale analysis to estimate each emphysema cluster's size was performed as follows. At first, Hole filling algorithm was performed on the emphysema mask and Gaussian low pass filter (LPF) with various size of kernel (15mm) was performed from large to small size, iteratively. Maximum density voxel in the each filtered volume was selected and dilated by the size of the kernel, which was regarded as the specific size emphysema mask. In this way, emphysema cluster with specific size range was classified and evaluated from the LAA mask. The accuracy of this classification result was evaluated and compared by an expert thoracic radiologist with 10 scale visual evaluation to determine size classifying accuracy and to determine probabilities for incorrect estimation. In addition, an artificial phantom study for mimicking emphysema and a COPD patients study were performed to evaluate the accuracy of this algorithm.

#### RESULTS

In phantom study, in case of sphere-like the shape of emphysema with various sizes from 1mm to 15mm, the method shows exact

estimation on every case. In the COPD patients, size based EI were  $3.48 \pm 1.97\%$ ,  $12.85 \pm 7.07\%$ ,  $7.07 \pm 7.88\%$ , and  $4.11 \pm 8.22\%$ , (size : 15mm), respectively. In addition, association study between blind visual evaluations of size based EI by an expert thoracic radiologist and our method showed all significant correlations  $r$  values : 0.499, 0.725, 0.768, 0.939, respectively) and probabilities for incorrect estimation were  $0.0 \pm 0.0\%$ ,  $0.67 \pm 0.2\%$ ,  $0.5 \pm 0.41\%$ , and  $1.17 \pm 0.26\%$  (size : 15mm), respectively. Overall underestimation and overestimation probabilities are 1.17% and 1.17%, respectively.

#### CONCLUSION

The methods proposed a robust emphysema clustering method, which could lead to new implication and progress of COPD

#### CLINICAL RELEVANCE/APPLICATION

This method is especially useful in measuring size based emphysema analysis and could be possible to evaluate etiology and progress of COPD using 3D volumetric chest CT.

### SSK20-03 • Virtual Non-contrast CT Using Dual Energy Spectral CT: Reproducibility of Calcium Mass for Coronary Calcium Scoring

**Myung Jin Chung MD \*** ; **Wan-Youk Kim** (Presenter) ; **Dong Ik Cha MD** ; **Sung Mok Kim MD** ; **Moon C Kim RT** ; **Kyung S Lee MD, PhD**

#### PURPOSE

To create virtual non-contrast CT, two-material decomposition is allowed from Spectral CT based on sinogram space, instead of three-material decomposition method allowed in image space. However, various virtual non-contrast images can be made from various material decomposition (MD) methods in spectral CT. We evaluated the feasibilities of three different virtual non-contrast (VNC) images derived from single source dual energy spectral CT compared to true non-contrast (TNC) image.

#### METHOD AND MATERIALS

This HIPAA-compliant study was approved by institutional review board and informed consent was provided from all patients. Twenty-four patients prospectively underwent non-contrast CT followed by contrast enhanced chest CT using single source fast kVp switching dual energy scan. Iodine eliminated images so called as VNC were reconstructed using two kinds of 2-material decomposition algorithms (MDW, material density-iodine/water; MDC, material density-iodine/calcium) and material suppression algorithm (MSI, iodine suppression image). Using third party workstation, semiautomatic calcium measurements were performed.

#### RESULTS

Quantified calcium scores (AJ score) from all three VNCs correlated well with that of TNC ( $R^2 = 0.95, 0.88, \text{ and } 0.88$  for MDW, MDC, and MSI, respectively). However correlation coefficients were less than 0.9 ( $C = 0.83, 0.62, \text{ and } 0.63$  for MDW, MDC, and MSI, respectively). Measured calcium volumes on VNCs also correlated well with that of TNC ( $R^2 = 0.94, 0.87, \text{ and } 0.90$  for MDW, MDC, and MSI, respectively), with correlation coefficients of 0.78, 0.59, and 0.63 for MDW, MDC, and MSI, respectively. Among the three VNCs, MDW correlated best with TNC.

#### CONCLUSION

VNC image from contrast enhanced CT using dual energy material decomposition/suppression is feasible for coronary calcium scoring. However, among various methods to make virtual noncontrast image from spectral CT, material quantifications are different depending on the decomposition methods. Furthermore, the absolute value on VNC tends to be smaller than that on TNC and should be considered with calibration.

#### CLINICAL RELEVANCE/APPLICATION

Absolute values of calcium scoring on VNC tend to be smaller than that on TNC and should be considered with calibration.

### SSK20-04 • Reproducibility of Imaging Features Computed from Same-day Repeat CT Scan Images Reconstructed at Different Acquisition Parameters

**Binsheng Zhao DSc** (Presenter) ; **Yongqiang Tan PhD** ; **Mingshi Wang** ; **Hyun-Ju Lee MD, PhD** ; **Chuanmiao Xie** ; **Jing Qi** ; **Ross C Ehmke BA** ; **Lawrence H Schwartz MD**

#### PURPOSE

Radiogenomics promises the genetic assessment of cancer patients with non-invasive radiographic imaging studies. To date, little attention has been paid to the sensitivity of imaging features to repeat scans and acquisition parameters. This study explored the reproducibility of imaging features computed on repeat CT scans reconstructed at different parameters.

#### METHOD AND MATERIALS

This study included a retrospective dataset containing 32 lung cancer patients, each having two same-day repeat CT scans and reconstructed into 6 image series, i.e., a combination of 3 slice intervals (5, 2.5 and 1.25mm) and 2 reconstruction algorithms [Lung (L) and Standard (S)]. Three radiologists independently used an in-house algorithm to segment 32 tumors ( $= 1 \text{ cm}$ ; one per patient) in all image series. 261 imaging features describing tumor size, histogram, shape, edge and texture were computed from the final tumor volumes, based on the common volumes obtained by 2 out of the 3 radiologists. The concordance correlation coefficient (CCC) was used to measure the agreement between each feature computed from two repeat scans reconstructed at the 6 series, i.e., 1.25L (first scan) and 1.25L (second scan), 1.25Sand1.25S, 2.5Land2.5L, 2.5Sand2.5S, 5Land5L and 5Sand5S.

#### RESULTS

Out of the 261 features, CCC of 32 features were  $= 0.95$  and of 169 features were  $= 0.75$  for all 6 series. Size and histogram features were highly reproducible for all parameter settings; shape index and boundary gradient strength were the least reproducible. For 2.5Sand2.5S re-scans, all run-length, GTDM and spatial correlation features had  $\text{CCC} = 0.95$ ; surprisingly, many features showed inferior reproducibility with 1.25Land1.25L re-scans, possibly due to noise.

#### CONCLUSION

Imaging parameters and repeat scans affect the reproducibility of imaging features to various degrees. Generally, the reproducibility of size, histogram, GTDM, run-length, spatial correlation, Laws', Gabor, wavelet, LoG and GLCM features (except 1.25Land1.25L for several features) at all parameter combinations ranged from acceptable ( $\text{CCC} = 0.75$ ) to excellent ( $\text{CCC} = 0.95$ ). The correlation of these features to gene expression warrants further investigation.

#### CLINICAL RELEVANCE/APPLICATION

Precautions should be taken with regard to CT imaging acquisition parameters when conducting radiogenomics studies.

### SSK20-05 • Improving CT Perfusion Image Quality Using Principal Component Analysis

**Timothy Pok Chi Yeung BSc** (Presenter) ; **Nathan De Haan** ; **Mark Dekaban** ; **Laura Morrison** ; **Lisa Hoffman** ; **Slav Yartsev** ; **Glenn S Bauman MD \*** ; **Ting-Yim Lee MSc, PhD \***

#### PURPOSE

Many CT perfusion (CTP) studies of small animal tumor models are performed using clinical CT scanner due to its availability, but the tradeoff between spatial resolution and image noise affects the quality of CT perfusion images. This study aimed to evaluate the ability of principal component analysis (PCA) in improving the contrast-to-noise ratio (CNR) of CTP images in a preclinical model of malignant glioma.

#### METHOD AND MATERIALS

Wistar rats ( $n = 8$ ) implanted with C6 glioma cells were scanned using CTP. Each CTP image set was filtered using 2, 4, 6, 8, and 10 principal components from PCA to result in 40 additional image sets. The noise level and CNR were used to quantify image quality in all



48 filtered and unfiltered image sets. The fractional residual information (FRI) was used to evaluate the amount of information loss after PCA filtering. Blood flow (BF), blood volume (BV), and permeability-surface area product (PS) before and after filtering were calculated. Noise level, CNR, BF, BV, and PS in the normal brain and tumor were expressed as mean  $\pm$  standard error of the mean. These metrics before and after filtering with different numbers of principal components were compared to evaluate the differences between the filtered and the unfiltered image sets.

#### RESULTS

PCA filtering significantly decreased noise level and increased CNR ( $p = 0.01$ ). An average of 26% (range, 11  $\diamond$  49%) of pixels in the tumor had information loss of  $\approx 5\%$  when filtering with only two principal components; this percentage decreased to an average of 1% (range, 0  $\diamond$  3%) with four or more components. Normal brain BV and PS were significantly different than the values in the tumor ( $p < 0.01$ ) without or with PCA filtering (using 4 or more principal components). Normal brain and tumor BF values were not significantly different without PCA filtering, but they became significantly different after filtering with 4 principal components ( $p = 0.03$ ).

#### CONCLUSION

PCA filtering improved the CNR in CTP studies. Four or more principal components are required to filter the CTP source images without substantial loss of information leading to higher contrast between tumor and normal brain tissue in BF maps.

#### CLINICAL RELEVANCE/APPLICATION

Lowering radiation exposure can lead to deterioration of CNR in CTP studies. PCA improves CNR to allow repeated ultralow dose CTP studies for assessing treatment response in the clinical setting.

### SSK20-06 • Image Registration for Prostate MR Guided Biopsy Using Automated Biomechanical Modeling

**Wendy Van De Ven** MSc (Presenter) ; **Nico Karssemeijer** PhD \* ; **Jelle O Barentsz** MD, PhD ; **Henkjan Huisman** PhD \*

#### PURPOSE

To investigate the effect of extending a non-rigid surface-based registration method with biomechanical modeling for prostate MR guided biopsies on the target registration error (TRE) using internal reference landmarks. The method is fully automated and we compare accuracy to previous results obtained with manual optimization of parameters in every patient.

#### METHOD AND MATERIALS

The accuracy of a novel non-rigid registration method involving biomechanical modeling to account for deformations inside the prostate was determined. While MR-TRUS registration is the ultimate goal, we used MR guided MR biopsy imaging data from six consecutive patients for this evaluation. The data included T2-weighted images (0.8x0.8x3.0 mm) before and after insertion of a needle guide causing deformation of the prostate. The needle guide had an orientation and dimension comparable to a transrectal ultrasound (TRUS) probe. The prostate in the two images was segmented and corresponding surface meshes were generated in both images by assuming identical prostate orientations. Next, a tetrahedral volume mesh was generated from the image before needle insertion. Prostate deformations due to needle insertion were simulated using the surface displacements as boundary condition. A 3D thin-plate spline deformation field was calculated by registering the mesh vertices. The TRE was defined as the Euclidean distance between registered and reference landmark position and was calculated for 45 reference landmarks manually annotated in both T2-weighted images. The results of this automated method were also compared to previous results obtained with manual optimization.

#### RESULTS

The median TRE of the automated surface-based registration method with biomechanical regularization was 2.21 mm (range 0.55-7.32 mm), which was significantly lower than a median TRE of 3.02 mm (range 0.85-7.95 mm) obtained without biomechanical regularization ( $PP=0.10$ ).

#### CONCLUSION

Non-rigid surface-based image registration extended with biomechanical modeling can be automated and improves the registration accuracy for prostate MR guided biopsies.

#### CLINICAL RELEVANCE/APPLICATION

The automated surface-based registration method extended with biomechanical modeling is applicable to MR-TRUS registration and can help to improve effectiveness of MR guided TRUS biopsy procedures.

### SSK20-07 • Validity of Myocardial Perfusion Asynchrony Measurements

**Andrew Van Tosh** MD \* ; **Nathaniel Reichel** MD ; **Christopher J Palestro** MD ; **Kenneth Nichols** PhD (Presenter) \*

#### PURPOSE

Left ventricular (LV) asynchrony can be quantified by both gated blood pool (BP) and myocardial perfusion (MP) tomography. A concern regarding MP phase measurements is their reliance on tracking myocardial walls in cases of severely reduced MP, for which counts are low. PET data are acquired in gated list mode and both BP and MP data are available for the same pts. To test validity of MP phase measurements for severely decreased MP we compared MP to BP phase measurements, which are not affected by decreased MP.

#### METHOD AND MATERIALS

Data were analyzed retrospectively for 67 pts (42 males; 23 females; 71 $\pm$ 12 yrs) with suspected heart disease evaluated by  $^{82}\text{Rb}$  PET/CT. Data were collected in gated list mode and rebinned into BP tomograms of tracer imaged during the first pass transit through the heart chambers, and separately into MP tomograms of tracer imaged during equilibrium. For BP PET data LV contraction phases were computed for each of 17 LV segments. Excluding the 3 most basal-septal segments to ensure LV cavity sampling the bandwidth (BW) of contraction phases were computed, defined as % of the R-R interval accounting for 95% of LV regional contractions. MP tomograms were analyzed by commercial algorithms, which computed summed rest scores (SRS) indicating severity of MP defects, and MP phase BW derived from phases of maximum count brightness corresponding to regional end-systole at each voxel at locations identified by algorithms as corresponding to the myocardial wall.

#### RESULTS

37 pts had negligible defects (SRS = 4) with BP phase BW = 16 $\pm$ 8%, lower than the 30 pts with significant MP defects (SRS > 4) (33 $\pm$ 22%,  $p = 0.0001$ ). BP and MP phase BW were similar for all pts (24 $\pm$ % versus 26 $\pm$ 16%,  $p = 0.49$ ), pts with SRS = 4 (16 $\pm$ 8% versus 19 $\pm$ 9%,  $p = 0.15$ ), and pts with SRS > 4 (33 $\pm$ 23% versus 36 $\pm$ 19%,  $p = 0.50$ ). BP and MP phase BW correlated significantly and similarly with SRS ( $r = 0.59$ ,  $p < 0.0001$  and  $r = 0.61$ ,  $p < 0.0001$ ), consistent with greater amounts of asynchrony being related to more severe myocardial damage. Differences between BP and MP phase BW had no correlation to SRS ( $r = 0.04$ ,  $p = 0.75$ ). Thus, severe MP defects had no deleterious effect on MP phase quantitation.

#### CONCLUSION

Detection of LV asynchrony by phase measurements derived from gated  $^{82}\text{Rb}$  PET/CT tomograms are robust and reliable, regardless of severity of MP defects.

#### CLINICAL RELEVANCE/APPLICATION

It is justifiable to include scintigraphic asynchrony measurements in forming clinical impressions for pts exhibiting severe MP defects.

### SSK20-08 • Classification of Osteoarthritic and Healthy Chondrocyte Patterns in Human Patellar Cartilage on Phase Contrast Computed Tomography through Topological and Geometric Features

**Mahesh Nagarajan** (Presenter) ; **Paola Coan** ; **Markus B Huber** PhD ; **Paul C Diemoz** PhD ; **Christian Glaser** MD ; **Axel Wismueller** MD, PhD

#### PURPOSE

Phase-contrast X-ray computed tomography (PCI-CT) has been demonstrated at achieving soft-tissue contrast with micrometer scale resolution while imaging cartilage. This study proposes to quantitatively evaluate the performance of topological and geometrical approaches in characterizing chondrocyte patterns as observed in PCI-CT of human patellar cartilage as healthy or osteoarthritic.

#### METHOD AND MATERIALS

Five osteochondral cylinders (7 mm diameter, 3 osteoarthritic, 2 healthy) extracted from post-mortem human patellae were subject to PCI-CT at 26 keV (European Synchrotron Radiation Facility, Grenoble, France). From reconstructed CT images of the cartilage, 842 regions of interest (ROI) of size 51x51 pixels capturing chondrocyte patterns were then annotated in the radial zone of the cartilage matrix from high resolution images (voxel size:  $8 \times 8 \times 8 \mu\text{m}^3$ ). Two texture analysis techniques - (1) Scaling Index Method (SIM), that estimates local scaling properties and (2) Minkowski Functionals (MF), that evaluates topological properties, were used to extract features from the ROIs. Random sub-sampling cross-validation was utilized in optimizing a support vector regression model with a radial basis function kernel for the classification task. Performance was measured using area under the Receiver-Operator Characteristic (ROC) curve (AUC) for each feature.

#### RESULTS

With the experimental conditions used in this study, the best classification performance was observed with the SIM histogram ( $0.95 \pm 0.06$ ) which was significantly better than the performance achieved by all Minkowski Functionals - Area ( $0.61 \pm 0.07$ ), Perimeter ( $0.85 \pm 0.10$ ) and Euler Characteristic ( $0.88 \pm 0.09$ ).

#### CONCLUSION

Our study investigates the use of advanced texture analysis techniques in images acquired with PCI-CT to quantitatively evaluate their ability in distinguishing between healthy and osteoarthritic cartilage. Our results show that geometrical features derived from SIM can capture differences in chondrocyte patterns annotated in the radial zone of knee cartilage matrix extracted from healthy and osteoarthritic specimens with high accuracy, and significantly outperform topological features derived from MF at the same task.

#### CLINICAL RELEVANCE/APPLICATION

Computer-aided feature analysis can distinguish between osteoarthritic and healthy chondrocyte patterns in knee cartilage as seen on Phase Contrast CT imaging studies with micrometer scale resolution.

### SSK20-09 • Analysis of Treatment Response of Bladder Cancers on CT Scans: Comparison of Computerized Volume Estimation with WHO and RECIST Criteria

**Lubomir M Hadjiiski** PhD (Presenter) ; **Alon Z Weizer** MD ; **Ajjai S Alva** MD ; **Elaine M Caoili** MD, MS ; **Richard H Cohan** MD \* ; **Heang-Ping Chan** PhD ; **Kenny H Cha** BEng ; **Stephen Dailey**

#### PURPOSE

To evaluate the accuracy of our Auto-Initialized Cascaded Level Set (AI-CALS) 3D segmentation system, the WHO and the RECIST criteria in estimation of treatment response of bladder cancer using CT scans.

#### METHOD AND MATERIALS

The AI-CALS system is designed to extract 3D lesion boundary based on level sets. The system uses as input an approximate bounding box for the lesion of interest. With IRB approval, pre- and post-chemotherapy treatment CT scans of 20 patients with bladder cancers were collected retrospectively for this preliminary study. For all cases, cystectomy was performed after treatment and the disease outcome was available as reference standard of treatment response. 35% of patients had pT0 disease (complete response) at cystectomy. A radiologist marked 20 temporal pairs of primary site cancers and also manually outlined full 3D contours on both the pre- and post-treatment scans using a GUI. For all cancers, following WHO and RECIST criteria two radiologists measured the longest diameter and its perpendicular on the pre- and post-treatment scans. Receiver operating characteristic (ROC) analysis was performed and the area under the ROC curve (AUC) was calculated to estimate the accuracy for prediction of pT0 stage (complete response) at cystectomy by the manual (3D), AI-CALS (3D), WHO (2D), and RECIST (1D) methods.

#### RESULTS

For the 20 cancers, the average pre- and post-treatment volumes from radiologist's segmentation were 36.0 and 17.6  $\text{cm}^3$ , respectively. The AUC for prediction of pT0 disease at cystectomy was  $0.68 \pm 0.13$  for the AI-CALS compared to  $0.72 \pm 0.11$  for the manual segmentation. The difference was not significant. Prediction of pT0 disease using the RECIST criteria by two radiologists was lower than the two 3D methods with AUCs of  $0.59 \pm 0.14$  and  $0.66 \pm 0.12$ , respectively. Prediction of pT0 disease using the WHO criteria by the two radiologists had AUCs of  $0.50 \pm 0.14$  and  $0.56 \pm 0.12$ , respectively, which were lower than all other methods.

#### CONCLUSION

The 3D pre- and post-treatment volume estimates obtained by manual radiologist segmentation and AI-CALS provided more accurate depiction of the irregular 3D tumor shapes and volume changes compared to the 1D (RECIST) and 2D (WHO) estimates.

#### CLINICAL RELEVANCE/APPLICATION

For tumors with irregular shape such as bladder cancers the 3D automated segmentation has the potential to accurately and efficiently determine tumor volume and response to treatment.

### Physics (Quantitative Imaging III)

Wednesday, 03:00 PM - 04:00 PM • N228

PH BQ

[Back to Top](#)

SSM19 • AMA PRA Category 1 Credit™:1 • ARRT Category A+ Credit:1

**Moderator**  
**Bram Van Ginneken**, PhD  
**Moderator**  
**Seungrong Cho**, PhD

### SSM19-01 • Automated Pulmonary Nodule Elastometry as a Potential Diagnostic Tool

**Mohammadreza Negahdar** (Presenter) ; **Billy W Loo** MD, PhD \* ; **Maximilian Diehn** MD, PhD \* ; **Dominik Fleischmann** MD \* ; **Lu Tian** ; **Peter G Maxim** PhD

### SSM19-02 • Multisite Quantitative Evaluation of the Accuracy and Precision of a Novel Test Bolus-based CT Angiography Contrast-enhancement Prediction Algorithm

**Johannes G Korporaal** PhD (Presenter) \* ; **Andreas H Mahnken** MD \* ; **Jiri Ferda** MD, PhD ; **Jorg Hausleiter** ; **Bernhard Schmidt** PhD \* ; **Thomas G Flohr** PhD \*

#### PURPOSE

To quantify the accuracy and precision of a novel test bolus-based CT angiography (CTA) contrast-enhancement prediction (CEP) algorithm by comparing the amplitude, timing and curve shape of the predicted and true enhancement in the descending aorta (DAo).

#### METHOD AND MATERIALS

After routine clinical scanning according to local scan and injection protocols, from three hospitals a total of 72 (3x24) anonymized cardiac CTA exams were collected for retrospective analysis. Patients (30f/42m) had a median age and body weight of respectively 74y (range 31-81) and 79kg (range 61-125).

Since existing data were retrospectively analyzed, injection protocols, image acquisitions and reconstructions differed substantially between hospitals. Test bolus (TB) scans were performed at the level of the pulmonary artery, after which the TB signal in the DAo was processed by the CEP-algorithm. This novel algorithm takes the injection protocols and kV settings of the TB and CTA scan into account, and uses population-averaged information to predict the CTA enhancement. The true enhancement was extracted from the CTA scan with a 6mm ROI along the DAo-centerline. For each patient, the relative errors in the accuracy and precision were calculated. Deviations in the amplitude were quantified with Bland-Altman analysis and shape differences with the mean absolute error (MAE) of the normalized curves. The predicted curve was shifted along the true enhancement to find the timing error, which is the time shift for which the MAE is minimal.

#### RESULTS

Although differences in injection and acquisition protocols existed, no significant differences in the precision and accuracy were found between the hospitals. For the entire patient group, the predicted enhancement has an average deviation of  $1.0 \pm 15.4\%$  in the amplitude,  $0.1 \pm 1.8$ s in the timing, and  $5.5 \pm 2.4\%$  in the curve shape.

#### CONCLUSION

No clinically relevant offsets in the timing and amplitude of the predicted enhancement exist, and the curve shape corresponds well with the true enhancement. With its excellent accuracy and good precision, this algorithm has high potential for CTA scan timing and injection protocol optimization.

#### CLINICAL RELEVANCE/APPLICATION

Most efficient usage of contrast agent, and thus maximum CNR in CTA images, can potentially be achieved by using this algorithm for scan timing and injection protocol optimization.

### SSM19-03 • Detecting Enhancing Lesions in Multiple Sclerosis Patients Using Visual Texture Analysis on Brain T2-weighted MR Images: A Feasibility Study

Nicolas Michoux (Presenter) ; Alain Guillet ; Denis J Rommel MD ; Thierry P Duprez MD

#### CONCLUSION

On-going research aims at assessing the performance of a texture-based decision system from T2 images acquired before Gd injection which, if effective, may offer an alternative to detect Gd-enhancing lesions in MS patients when Gd injection is contra-indicated or impossible. **References**

1. NMR Biomed 2010;23:865-72.
2. Am J Neuroradiol 2010;31:809 -16.
3. IEEE Trans Syst Man Cybern 1973;SMC-3:610-621.
4. IEEE Trans Image Process 1998;7:1602-9.

#### Background

MRI is the most sensitive technique for detecting multiple sclerosis (MS) lesions. While DCE-MRI is routinely used for evaluating the inflammatory activity, diffusion MRI is controversial (1). Texture analysis has been used with success to investigate pathological brain tissues (2). This study assesses the feasibility of **texture analysis on T2-weighted MRI** to detect changes within white matter in MS patients.

#### Evaluation

##### Patients

This retrospective study was approved by our institutional ethical committee. From post-Gd T1-weighted imaging, 44 enhancing lesions (EL), 37 non-enhancing lesions (non-EL) and contra-lateral regions in normal appearing white matter (NAWM) were identified in 21 patients diagnosed with MS.

##### MRI

Examinations were performed using a 3.0T whole body imaging system and a SENSE head 32 receiving coil. FSE T2, FSE FLAIR, EPI diffusion and 3D post-Gd GRE T1 sequences were acquired.

##### Computing

A 21-components vector (20 Textons + ADC) was derived for each region from grey level co-occurrence and run length matrices (3, 4).

##### Results

Differences between EL/non-EL and NAWM were statistically significant ( $p < 0.05$ ) except for one Texton. Differences between EL and non-EL were significant except for one Texton and ADC. ROC analysis showed a performance of Textons and ADC ranging from moderate ( $AUC_{ADC} = 0.58$ ) to good ( $AUC_{Texton} = 0.84$ ). A good predictive model of EL ( $Se = 88\%$ ,  $Sp = 81\%$ ) was achieved based on a partial least squares classifier and a set of 6 Textons.

#### Discussion

Textons values result from the structural characteristics of the tissues and thus are affected by pathologic changes. Applying texture analysis to T2-weighted MRI is feasible and may help differentiating EL from non-EL in MS.

### SSM19-04 • Comparison Study of Spectral Imaging Associated with Iso-Osmolar Contrast Media on Vascular Evaluation in Rabbits

Pan Liang (Presenter) ; Jianbo Gao MD

#### PURPOSE

To compare the vascular enhancement between spectral imaging associated with iso-osmolar contrast media and traditional 120kVp scans with high-osmolar contrast media on vessel.

#### METHOD AND MATERIALS

6 adult New Zealand rabbits of similar age and size were enrolled in this study. Each rabbit underwent two epigastric CT protocols and interval time among every protocol is 24 hours. Protocol A: traditional CT gastric angiography (CTGA) with Iopromide 350 (2ml/kg, 1.5ml/s). Protocol B: spectral CT enhanced sequence with Iodixanol 270 (2ml/kg, 0.5ml/s). Images of spectral CT series will be reconstructed at 55 keV. Signal intensity, image noise, signal-to-noise ratio (SNR) and contrast-to-noise ratio (CNR) measured within the parallel groups in aortaventralis and left gastric artery were calculated and compared. Overall diagnostic quality of images were evaluated using a five-point scale. Comparison of percentages of diagnostic images (score=3) were performed.

#### RESULTS

Compared with the traditional CTGA scans, 55 keV images demonstrated significantly higher signal intensity ( $p=0.000$ ) in aortaventralis and left gastric artery, and inferior noise ( $p=0.029$ ) only in left gastric arteries. The SNR and CNR of the 55 keV images had no significant differences from that of the traditional CTGA images ( $23.33 \pm 5.54$  vs.  $24.45 \pm 1.65$ ,  $P=0.646$ ;  $18.19 \pm 4.28$  vs.  $17.74 \pm 1.03$ ,  $P=0.806$ ). Also, spectral CT images provide better overall image quality scores ( $p>0.05$ ), the proportion of diagnostic images was higher (p

#### CONCLUSION

Spectral imaging associated with iso-osmolar contrast media of Iodixanol 270 can provide excellent gastric vascular images at 55 keV at equivalent radiation of traditional CTGA scans. In the meanwhile, contrast media dose can be greatly reduced.

#### CLINICAL RELEVANCE/APPLICATION

The association of iso-osmolar contrast media with spectral imaging can greatly reduce the amount of iodine while maintaining high quality of vascular images.

### SSM19-05 • Assessment of a New Image-based Method of Monoenergetic Imaging

Katharine Grant PhD (Presenter) \* ; Bernhard Krauss PhD \* ; Martin U Sedlmair MS \* ; Thomas G Flohr PhD \* ; Christian

PURPOSE

Following the trend of low dose imaging, concerns regarding the detectability of low contrast lesions have been growing. The goal of this research is to evaluate if a new image-based algorithm (mono+) for monoenergetic imaging can improve the contrast-to-noise ratio and conspicuity of these low contrast objects.

METHOD AND MATERIALS

Three different anthropomorphic dual energy phantoms of different size representing a small medium and large phantoms containing 3 different iodine inserts (known values of 20, 50 and 100HU @120kV) were scanned at 3 different dose levels (full, half and quarter dose). Images were reconstructed at both 40keV and 70keV using both a standard image-based monoenergetic algorithm and mono+ at all three dose levels, resulting in 12 different images sets per phantom size. Hounsfield units and standard deviation (noise) measurements were recorded from ROIs placed within the three inserts and one background for each image set. To calculate monoenergetic images, similar to raw data approaches a two material decomposition into base materials is performed. Based on tabulated data, from the two material images, monoenergetic (keV) images can be calculated. Since by theory, any decomposition leads to an increase in noise, keV images of very low or high energy (e.g. 40 keV or 190 keV) show a substantial noise increase. Our newly developed method to calculate keV images suppresses this increase by applying a regional analysis-dependent frequency-based recombination of the high signal at lower energies and the superior noise properties at medium energies.

RESULTS

The mono+ algorithm resulted in a greatly improved image quality for both the 40 keV (Fig 1.) and 70 keV. Both keV level displayed lower image artifacts and a significant reduction in image noise. CNR improved for all inserts using mono+ compared to the standard algorithm. For example for the small phantom CNR could be improved for the 40 keV by about 50%.

CONCLUSION

Mono+ improves CNR and low contrast lesion conspicuity in particular for low dose imaging, independent of phantom size.

CLINICAL RELEVANCE/APPLICATION

Mono+ provides significantly increased CNR, resulting in increased lesion conspicuity. These improvements should allow for added diagnostic confidence, higher throughput and reduced reader fatigue.

**SSM19-06 • Automated and Optimized Imaging Simulation Platform for Virtual Clinical Trials of Breast Cancer Screening**

**Predrag R Bakic** PhD (Presenter) \* ; **Andrew D Maidment** PhD \* ; **Joseph H Chui** MSc \* ; **Ali N Avanaki** PhD \* ; **Cedric Marchessoux** \* ; **David D Pokrajac** PhD ; **Kathryn S Espig** MSc \* ; **Tom Kimpe** PhD \* ; **Albert Xthona** \* ; **Miguel A Lago** ; **Varsha Shankla**

PURPOSE

We have developed an automated pipeline for the simulation and analysis of x-ray breast images. The simulation has been used to conduct Virtual Clinical Trials (VCTs) of digital mammography and digital breast tomosynthesis imaging.

METHOD AND MATERIALS

An automated pipeline has been developed (in C++ and OpenCL) that includes simulation of the normal breast anatomy and lesions (e.g., microcalcification clusters), breast deformation, image acquisition, image processing, display modeling, and image analysis using model observers. The breast anatomy is simulated using an octree-based recursive partitioning method, which allows for fast simulation of a large number of phantoms with very small voxel size. Clusters of microcalcifications (derived from stereomammographic clinical images) are added after identifying potential locations of cluster insertion based upon the convolution of simulated dense tissue regions with the minimal bounding box surrounding the cluster. The phantom deformation resulting from mammographic compression is simulated using a finite element model. Images of the deformed breast are then synthesized using a fast ray tracing method. Image processing is applied to create DICOM images and display modeling takes into account medical monitors effects including temporal effects and an accurate browsing speed simulation. Detection of microcalcifications is estimated using 2D, 2D+time, and 3D channelized Hotelling observers equipped with the spatio-temporal contrast sensitivity function of the human visual system in response to the simulated display of images.

RESULTS

The developed pipeline supports the simulation of 2D and 3D breast imaging. The GPU implementation has resulting in significant acceleration, with the simulation duration at each pipeline stage now being on the order of seconds. For example, compressed versions of 450ml breasts with voxel size of 200 microns are generated at a rate of more than 30 per minute. Extensive pipeline testing has demonstrated that detection results follow the same trends as human observers in terms of contrast and browsing speed.

CONCLUSION

We have developed an automated and accelerated pipeline for performing VCTs of breast imaging.

CLINICAL RELEVANCE/APPLICATION

VCTs have role as a preclinical optimization and validation tool prior to clinical trials of new imaging equipment.

**Quantitative Imaging: Volumetric CT as a Biomarker for Disease**

Thursday, 08:30 AM - 10:00 AM • N226

PH CT BQ

[Back to Top](#)

**RC625 • AMA PRA Category 1 Credit™:1.5 • ARRT Category A+ Credit:1.5**

**Director**

**Michael F McNitt-Gray**, PhD \*

**RC625A • Why is Quantitative Imaging (Tumor Volumes) Needed in Oncologic Imaging**

**Lawrence H Schwartz** MD (Presenter)

LEARNING OBJECTIVES

1) To understand the role and value of quantitative volumes in oncology. 2) To understand the challenges associated with quantitative volume calculations in oncology.

**RC625B • Understanding Measurement Variation: Lessons Learned from Phantom Studies**

**Nicholas Petrick** PhD (Presenter)

LEARNING OBJECTIVES

1) To review how changes in CT acquisition parameters and nodule characteristics affect measurement error. 2) To review how phantom studies can be used to systematically probe, identify and potentially minimize measurement error and improve our ability to perform quantitative CT imaging. 3) To understand which CT and analysis parameters should be held constant across multiple CT scans, if at all possible, to optimize the evaluation of a patient's response to therapy.

ABSTRACT

In this refresher course, we will update the audience on the methods and results obtained from various phantom studies developed to assess both absolute lesion size measurements and change over time measurements involving both automated and semi-automated lesion sizing tools.

## RC625C • Variability in CT Measurement of Tumor Volumes and Its Impact on Response Assessment

**Binsheng Zhao** DSc (Presenter)

### LEARNING OBJECTIVES

1) Demonstrate the feasibility of computer-aided (tumor) volume measurement and explain its potential to improve conventional response assessment in oncology. 2) Familiarize the audience with sources of variation in measuring tumor volume and tumor volume change. 3) Discuss the need for standardizing both imaging and measurement techniques in the interpretation of tumor measurement and thus in response assessment.

### ABSTRACT

Volumetric CT (VolCT) shows potential as a better method to assess tumor response, especially early response, to therapy than the conventional diameter methods. This refresher course will first show how the volumes of solid tumors can be accurately and practically obtained with the help of computer software, then discuss the factors that can affect measurement reproducibility of in vivo tumors during image acquisition and tumor measurement. By becoming acquainted with a well-designed series of (clinical) variability studies, the audience will learn the magnitudes of variability that can occur in the measurement of tumor volumes, as well as in tumor diameter(s).

## Chest Series: Hot Topics in Chest Imaging: Emerging Technologies and Clinical Applications

Thursday, 08:30 AM - 12:00 PM • E351

[CT](#) [BQ](#) [CH](#)

[Back to Top](#)

**VSCH51** • AMA PRA Category 1 Credit™:3.25 • ARRT Category A+ Credit:3.75

### Moderator

**Jonathan G Goldin**, MBChB, PhD

### Moderator

**Jens Bremerich**, MD

## VSCH51-01 • Quantitative Imaging: Lung Nodule Analysis

**Jane P Ko** MD (Presenter)

### LEARNING OBJECTIVES

1) To increase understanding of the advancements in computer-assisted quantification of lung nodule size and features. 2) To enhance knowledge of the challenges pertaining to nodule evaluation techniques and their clinical applications.

### ABSTRACT

## VSCH51-02 • Quantitative Imaging: COPD and Airways

**Alexander A Bankier** MD, PhD (Presenter) \*

### LEARNING OBJECTIVES

1) To present up-to-date imaging techniques for assessing airways and lung parenchyma in patients with COPD. 2) To present quantitative imaging approaches to COPD. 3) To discuss the clinical impact of quantitative imaging, notably for phenotyping patients with COPD.

### ABSTRACT

This presentation will present current imaging techniques used to assess changes in lung parenchyma and airways in patients with COPD. It will discuss the importance of a quantitative approach to image COPD, notably as to phenotyping patients with this disease. Finally, potential future trends in imaging COPD will be discussed.

## VSCH51-03 • Reproducibility of Automated Three-dimensional Airway Wall Thickness Measurements in Thoracic Computed Tomography and Influence of Inspiration Depth

**Michael Schmidt** MSc ; **Eva M Van Rikxoort** PhD ; **Onno M Mets** MD ; **Pim A De Jong** MD, PhD ; **Jan-Martin Kuhnigk** PhD, MS (Presenter) ; **Matthys Oudkerk** MD, PhD ; **Harry De Koning** \* ; **Bram Van Ginneken** PhD

### PURPOSE

Pathological changes of the airways are strongly associated with lung function impairment in chronic obstructive pulmonary disease (COPD). We investigate the reproducibility of CT-based airway dimension measurements and their dependence on the level of inspiration.

### METHOD AND MATERIALS

We analyzed 740 pairs of low-dose chest CT scans of male (former) smokers who were recalled for a three-month follow up scan in the NELSON lung cancer screening trial. Given the slow progression of COPD, we expect that no significant COPD-related changes in airway dimensions should exist between baseline and three month follow-up. Each scan was analyzed fully automatic using CIRRUS Lung 13.03 and airway wall thickness (Pi10) and lung volume were recorded. Subjects where processing failed for any of the two scans were excluded for analysis (n=32). First, we analyzed the differences in airway wall thickness measurements for all scan pairs. Next, we determined reproducibility in absence of significant changes in inspiration depth by repeating the analysis for the subset of scans where the difference in lung volume between baseline and follow-up was less than 200ml (n=312). Finally, we investigated the correlation between difference in inspiration depth and airway wall thickness measurements, established a linear correction model for the airway measurements and analyzed differences for corrected measurements.

### RESULTS

### CONCLUSION

Changes in level of inspiration are significantly associated to changes of airway wall thickness and accounted for approximately 25% of the total differences between baseline and follow-up measurements.

### CLINICAL RELEVANCE/APPLICATION

Inspiration depth should be controlled or linear correction should be applied for monitoring of airway wall thickness. This may help to better differentiate COPD subtypes in chest CT scans.

## VSCH51-04 • Quantitative Imaging: Interstitial Lung Disease

**Jonathan G Goldin** MBChB, PhD (Presenter)

### PURPOSE

The learning objectives are the following: Approaches to Quantitative Imaging in ICD, Quantitative Imaging in Clinical Trials as a Biomarker and Quantitative Imaging in Clinical Practices.

## **VSCH51-05 • Phenotypes of Pulmonary Fibrosis in the MUC5B Promoter Site Polymorphism (SNP)**

**Jonathan H Chung MD (Presenter) \* ; Ashish Chawla MD, MBBS ; David Mckean ; Janet Talbert ; Anna Peljto ; David A Lynch MBBCh \* ; Marvin I Schwarz MD ; David Schwartz**

### **PURPOSE**

The purpose of this study was to determine the variation of phenotypic manifestations of pulmonary fibrosis with regard to the MUC5B promoter site (rs35705950) polymorphism, which has been strongly associated with IPF and familial pulmonary fibrosis.

### **METHOD AND MATERIALS**

HRCT scans of 1,764 subjects were scored as part of a genome-wide association study. Two thoracic radiologists independently evaluated the HRCT scans. Discrepancies were resolved by a third thoracic radiologist. All patients were genotyped specifically for the rs35705950 SNP. Two-tailed Fisher exact or Chi-square tests and t-test or one-way ANOVA tests were used to compare proportions and means, respectively. A p-value of 0.05 was considered statistically significant.

### **RESULTS**

The major and minor alleles at the rs35705950 SNP are guanine (G) and thymine (T), respectively. There were 670 GG, 958 GT, and 136 TT subjects. This distribution showed significant departure from Hardy-Weinberg equilibrium (p

### **CONCLUSION**

Polymorphisms at the MUC5B promoter site are associated with different phenotypes of lung fibrosis on chest CT.

### **CLINICAL RELEVANCE/APPLICATION**

Integration of imaging and genotypic information may provide valuable information regarding patient prognosis and optimal treatment in fibrotic lung disease.

## **VSCH51-06 • Dual Energy CT: Emerging Applications**

**Ioannis Vlahos MRCP, FRCR (Presenter) \***

### **LEARNING OBJECTIVES**

1) To understand the current potential for dual energy CT in thoracic imaging. 2) To review select current literature supporting the use of dual energy imaging. 3) To highlight emerging areas of clinical evaluation.

## **VSCH51-07 • Dual-energy CT with Reduced Iodine Load: A New Option for Standard Chest CTA in Patients with Superior Vena Cava Syndrome**

**Sofiane Bendaoud MD (Presenter) ; Olivier Vanaerde MD ; Francesco Molinari MD ; Arianna Simeone MD ; Emanuela Algeri MD ; Martine J Remy-Jardin MD, PhD \***

### **PURPOSE**

To evaluate the interpretive conditions for analysis of all thoracic circulations on a chest CT angiographic examination optimized for suspicion of superior vena cava syndrome (SVCS).

### **METHOD AND MATERIALS**

41 patients with suspected SVCS underwent a dual-source, dual-energy CT angiographic examination of the chest with bi-brachial administration of a low-concentration contrast agent (160 mg iodine /mL). From each data set, 3 series of images were systematically reconstructed: (a) the 2 polychromatic series acquired at 80 and 140 kV; and (b) the fused images from both tubes, with a weighting factor of 0.6 (i.e., averaged images equivalent to images acquired at 120 kV). On each series of images, a quantitative and qualitative analysis of 3 anatomical compartments was performed, including the: (a) superior vena cava; (b) pulmonary arteries; and (c) aorta. In the quantitative evaluation: (a) ROIs were placed in each vessel-of-interest to measure mean  $\pm$ SD attenuation; (b) the signal-to-noise (SNR) and contrast-to-noise (CNR) ratios were calculated. Qualitative analysis evaluated the presence and severity of streak artifacts at the level of 3 nodal stations (i.e., 2R, 4R, 10R). On a patient-by-patient basis, the number of series to-be-interpreted for optimal analysis of all anatomical regions was then assessed.

### **RESULTS**

Averaged images provided (a) a good to excellent level of opacification within the SVC (n=40 ; 98%) without artifacts at the level of 2R (n=26 ; 63%), 4R (n=40 ; 98%) and 10 R (n=41 ; 100%) ; (b) analyzability of pulmonary arteries down to the subsegmental level (n=31 ; 76%) ; and (c) a good to excellent opacification of the aorta (n=35; 85%). In 29 patients (29/41; 71%), averaged images alone provided optimal evaluation of all vascular compartments; in 12 patients (12/41; 29%), they had to be completed by images at 140 kV (n=6) to suppress artifacts at the level of the nodal station 2R and/or images at 80 kV (n=10) to improve the CNR at the level of subsegmental pulmonary arteries and/or the aorta.

### **CONCLUSION**

Dual-energy CT enables combination of optimal evaluation of SVCS and diagnostic image quality at the level of the other thoracic circulations.

### **CLINICAL RELEVANCE/APPLICATION**

On dual-energy CT angiograms obtained with low-concentration contrast material, an optimal analysis of all thoracic vessels requires the reading of a single series of images in the majority of cases.

## **VSCH51-08 • CT Innovations for Radiation Dose Reduction**

**John R Mayo MD (Presenter) \***

### **LEARNING OBJECTIVES**

1) To identify the patient factors that increase CT radiation dose risk. 2) To describe current CT radiation dose reduction techniques. 3) To outline the relationship between CT image noise and the detection of abnormalities. 4) To evaluate the impact of iterative reconstruction on CT radiation dose reduction.

## **VSCH51-09 • Incidental Findings Detection on CT Pulmonary Angiography Images with Low kVp Techniques**

**Kanako K Kumamaru MD, PhD (Presenter) ; Rachna Madan MD ; Ritu R Gill MBBS \* ; Nicole Wake MS ; Frank J Rybicki MD, PhD \* ; Andetta R Hunsaker MD**

### **PURPOSE**

To evaluate the effect of reduced kVp on detection of incidental findings in the lungs and mediastinum in patients who underwent CT Pulmonary Angiography (CTPA) for suspected acute pulmonary embolism.

### **METHOD AND MATERIALS**

This IRB-approved HIPAA-compliant study included consecutive CTPA studies performed from January 2008 to April 2010 which used low kVp technique (80kVp for patients weighing

### **RESULTS**

Compared with standard kVp settings, objective/subjective noise scores were significantly greater at lower kVp, while the SNR/CNR/contrast opacification scores were not significantly different, in both weight cohorts. Confidence level of clinical interpretation tended to be lower at low kVp, with a significant decrease for mediastinal lesions interpreted by one of two readers (coefficient=-2.35, 95%CI=-2.89 to -1.82, p0.1). Multivariate analysis did not show a significant correlation between accuracy of interpretation and kVp

settings for lung nodules and mediastinal nodal detection (adjusted odds ratio=0.67-1.22, p-values >0.2).

#### CONCLUSION

Despite the increased image noise, lower kVp techniques in CTPA studies in patients suspected of acute pulmonary embolism does not adversely affect the detection of lung nodules or mediastinal nodes.

#### CLINICAL RELEVANCE/APPLICATION

Lower kVp does not adversely affect the detection of lung nodules or mediastinal nodes on CTPA studies, despite the increased noise and decreased confidence in the interpretation.

### VSCH51-10 • Hyperpolarized Gas MR Imaging

**Talissa A Altes** MD (Presenter) \*

#### LEARNING OBJECTIVES

1) Understand the limitations of proton lung MRI and the strengths and weaknesses of hyperpolarized gas MRI of the lung. 2) Learn about potential research and clinical applications of hyperpolarized gas lung MRI in lung diseases such as CF, asthma, and COPD.

#### ABSTRACT

### VSCH51-11 • Are Hyperpolarized <sup>3</sup>He Magnetic Resonance Imaging Ventilation Defects Clinically Relevant in Ex-smokers without Airflow Limitation?

**Damien Pike** BSC (Presenter) ; **Miranda Kirby** PhD ; **Sarah Svenningsen** BSC ; **Harvey O Coxson** PhD \* ; **David McCormack** MD ; **Grace Parraga** PhD

#### PURPOSE

In early or mild chronic obstructive pulmonary disease (COPD), spirometry measurements are relatively insensitive to changes in the  $\diamond$ silent zones $\diamond$  of the lung in the small airways (1). However, hyperpolarized <sup>3</sup>He magnetic resonance imaging (MRI) has provided evidence of early or very mild emphysema in never-smokers with exposure to second hand smoke (2) as well as early emphysema (3) and airways abnormalities (4) in asymptomatic ex-smokers. We recently evaluated 160 ex-smokers and 71/160 (44%) did not have spirometry measurements diagnostic for COPD. We hypothesized that <sup>3</sup>He MRI and computed tomography (CT) measurements of airways disease and emphysema would detect a subgroup of ex-smokers without airflow limitation but with clinically relevant structure-function pulmonary abnormalities.

#### METHOD AND MATERIALS

Seventy-one ex-smokers (69±10yr, FEV1/FVC=.70) underwent spirometry, <sup>3</sup>He MRI, thoracic CT and the St. George's Respiratory Questionnaire (SGRQ). CT-derived measurements were generated for wall area percent (WA%) and lumen area (LA) of the sub-segmental lower right (RB8) airway and the relative area at -950 Hounsfield units of the CT density histogram (RA950). Hyperpolarized <sup>3</sup>He MRI ventilation defect percent (VDP), a surrogate of airways and bullous disease, and apparent diffusion coefficients (ADC), a surrogate of emphysema was generated for whole lung (WL) and lower right lobe (LRL) pulmonary measurements.

#### RESULTS

Subjects were classified into two sub-groups: ex-smokers with a LRL <sup>3</sup>He MRI defect (Defect, n=9) and ex-smokers with no LRL defect (No Defect, n=62). Subjects with a defect had significantly greater VDP, RB8 WA%, smaller RB8 LA and worse symptoms than subjects without a LRL defect.

#### CONCLUSION

In 9/71 (13%) ex-smokers without airflow limitation and a LRL ventilation defect, symptoms were worse and <sup>3</sup>He MRI and CT measurements showed abnormal airway structure and function that was significantly worse than in a subgroup of ex-smokers without an LRL ventilation defect.

#### CLINICAL RELEVANCE/APPLICATION

In ex-smokers without airflow limitation and previously undetected but clinically relevant symptoms, lung imaging provided evidence of structure-function abnormalities that require clinical follow-up.

### VSCH51-12 • MR Imaging: Recent Advances for Chest Imaging

**Jens Bremerich** MD (Presenter)

#### LEARNING OBJECTIVES

1) Understand physical limitations specific to the chest and how to improve image quality. 2) Current applications of MR for imaging pulmonary morphology and function. 3) Oversee emerging techniques for MR imaging of the entire chest.

#### ABSTRACT

##### Introduction:

Magnetic Resonance is an attractive tool for imaging of morphology and function of the chest with ionizing radiation. Magnetic properties of the chest, however, remain unfavourable for MR because of low water proton density and considerable magnetic field inhomogeneities. Recently new imaging protocols and sequences became available that may overcome these limitations. This abstract reviews current applications and recent advances of MR of the chest. Methods:

Fast imaging techniques such as turbo spin echo or segmented gradient echo can reduce susceptibility artefacts and enable breath held acquisitions. Free breathing respiratory gated sequences may be used alternatively. Standard imaging protocols comprise T1 and T2 weighted images for morphology assessment and edema detection. Diffusion weighted MR may be added to identify diffusion restriction which may indicate malignancy. Pleural infiltration of peripheral masses may be assessed by means of cine imaging during in- and expiration. For further characterisation of masses and inflammatory diseases T1 weighted images pre and post gadolinium may be used. Emerging techniques based on fourier decomposition for assessment of perfusion and ventilation are currently under investigation. Results: Magnetic Resonance may be used to identify and characterise pulmonary masses, monitor pulmonary perfusion and ventilation, assess chest wall motion, identify involvement of chest wall in peripheral lung tumors and to identify pulmonary embolism. Fourier decomposition may enable assessment of perfusion and ventilation and is currently under investigation. Conclusion: Today, MR is a useful tool for assessment of pulmonary morphology, function and tissue characterisation. Recent advances in MR of the chest include fourier decomposition techniques which may enable assessment of perfusion and ventilation without injection of contrast material.

### VSCH51-13 • SUVmax Correlation between PET/MRI and PET/CT in FDG Avid Lesions of the Chest Using a Three Segment Model Attenuation Correction

**Andres Kohan** MD (Presenter) \* ; **Christian Rubbert** MD \* ; **Jose L Vercher-Conejero** MD \* ; **Sasan Partovi** BS \* ; **Karin A Herrmann** MD ; **Luis A Landeras** MD ; **Peter F Faulhaber** MD \*

#### PURPOSE

PET/MRI combines the superior tissue resolution and multiparametric capabilities of the MRI with the functional capabilities of PET. It  $\diamond$ s theorized to improve oncologic imaging in multiple areas of the body, specially: brain, liver, pelvis and bone. Nonetheless other areas are bound to benefit from this technology.

However, SUVs obtained from FDG avid lesions in PET/MRI remains a concern, mainly due to the migration from CT attenuation correction to MRI attenuation correction (MRAC). One area of major concern is the chest, where two critical tissue interfaces with very different attenuation coefficients can be found.

We studied FDG avid lesions in the chest to determine the correlation between the SUVmax from PET/MRI and PET/CT using a three

segment model MRAC.

#### METHOD AND MATERIALS

First 47 oncologic consecutive patients from a research protocol were included. Final n was 19 due to 6 failed MRAC and 22 patients without chest lesions to analyze. All patients underwent PET/CT (Gemini TF) and PET/MRI (Ingenuity TF) with a single FDG injection. Lesions were identified by direct comparison and sub-classified as mediastinal, lung or chest wall lesions. SUVmax was determined with a spherical ROI including the lesion. Spearman Ranked correlation was performed.

#### RESULTS

Out of all patients (5 male, 14 female): 9 had lung cancer, 3 breast cancer, 2 head and neck cancer, 2 lymphoma, 1 melanoma, 1 pancreas and 1 colon cancer. Seventy six lesions were analyzed: 21 in the lung, 14 in the chest wall and 41 in the mediastinum. Mean exam scan time: 18±4min (PET/CT) and 21±3 (PET/MRI). Mean time from FDG injection: 66±8min (PET/CT) and 105±20min (PET/MRI). Spearman for SUVmax was 0.93, 0.95, 0.84 and 0.96 for overall, lung, chest wall and mediastinal lesions respectively (p

#### CONCLUSION

Chest wall lesions had a somewhat lower correlation (0.84) than the others (>0.90), probably related to more than half of the lesions being in vertebrae and ribs, whereas the MRAC cannot identify bone tissue. Nonetheless, correlation between SUVmax was very strong (rho>0.8) for all lesions in all areas which raises the question whether there is any clinical relevance to the findings seen in the chest wall.

#### CLINICAL RELEVANCE/APPLICATION

Reliability of SUVs in an area with air/soft tissue boundaries is vital for PET/MR to succeed in chest oncologic imaging. The high correlation to PET/CT SUVs seen here is a step into that direction.

### VSCH51-14 • Innovations in Chest Radiography

**Heber Macmahon MD (Presenter) \***

#### LEARNING OBJECTIVES

1) Understand the newer enhancements that have become available for digital chest radiography. 2) Learn how these techniques may improve diagnostic accuracy. 3) Appreciate the benefits and limitations of dual energy radiography, bone suppression, computer-aided nodule detection in clinical practice.

### VSCH51-15 • Digital Chest Tomosynthesis

**Ase A Johnsson MD, PhD (Presenter)**

#### LEARNING OBJECTIVES

1) The benefits of chest tomosynthesis in comparison to chest radiography. 2) The limitations of chest tomosynthesis in comparison to computed tomography. 3) The role of chest tomosynthesis as a problem solver in daily clinical practice.

ABSTRACT

## Breast Imaging (CAD/Quantitative Imaging)

Thursday, 10:30 AM - 12:00 PM • E450A

[IN](#) [MR](#) [DM](#) [BQ](#) [BR](#)

[Back to Top](#)

**SSQ02 • AMA PRA Category 1 Credit™:1.5 • ARRT Category A+ Credit:1.5**

#### Moderator

**Despina Kontos**, PhD

#### Moderator

**Jennifer A Harvey**, MD \*

#### Moderator

**Christopher E Comstock**, MD

### SSQ02-01 • Computer Derived Texture Features on DCE-MRI Can Separate ER+ Breast Cancers with Low and High Oncotype DX Scores

**Tao Wan** PhD (Presenter); **Boris N Bloch** MD; **Donna M Plecha** MD\*; **Cheryl Thompson** BS; **Hannah Gilmore**; **Norbert Avril** MD; **C. Carl Jaffe** MD; **Lyndsay Harris** MD; **Anant Madabhushi** MS\*

#### PURPOSE

Oncotype DX (ODX) is a gene-expression based assay for predicting response to hormonal therapy in estrogen receptor positive (ER+) breast cancers (BCa) patients. The goal of this study was to identify whether computer derived texture features on DCE-MRI can distinguish low and high ODX scores (i.e. ER+ BCa patients who would and would not benefit from adjuvant chemotherapy), thereby providing a non-invasive pertherapeutic gene-expression assessment tool predicting tumor treatment response.

#### METHOD AND MATERIALS

A total of 57 ER+ BCa patient studies were collected, in which 21 breast MRIs were acquired from a Phillips 1.5T magnet with a 7-channel breast coil, and 36 MRIs were acquired using a Siemens 1.5T magnet with a 8-channel breast coil, including DCE images obtained prior to, during, and after administration of 0.1 mmol/kg of Gd-DTPA. Each study was accompanied by: i) lesion annotations from an expert radiologist; and ii) ODX scores. A set of 6 morphological features, 3 pharmacokinetic features, 12 enhancement kinetic features (EKF), 12 intensity kinetic features, 312 textural kinetic features, 6 dynamic local binary patterns (DLBP), and 5 dynamic histogram of oriented gradients (DHoG) features were extracted and used to characterize the appearance of the breast lesions. The computed features were evaluated by a linear discriminate analysis (LDA) classifier in terms of their ability to distinguish ER+ BCa with low or high ODX scores via a 2-fold randomized cross validation scheme.

#### RESULTS

The DHoG, DLBP, and EKF texture features yielded AUC values of 0.85, 0.82, and 0.80 in conjunction with the 2-class LDA classifier for separating low and high ODX ER+ breast lesions.

#### CONCLUSION

This work to our best knowledge, the first attempt to quantitatively correlate texture measurements on DCE-MRI to patient outcome prediction via the ODX assay. Our results suggested that the DHoG, DLBP, and EKF were robust and stable DCE-MRI markers in distinguishing between low and high ODX scores.

#### CLINICAL RELEVANCE/APPLICATION

An MRI-based assay to identify ER+ BCa patients that could non-invasively predict which patients would benefit from adjuvant chemotherapy, and could serve as a complement to Oncotype DX assay.

### SSQ02-02 • Computerized Characterization of Mass and Non-mass-Like Lesions on Breast MRI

**Hui Li** PhD (Presenter); **Maryellen L Giger** PhD\*; **Li Lan**; **Sunny Y Duan**; **Stephan Hu**; **Gillian M Newstead** MD\*; **Hiroyuki Abe** MD; **Michelle Lindgren** MD



#### PURPOSE

To investigate the potential usefulness of quantitative imaging analysis on characterizing both mass and non-mass-like enhancement breast lesions in the task of distinguishing between malignant and benign lesions

#### METHOD AND MATERIALS

Study was performed on 123 biopsy-proven lesions from 103 MRI studies acquired between January 2009 and April 2010, including 35 benign mass, 50 malignant mass, 11 benign non-mass-like and 27 malignant non-mass-like lesions. Our quantitative imaging analysis method incorporated computerized 3D lesion segmentation and feature extraction, including kinetic, enhancement-variance kinetic, morphological, size, and texture features. Output from the system yielded the probability of malignancy from a Bayesian artificial neural network (BANN). Classification performance was evaluated with a leave-one-case-out method using ROC analysis with area under the ROC curve as the figure of merit.

#### RESULTS

For mass lesions, the kinetic features of time to peak and curve shape index statistically differed between malignant and benign lesions. However, kinetic features did not contribute significantly in the diagnostic task with non-mass-like breast lesions. By merging computer-selected features with BANN classifiers, AUC values of 0.88 (SE=0.03), 0.95 (SE=0.02), and 0.82 (SE=0.08) were obtained in the task of distinguishing between malignant and benign lesions on the entire dataset, between malignant and benign mass lesions, and between malignant and benign non-mass-like lesions, respectively.

#### CONCLUSION

Kinetic characteristics are useful in differentiating malignant from benign mass lesions; however, their performance is reduced when the lesions are non-mass-like. Thus, quantitative analysis for diagnostic decision-making should be performed separately on mass and non-mass-like lesions.

#### CLINICAL RELEVANCE/APPLICATION

In order to improve clinical diagnostic accuracy, quantitative analysis for diagnostic decision-making should be performed separately on mass and non-mass-like lesions in the classification task.

### SSQ02-03 • Use of Quantitative 3D Breast Image Analysis to Inform DCIS Staging

**Stephanie M Burda** (Presenter) ; **Maryellen L Giger** PhD \* ; **Li Lan** ; **Kathy Rodogiannis** ; **Hui Li** PhD ; **Gillian M Newstead** MD \* ; **Ken Yamaguichi** ; **Koichi Ishiyama** MD ; **Hiroyuki Abe** MD ; **Michelle Lindgren** MD ; **Adam Starkey**

#### PURPOSE

Uncertainty on which ductal carcinoma in situ (DCIS) cases will progress to invasive breast cancer currently results in overtreatment. Our purpose was to discern quantitative characteristics of pure DCIS, DCIS with an invasive component, and invasive cancers without DCIS to inform prognosis of patients with lesions presenting initially as DCIS.

#### METHOD AND MATERIALS

Retrospective, IRB-approved review of our radiology database 2005-2012 identified 303 pathology-proven cancers with correlative MR imaging. Histology yielded 54 pure DCIS lesions, 56 with both DCIS and invasive pathology, and 193 invasive cancers without DCIS. Quantitative 3D image analysis yielded morphological, kinetic, and texture lesion descriptors following semi-automated lesion segmentation. ROC analysis was performed on these image-based phenotypes comparing pure DCIS lesions, DCIS lesions with an invasive component and invasive cancers without an in situ component.

#### RESULTS

The combination of features that best distinguished pure DCIS from invasive cancer included kinetic feature time to peak, texture features of contrast and correlation, and morphological features of circularity, margin, and surface area. The combination of features that was best able to distinguish pure DCIS from invasive cancers with a DCIS component included contrast, margin, and ratio of surface area to volume. The margin characteristics (determined by spiculation and sharpness) and contrast (the difference between the average gray level of the cancer and the surrounding area) were found to be insightful in both comparisons. Time to peak was also significant in the comparison of Pure DCIS and invasive cancers, yielding an AUC value of 0.77. Round-robin evaluation of an LDA yielded AUCs of 0.85 and 0.74 distinguishing pure DCIS from invasive cancers and invasive cancers with a DCIS component, respectively.

#### CONCLUSION

Image-derived quantitative phenotypes, which indicate a likelihood of invasive disease-of pure DCIS, could patient guide management of DCIS lesions, thus potentially reducing overtreatment.

#### CLINICAL RELEVANCE/APPLICATION

Image-derived quantitative phenotypes, which indicate a likelihood of invasive disease-of pure DCIS, could patient guide management of DCIS lesions, thus potentially reducing overtreatment.

### SSQ02-04 • Undetected Breast Cancers on Commercial Breast MRI CAD (Computer-aided Detection) System

**Chae Hyun Kim** (Presenter) ; **Seon Hyeong Choi** ; **Ji Yeon Park** ; **Yoonjung Choi** MD ; **Shin Ho Kook** MD

#### PURPOSE

To evaluate the immuno-histological factors of breast cancer not detected on breast MRI CAD system.

#### METHOD AND MATERIALS

The study included 327 preoperative breasts MRI of histologically proven breast cancer from July 2011 to February 2013. We retrospectively reviewed the MRI CAD results, corresponding immune-histopathologic features, lesion size and age to determine factors affecting MRI CAD detectability. We categorized tumors into two groups: detected and undetected groups.

#### RESULTS

Of the 327 cases, the CAD system marked 259 (79.2%) lesions correctly and 68(20.8%) were undetected on breast MRI CAD. The mean size and age were 18 mm (range:1-70) and 50.0 yo (SD:9.9) in the undetected group and 22.8 mm (range: 3-120) and 51.4 yo (SD: 10.7) in the detected group. Detectability rates for IDCs, DCIS were 86.7% (208 of 240) and 44.6 % (25 of 56), respectively. The tumor type was a significant (p

#### CONCLUSION

Though the commercial breast MRI CAD system showed good performance, about 20% of breast cancers were not detected on MRI CAD. DCIS, low nuclear grade, low Ki-76 percentage, and HER-2 negative influenced the breast MRI CAD detectability in breast cancer patients.

#### CLINICAL RELEVANCE/APPLICATION

DCIS, low nuclear grade, low Ki-67, and HER-2 negative can influence CAD detectability. So, radiologist should check immunohistologic profiles and original images when interpreting breast MRI CAD.

### SSQ02-05 • Immunohistological Factors Affecting the Breast Cancer Size Measurement by MRI Computer-aided Detection (CAD) System

**Ji Yeon Park** (Presenter) ; **Seon Hyeong Choi** ; **Yoonjung Choi** MD ; **Chae Hyun Kim** ; **Shin Ho Kook** MD

#### PURPOSE

To investigate immunohistological factors affecting the breast tumor size measurement discrepancy between the MRI CAD and the pathologic specimen.

#### METHOD AND MATERIALS

We retrospectively reviewed the 244 cases of breast MRI CAD images and pathologic findings of the 244 patients who underwent operation for breast cancer between July 2011 and December 2012. We compared the CAD generated tumor size with tumor size measured on pathologic specimen. We classified the tumors into three groups: underestimated, adequately measured and overestimated group. We investigated the statistical difference in histopathology including histologic type, presence of DCIS, extensive intraductal component, nuclear grade, ER, PR and HER-2, among the 3 groups.

#### RESULTS

Median tumor size on CAD and specimen were 20 mm (2-163 mm) and 17 mm (0.8-82 mm), respectively. Adequately measured group was 68.6% (n=168). Invasive ductal carcinoma (IDC) showed significantly more adequate measurement, compared with DCIS (p=0.025). Among IDC, the presence of extensive intraductal component was significantly higher in overestimated group (p

#### CONCLUSION

Size assessment using breast MRI CAD was accurately measured in 68.6%. On MR CAD, breast cancer size was frequently overestimated in cases of DCIS, the presence of extensive intraductal component, and HER-2(+).

#### CLINICAL RELEVANCE/APPLICATION

Accurate tumor size measurement is critical to surgical plan for breast conservation.

Size assessment by breast MRI CAD is accurate but it can be overestimated in cases of DCIS, EIC, and HER-2(+).

### SSQ02-06 • Quantitative MRI-based Phenotypes of Triple Negative Breast Cancers

**Hui Li** PhD (Presenter) ; **Maryellen L Giger** PhD \* ; **Li Lan** ; **Hiroyuki Abe** MD ; **Michelle Lindgren** MD ; **Eric M Blaschke** MD ; **Gillian M Newstead** MD \*

#### PURPOSE

To investigate the potential usefulness of quantitative image analysis on characterizing the molecular subtypes of breast cancer in order to better understand the difference between triple negative and other molecular subtypes of breast cancer

#### METHOD AND MATERIALS

Study was performed on 168 biopsy-proven breast cancer MRI studies acquired between November 2008 and August 2011, in which 40 cases were triple negative (ER-, PR-, and HER2-) breast cancers and 128 cases were of other molecular subtypes including Luminal A, Luminal B, and HER2. Quantitative MRI analysis included: 1) 3D lesion segmentation based on a fuzzy c-means clustering algorithm; 2) computerized feature extraction; 3) leave-one-out linear stepwise feature selection; and 4) discriminant score estimation using Linear Discriminant Analysis (LDA). The classification performance between triple negative and other molecular subtypes of breast cancer was evaluated using ROC analysis with area under the ROC curve (AUC) as the figure of merit.

#### RESULTS

The triple negative classification, in a round-robin evaluation, yielded AUC values of 0.90 (SE=0.05) and 0.67 (SE=0.05) on 3T and 1.5T MR scanners, respectively, in the task of distinguishing between triple negative and other molecular subtypes, statistically significantly higher than an AUC value of 0.5 (p-value

#### CONCLUSION

The results from this study indicate that quantitative MRI analysis shows promise in the discrimination of triple negative breast cancer from other molecular subtypes of breast cancer.

#### CLINICAL RELEVANCE/APPLICATION

Identification of the molecular subtypes of breast tumors is expected to allow for improved prognostic assessment and more effective cancer treatment plans.

### SSQ02-07 • Features of Undiagnosed Breast Cancers at Screening Breast MRI: Potential Utility and Limitation of Computer-aided Evaluation

**Mirinae Seo** MD (Presenter) ; **Nariya Cho** MD ; **Min Sun Bae** MD, PhD ; **Eun Bi Ryu** MD ; **Jung Min Chang** MD ; **Hye Ryoung Koo** MD ; **Su Hyun Lee** MD ; **Won Hwa Kim** MD, MS ; **Woo Kyung Moon** ; **Hye Mi Gweon** MD ; **A Jung Chu** MD

#### PURPOSE

To evaluate the features of undiagnosed cancers at prior screening breast MRIs in patients who subsequently developed breast cancers and the potential utility and limitation of computer-aided evaluation (CAE).

#### METHOD AND MATERIALS

Between March 2004 and March 2013, 65 pairs of dynamic contrast enhanced breast MRIs including prior negative screening MRIs and subsequent MRIs with developed cancers (mean interval 36.5 months, range 5.4 - 96.7 months) were identified. The mean histological sizes of developed cancers was 2.0cm (range 0.5 - 9.5 cm) for invasive cancers (n=44) and 1.9cm (range 0.5 - 4.1 cm) for DCIS (n=21). Visible findings, their maximum lesion size and actionability, as well as causes for overlooked cancers on prior MRI were determined and classified by two experienced radiologists in consensus. A commercially available CAE program was retrospectively applied to the prior MRIs with visible findings for generation of kinetic features including washout, plateau, and persistent enhancement proportions. Presence of a washout component on CAE was also described.

#### RESULTS

Of the 65 areas where cancer later developed, 51% (33 of 65) of prior MRIs had visible findings and their mean lesion size was 1.0cm (range 0.4 - 5.2 cm). Of these visible findings, 24% (8 of 33) were classified as actionable and 76% (25 of 33) as underthreshold. Causes for actionable findings were mimicking of physiologic enhancement (n=3), mismanagement after benign results of biopsy (n=3), and satisfaction of search (n=2). Those of underthreshold findings were small lesion size (n=6), moderate to marked background parenchymal enhancement (n=11), mimicking of post-op scar (n=7), and peripheral location (n=1). Twenty three of the visible findings were available for CAE and the washout component was found in 14. However, 4 of 14 lesions with a washout component were not marked due to marked background enhancement with multiple enhancing lesions with a washout component. CAE did not show the washout component in 9 of 23 lesions.

#### CONCLUSION

On prior screening breast MRIs in which cancer later developed, 51% (33 of 65) had visible findings (24% actionable, 76% underthreshold). The addition of CAE has the potential to identify 43% (10 of 23) of overlooked findings. Yet, there are still some limitations on CAE.

#### CLINICAL RELEVANCE/APPLICATION

When an enhancing lesion shows a washout component on MR-CAE of screening breast MRI, closer attention is warranted.

### SSQ02-08 • Evaluation of a Commercial CAD System for Detecting Lesions at Breast Digital Tomosynthesis

**Lia Morra** PhD \* ; **Silvano Agliozzo** PhD \* ; **Luca A Carbonaro** MD \* ; **Manuela Durando** (Presenter) ; **Barbara Pesce** MD ; **Giovanna Mariscotti** ; **Alberto Bert** PhD \*

#### PURPOSE

To evaluate the performance of a commercial computer aided detection (CAD) system (CAD BREAST DTS, im3D S.p.A.) for detecting lesions at digital breast tomosynthesis (DBT) on an independent testing set.

#### METHOD AND MATERIALS

The CAD system was retrospectively tested on a set of 143 patients. Craniocaudal (CC) and mediolateral oblique (MLO) DBT projections were acquired with a Hologic Selenia Dimensions system and reconstructed with the Briona library (Real Time Tomography LLC). All patients signed an informed consent form. A total of 80 histologically confirmed malignant lesions (57 masses, 18 microcalcification

clusters and 6 masses with associated microcalcifications) were detected and annotated by experienced radiologists who drew a 3D bounding box around each lesion view. CAD BREAST DTS yields both masses and microcalcification clusters candidates. For masses, a CAD true positive was registered when the CAD marking overlapped by at least 20% the radiologists marking; for microcalcification clusters, when at least two of the microcalcifications identified by CAD fell within the radiologists marking. A CAD false positive was registered in all other cases, to avoid chance matchings. Masses with associated microcalcifications were considered correctly identified if CAD marked at least a mass or a microcalcification cluster.

#### RESULTS

At the selected operating point, per-lesion sensitivity was 89% (95% C.I. 80-94%). The system detected 48/56 masses, 17/18 microcalcification clusters and 6/6 masses with microcalcifications. Mean number of false positives per view was  $2.8 \pm 1.9$  (mean  $\pm$  standard deviation), of which 2 were marked as masses and 0.8 as microcalcification clusters.

#### CONCLUSION

The DBT CAD sensitivity is comparable to that observed for 2D digital mammography CAD systems, with a fairly low number of false positives per view. Further work, especially on difficult cases such as screening interval cancers, and comparing reading with and without CAD, is needed to understand its role in clinical practice.

#### CLINICAL RELEVANCE/APPLICATION

A commercial CAD system for masses and microcalcification clusters detection is evaluated on an independent testing set.

### SSQ02-09 • Quantitative MRI Morphological Features of Breast Cancer: Correlation with Immunohistochemical Biomarkers and Subtypes

**Min Sun Bae MD, PhD (Presenter) ; Mirinae Seo MD ; Woo Kyung Moon ; Nariya Cho MD ; Jung Min Chang MD ; Hye Ryoung Koo MD ; Won Hwa Kim MD, MS ; Su Hyun Lee MD ; Hye Mi Gweon MD**

#### PURPOSE

To investigate the correlation of the tumor roundness measured quantitatively at contrast-enhanced magnetic resonance imaging (MRI) and immunohistochemical biomarkers and subtypes in breast cancer.

#### METHOD AND MATERIALS

After IRB approval, we retrospectively reviewed 280 consecutive women (median age, 50 years; range, 28-79 years) with 282 invasive breast cancers (< 5 cm size). All patients underwent preoperative breast MRI. Images were assessed independently by the two radiologists who were unaware of pathological findings. Tumor roundness was measured quantitatively by a software developed in-house and was calculated according to the following equation:  $\text{roundness} = 4\pi \times A / P^2$  (A is the cross-sectional area of the tumor and P is the measured perimeter length of the tumor). The means of values measured by the two observers were recorded and interobserver variability was calculated. Associations between the tumor roundness (1-100 %) and biomarker (estrogen receptor [ER], progesterone receptor [PR], HER2, and Ki67) features were evaluated using Pearson's correlation coefficient and a multiple linear regression analysis. Tumor roundness was compared between breast cancer subtypes (luminal A, luminal B, HER2-enriched, and triple-negative).

#### RESULTS

Interobserver agreement for MRI measurements was moderate with intraclass correlation coefficients of 0.75 (95% confidence interval: 0.67-0.80). A moderate inverse correlation was observed between the ER score and tumor roundness ( $-0.408, P < .0001$ ). PR score, Ki67 index, and tumor grade correlated with the tumor roundness ( $P < .0001$ ). In multiple linear regression, ER score ( $P < .0001$ ) and Ki67 index ( $P = .003$ ) were independent factors determining tumor roundness. Triple-negative tumors showed the highest mean roundness score compared with other subtypes (67.3 for triple-negative vs. 55.9 for HER2-enriched, 53.8 for luminal B, and 51.7 for luminal A;  $P < .0001$ ).

#### CONCLUSION

Tumor roundness measured quantitatively at MRI correlated with ER score and Ki67 index in breast cancer. Triple-negative tumors showed the highest mean roundness score compared with other subtypes.

#### CLINICAL RELEVANCE/APPLICATION

Our data may have implications for possibly stratifying breast cancer patients with different clinical outcomes by using MRI morphological features.

---

### Thursday Plenary Session

---

Thursday, 01:30 PM • Arie Crown Theater

**PH** **RO** **OI** **BQ**

[Back to top](#)

**PS50 • AMA PRA Category 1 Credit™: 1.25 • ARRT Category A+ Credit: 1.5**  
To receive credit, relinquish attendance voucher at end of session.

#### RSNA/AAPM Symposium

##### Moderator

**Jeffrey H Siewerdsen**, PhD \*, Baltimore, MD  
AAPM Liaison to the RSNA Scientific Program Committee

##### LEARNING OBJECTIVES

1) Learn how multi-modality imaging methods are being used in combination with high-precision radiation therapy delivery techniques to understand fundamental mechanisms of cancer pathogenesis, progression, and treatment response. 2) Learn the challenges and advances associated with quantitative imaging, and understand how more accurate and quantitative imaging is central to advancing the understanding of major questions in 21st century medicine. 3) Learn how imaging in partnership with medical physics and other technical and clinical disciplines provides a vital tool and multidisciplinary expertise for such advances.

#### Imaging in Partnership: With Radiation Therapy

**David A Jaffray**, PhD \*, Toronto, ON, CANADA

##### LEARNING OBJECTIVES

View learning objectives under main course title.

#### Imaging in Partnership: With Physics and Quantitative Medicine

**James A Deye**, PhD, Bethesda, MD

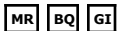
##### LEARNING OBJECTIVES

View learning objectives under main course title.

---

### Hot Topic Session: MR Quantification Techniques in the Liver (Fat, Iron, Fibrosis)

---

**SPSH52** • AMA PRA Category 1 Credit™:1 • ARRT Category A+ Credit:1**Moderator**  
**Claude B Sirlin**, MD \***SPSH52A • MR Quantification of Liver Fat****Scott B Reeder** MD, PhD (Presenter)

## LEARNING OBJECTIVES

1) Understand the relative accuracy and performance of US, CT and MRI for the detection and quantification of hepatic steatosis. 2) Understand the fundamentals of emerging confound-corrected MRI methods to quantify liver fat content.

**SPSH52B • MR Quantification of Liver Iron****Diego Hernando** PhD (Presenter)

## LEARNING OBJECTIVES

1) Understand the fundamentals of MR methods to quantify liver iron. 2) Understand the main advantages and disadvantages of different methods.

## ABSTRACT

Assessment of liver iron levels is necessary for detection and quantitative staging of iron overload, and monitoring of iron-reducing treatments. This lecture discusses the need for non-invasive assessment of liver iron, and reviews qualitative and quantitative methods with a particular emphasis on MRI. Methods that are in clinical use, as well as their limitations, are described. Remaining challenges, unsolved problems, and recently introduced techniques to provide improved characterization of liver iron deposition are discussed.

## URL

**SPSH52C • MR Quantification of Liver Fibrosis****Richard L Ehman** MD (Presenter) \*

## LEARNING OBJECTIVES

1) Briefly review different MR-based techniques to evaluate liver fibrosis. 2) Understand the fundamentals of MR elastography. 3) Understand the performance of MR elastography for evaluating liver fibrosis.

**Quantitative Imaging: Informatics**

Thursday, 04:30 PM - 06:00 PM • E352

**RC725** • AMA PRA Category 1 Credit™:1.5 • ARRT Category A+ Credit:1.5**Director**  
**Michael F McNitt-Gray**, PhD \***RC725A • The Role of Informatics in Quantitative Imaging****Katherine P Andriole** PhD (Presenter)

## LEARNING OBJECTIVES

1) Understand the role of informatics in quantitative imaging. 2) Be able to identify existing limitations in information technologies with respect to quantitative imaging, and conversely see how informatics may assist in filling some of the current gaps in quantitative imaging methods. 3) Become familiar with on-going efforts to address current challenges facing research into and clinical implementation of quantitative imaging applications.

## ABSTRACT

Quantitative imaging is increasingly becoming an essential part of biomedical research as well as being incorporated into clinical diagnostic activities. Referring clinicians are asking for more objective information to be gleaned from the imaging tests that they order so that they may make the best clinical management decisions for their patients. Medical Physicists, Researchers, Imaging Scientists, and others may be called upon to identify existing issues as well as develop, validate and implement new approaches and technologies to help move the field further toward quantitative imaging methods. Biomedical imaging informatics tools and techniques such as standards, integration, data mining, cloud computing and new systems architectures, ontologies and lexicons, data visualization and navigation tools, and business analytics applications can be used to overcome some of the existing limitations. The RSNA's Quantitative Imaging Biomarkers Alliance (QIBA) is an initiative with international participation from medical physicists, clinicians, researchers, industry scientists, and government officials all interested in optimizing the potential of quantitative imaging. A major QIBA informatics activity, the imaging data warehouse is in progress. Current status and future plans will be described.

**RC725B • Standards for Quantitative Imaging****David A Clunie** MBBS (Presenter) \*

## LEARNING OBJECTIVES

1) Identify the importance of quantitative imaging principles in the setting of clinical trials. 2) identify the role of standards, including DICOM and others, in the successful application of quantitative imaging principles. 3) Analyze quantitative imaging techniques and apply this knowledge to protocol development in the setting of clinical trials.

**RC725C • Clinical and Research Needs for Quantitative Imaging Informatics Tools****Bradley J Erickson** MD, PhD (Presenter) \*

## LEARNING OBJECTIVES

1) Become familiar with the quantitative imaging tools that are available for clinical and research uses. 2) Become familiar with the clinical and research problems that are being addressed by quantitative imaging. 3) Become familiar with the clinical and research problems that might be addressed by quantitative imaging in the near future and how to prepare one's practice for these uses.

## ABSTRACT

Quantitative imaging is more than just the measurement of structures in images. It is a new way of approaching diagnosis and therapy assessment. While simple linear measurements might qualify as quantitative imaging, it is important to think of QI in a much broader context. In addition to measuring spatial quantities like length, area, and volume, one can measure image values on functional imaging, which might represent a physiologic value. One can measure textures and edge properties, potentially replacing the "it just looks like it"

answer to why an expert can diagnose a certain disease. Measuring change can also be more than just spatial. Spatial change detection is important, of course, and doing it well is a critical component of QI. Measuring change in non-spatial properties is likely to become more important in the future. Finally, while some might believe that genomics will largely replace imaging, there is currently much interest in the use of imaging to provide pervasive and non-destructive prediction of genomic, proteomic, and metabolomic properties that are likely to be of great value to patient care.

---

## Techniques for Quantitative Cancer Imaging: Current Status

---

Friday, 08:30 AM - 10:00 AM • S404CD

---

[Back to Top](#)

**RO** **OI** **BQ**

**RC818** • AMA PRA Category 1 Credit™:1.5 • ARRT Category A+ Credit:1.5

### RC818A • Computed Tomography

**Binsheng Zhao** DSc (Presenter)

#### LEARNING OBJECTIVES

1) Familiarize the audience with conventional CT response assessment methods and their limitations, especially in the era of new drug development. 2) Provide examples of modified RECIST methods in several types of cancers. 3) Raise awareness of the need to re-evaluate RECIST guidelines and establish new response assessment criteria based on tumor volume and density changes. 4) Discuss the effects of CT imaging parameters on tumor measurement and the importance of standardizing an imaging acquisition protocol in response assessment.

#### ABSTRACT

Computed tomography (CT) has been widely used in assessing tumor response to therapy. This refresher course will familiarize the audience with conventional response assessment methods and their limitations, especially at a time of target drug development. Potential improvements will be discussed, including re-evaluating the RECIST (Response Assessment Criteria in Solid Tumors) guidelines and establishing new response assessment criteria based on tumor volume and density changes on CT. Several examples of modified RECISTs for lymphoma, mesothelioma, hepatocellular carcinoma (HCC) and gastrointestinal stromal tumor (GIST) will be provided. Last but not least, measurement variability will be addressed and the importance of standardizing an imaging acquisition protocol in oncologic response assessment will be discussed.

### RC818B • Magnetic Resonance Imaging

**Gregory S Karczmar** PhD (Presenter) \*

#### LEARNING OBJECTIVES

1) Gain familiarity with methods used for accurate measurements of tumor volumes with MRI, advantages of MRI, challenges, and sources of error. 2) Understand basic principles and clinical applications of dynamic contrast enhanced MRI; possibilities for standardized measurements of perfusion and capillary permeability, and sources of error. 3) Understand basic principles and clinical applications of diffusion-weighted imaging, measurements of the apparent coefficient of diffusion (ADC), and sources of error.

#### ABSTRACT

Anatomic and functional MRI is increasingly used for diagnosis and staging of cancer, and for detection of response to therapy. However, standardized, quantitative measurements remain challenging. We will review use of MRI to reliably measure tumor volume, and two widely used functional MRI methods: dynamic contrast enhanced MRI (DCEMRI) and diffusion-weighted imaging (DWI). We will discuss methods used to standardize DCEMRI measurements, including quantitative measurements of contrast media as a function of time, measurement of the arterial input function, and use of an appropriate model for calculation of perfusion/capillary permeability, as well as 'model-free' approaches. We will discuss methods used to measure the apparent diffusion constant (ADC) and the relationship between the ADC and underlying physiology/anatomy at the microscopic level.

### RC818C • Positron Emission Tomography

**Paul E Kinahan** PhD (Presenter) \*

#### LEARNING OBJECTIVES

1) Understand the advantages and disadvantages of PET/CT as a quantitative imaging technique. 2) Understand sources of bias and variance in quantitative PET/CT imaging, both in data acquisition and analysis. 3) Learn techniques for limiting variability in quantitative PET/CT imaging.

#### ABSTRACT

Dual-mode positron emission tomography / x-ray computed tomography (PET/CT) imaging has become a standard tool in cancer imaging for detection, diagnosis and staging over the last decade, and is increasingly being used in therapy planning and assessing response to therapy. This refresher course will familiarize the audience with response assessment methods used in PET/CT imaging and their limitations. Recently proposed criteria will be discussed, including the PERCIST (PET Response Criteria in Solid Tumors) guidelines. Measurement variability will be addressed and the importance of standardizing an imaging acquisition protocol in oncologic response assessment with PET/CT will be discussed.

---

## Quantitative Imaging: Quantitative Imaging in Ultrasound

---

Friday, 08:30 AM - 10:00 AM • E263

---

[Back to Top](#)

**PH** **US** **BQ**

**RC825** • AMA PRA Category 1 Credit™:1.5 • ARRT Category A+ Credit:1.5

**Director**

**Michael F McNitt-Gray**, PhD \*

### RC825A • Elasticity and Backscatter Related Measures

**Timothy J Hall** PhD (Presenter) \*

#### LEARNING OBJECTIVES

1) Describe the various approaches and history of Quantitative Ultrasound. 2) Understand the difference in system-dependent and system-independent backscatter parameters. 3) Understand the benefits of system-independent backscatter parameters. 4) Describe the state of the art in elasticity imaging and quantitative ultrasound from backscattered echoes.

#### ABSTRACT

There is a long history of attempts to use the backscattered echo signals from medical ultrasound to describe disease conditions of various tissue types. For example, from the initial application of ultrasound in breasts, the investigators attempted to differentiate benign from malignant disease based on characteristics of the echo signals. Along the way, there have been substantial successes. For example, it was only 30yrs ago that we debated how to estimate blood flow based on ultrasound echo signals and how to interpret that data. Just

over 20yrs ago we began to display flow dynamics with color flow imaging. More recently, elasticity imaging methods, which also began in the tissue characterization or quantitative ultrasound community, have become commercially viable products with clear diagnostic potential. These were tissue characterization methods in their early days. Now they are recognized as specific procedures with quantifiable diagnostic merit. Numerous other quantitative ultrasound (QUS) methods have been proposed, developed, tested and have demonstrated varying degrees of success. Many of these methods are still under development. This presentation will discuss quantitative ultrasound methods based on backscattered echo signals focusing on the most recent techniques that are either commercially available or that show the greatest potential as diagnostic tools.

## RC825B • Volume Flow and Measures From Contrast Agents

**Oliver D Kripfgans** (Presenter) \*

### LEARNING OBJECTIVES

1) Understand the pitfalls of ultrasound based blood flow acquisition, analysis, and interpretation. 2) Become familiar with current approaches of quantitative estimation of blood flow and learn how to minimize associated errors. 3) Obtain an overview of current commercial ultrasound contrast agents as well as their availability in the US. 4) Learn about contrast agent enhanced measurements in a clinical setting.

### ABSTRACT

Clinical ultrasound scanners typically offer three methods of blood flow acquisition, namely pulse wave, color flow and power Doppler. While real-time blood flow visualization is one of the perks of ultrasound, standardized quantitative methods are still unavailable to the radiologist. Pulse wave offers volumetric flow computation based on assumptions that are often violated. Color flow has never been directly quantitative as no angle correction can be dialed-in. The advent of 2D ultrasound arrays (electronic or mechanically swept) has enabled color flow and power Doppler acquisition in the coronal plane thus yielding Doppler angle as well as geometry independent flow information for direct quantification of in situ real-time volumetric flow. Ultrasound contrast agents have been approved for many clinical applications in Europe, Asia and Canada. The FDA has limited the use of ultrasound contrast agents in the US and essentially only cleared ultrasound contrast agents for cardiac applications. However, off-label application is practiced in the US. Its extend and benefits will be discussed in this course along with current approaches for ultrasound contrast agents based clinical measurements.

### URL's

[www.ultrasound.med.umich.edu/ODK/RSNA2012](http://www.ultrasound.med.umich.edu/ODK/RSNA2012)

## RC825C • Ultrasound Measurements and FDA Criteria for Display of New Quantitative Measures

**Brian S Garra** MD (Presenter)

### LEARNING OBJECTIVES

1) Review the main types of quantification of Ultrasound images. 2) Review some recent examples exploring sources of error in ultrasound morphometric quantification. 3) Summarize new ultrasound based parameters that might be displayed. 4) Discuss the formation of the Ultrasound QIBA Technical Committee and its objectives. 5) Review recent changes in FDA policy regarding display of quantitative features on ultrasound images.

### ABSTRACT

Ultrasound images are probably the most frequently measured images and extensive literature on a wide variety of ultrasound image measurements exists going back to the 1960's. Most morphometric and Doppler measurements are well documented and are at a mature stage. Automated measurements of volume and structures such as arterial intimal medial thickness are also finding increasing clinical application but each method of image segmentation and quantification has its own characteristic problems and sources of error. Some newer measurements including measurement of tissue strain (elastography) and strain rate and one of the newest, shear wave speed, are the subject of considerable research activity and the sources of error and bias are just now being identified and quantified. The RSNA Quantitative Imaging Biomarker Alliance (QIBA) has recently undertaken the task of developing standardized protocols for measurement of ultrasound related parameters. The first project of the US QIBA technical committee is to develop a profile for measurement of shear wave speed in tissue using ultrasound. The FDA has long allowed many types of measurements to be displayed as part of the ultrasound image. A demonstration of reasonable accuracy and precision important for obtaining clearance to display a new measurement. Display of measurement accuracy may also be required and users should be informed of situations where the measurement may be inaccurate. The efforts of the QIBA may provide data that in the future will help to speed up FDA clearance for display of new types of measurements.

## Neuroradiology (Quantitative Neuroimaging)

Friday, 10:30 AM - 12:00 PM • N230

**MR** **BQ** **NR**

[Back to Top](#)

**SST11** • AMA PRA Category 1 Credit™:1.5 • ARRT Category A+ Credit:1.5

### Moderator

**Pratik Mukherjee**, MD, PhD \*

### Moderator

**Haris I Sair**, MD

## SST11-01 • Geometrical Assessment of the Membranous Semicircular Canals: Using Three-dimensional Reconstructed High Resolution Magnetic Resonance Imaging of the Inner Ear

**Ahmed F Emam** MBBCh (Presenter); **Nagy N Naguib** MSc; **Nour-Eldin A Nour-Eldin** MD, MSc; **Mohammed A Alsubhi** BMBS; **Thomas J Vogl** MD, PhD

### PURPOSE

To estimate the angles between and to assess the length of the Superior (S), Posterior (P), Lateral (L), Crus commune (CC) semicircular canals (SCC) of the Inner Ear using three dimensional (3D) reconstruction of the high resolution MR-Imaging sequences

### METHOD AND MATERIALS

The retrospective study was performed on 2100 SCC's (in 350 patients with a mean age of 48.5 year). Measurements were performed using 3D reconstruction of a high resolution MR-Imaging ISO-Space sequence with 0.6 mm slice thickness. 3D reconstructions were performed using Advantage Workstation for diagnostic imaging. The assessment was manually performed for each side in all patients. For each side the angles between the superior and posterior SCC (X), between the Superior and lateral SCC (Y) and between the Posterior and lateral SCC (Z) were measured. In addition, the individual length of each SCC and the CC was performed. The mean, standard deviation (SD) and range of each measurement were calculated.

### RESULTS

Of the 2100 angles measured 37 were not visualized due to unclear appearance of the SCC in the region of the angle. In addition the length of 163 SCCs was not assessed due to fragmentation or unclear visualization. The angles between the left SCCs showed a mean value of X: 108.31° (SD:10.15, Range:77°-145°), Y: 72.11° (SD:12.28, Range:41°-116°) and Z: 84.85° (SD:12.45, Range:48°-123°). The angles between the right SCCs showed a mean of X: 110.34° (SD:10.26, Range:80°-150°), Y: 71.13° (SD:13.15, Range:42°-113°), and Z: 85.33° (SD:13.07, Range:48°-138°). The mean Length of the Superior, Posterior, Lateral, Crus commune SCC of the left Inner Ear was S: 19.66mm (SD:1.64,

Range:14-25mm), P: 21.54mm (SD:1.99, Range:7.3-27mm), L: 13.31mm (SD:1.48, Range:8-18mm) CC: 3.78mm (SD:0.44, Range:3-5mm). The mean Lengths on the right side were S: 19.47mm (SD:1.67, Range:15-26mm), P: 22.30mm (SD:2.06, Range:16-29mm), L: 13.39mm (SD:1.46, Range:7-18mm), CC: 3.78mm (SD:0.44, Range:2.7-5mm).

#### CONCLUSION

This descriptive study showed that angles between the Semicircular canal planes have a wide range of degrees..

#### CLINICAL RELEVANCE/APPLICATION

Contrary to previous reports in the literature (that the angle between the SCCs is around 90°) the current study results shows a wide range of variations between the angles.

### SST11-02 • Clinical Evaluation of Synthetic Brain MRI at 3.0 Tesla

**Michael Nelles MD** (Presenter) ; **Juergen Gieseke DSc** ; **Dariusch R Hadizadeh Kharrazi MD** ; **Horst Urbach MD** ; **Hans H Schild MD**

#### PURPOSE

Prospective intra-individual comparison of synthetic quantitative versus regular MR imaging (MRI) of the brain at 3.0T.

#### METHOD AND MATERIALS

A 3.0T MR system (Achieva 3.0T TX, Philips Healthcare, The Netherlands) and a stand-alone postprocessing software (SyntheticMR, Sweden) were used to create T1, T2 and FLAIR contrast-weighted synthetic MR images of the brain. The quantitative mapping was based on the QRAPMASTER method ("Quantification of Relaxation Times and Proton Density by Multiecho acquisition of a saturation-recovery using Turbo Spin-Echo Readout"), using a multislice, multiecho, and multidelay acquisition with a scan time of 4:50 minutes. 25 consecutive patients underwent MRI of the brain including synthetic quantitative and regular T1, T2 and FLAIR sequences. Contrast ratios (CRs) were calculated between gray matter (GM) and white matter (WM) for synthetic and regular sequences. Diagnostic quality of synthetic MR examinations was scored as follows: Score of 4, excellent (sharp depiction of the GM/WM junction and subcortical GM without interfering artifacts). Score of 3, adequate for diagnosis (minor artifacts or noise present not interfering with image interpretation). Score of 2, questionable for diagnosis (impaired by artifacts, noise and / or changes in contrast). Score of 1, non-diagnostic.

#### RESULTS

#### CONCLUSION

Synthetic quantitative MRI is capable of generating accurate conventional contrast images within a clinically acceptable time. The diagnostic image quality is readily comparable to that of regular MRI sequences in the majority of cases.

#### CLINICAL RELEVANCE/APPLICATION

Synthetic MRI holds the promise of replacing the acquisition of different regular MR series in selected patients, suitable for disease monitoring in e.g. MS or glioma patients.

### SST11-03 • Multivariate Longitudinal Shape Statistics of Brain Lateral Ventricles during the First Eighteen Months of Human Life

**Lucile Bompard** (Presenter) ; **Shun Xu** ; **Martin Styner** ; **Wei Gao** ; **Valerie L Jewells DO** ; **Beatriz Paniagua** ; **Weili Lin PhD**

#### PURPOSE

The human brain undergoes dramatic structural changes in the first few years of life. Of particular interest are the lateral ventricles (LVs) of the brain because of their association with many psychiatric and developmental disorders. The primary aim of this research is to discern the tempo-spatial growth characteristics of the LVs to develop a normative data-base.

#### METHOD AND MATERIALS

24 healthy subjects were imaged using a 3T MR scanner as frequently as 3 months from 2 weeks of age to 12 months of age, and again at 18 months. A minimum of 4 scans was performed per subject. T2- weighted images were employed to segment the LVs, resulting in 127 left and 119 right LVs. Due to significant variation, the tail of the ventricular horn was manually removed. Subsequently, a densely sampled surface representation was computed for each LV using spherical harmonics based point distribution models, allowing group analysis of the spatiotemporal growth of the LVs during the first 18 months of life. Volumetric measures, cross-sectional areas, and growth rates were calculated.

#### RESULTS

Volumetric measurements reveal a continuous growth of the LVs in the first 12 months, followed by 11±27% reduction from 12 to 18 months. In addition, the left LV is consistently larger (10±23% at 2wks and 9±20% at 18month) than that of the right LV. By grossly separating the LVs into the anterior and posterior horns and the mid-body, additional insights are revealed. Measurements of regional cross-sectional areas of LVs, the mid-body mainly elongates and the horns thicken with time. Specifically, the ventricle horns exhibit the fastest growth rates between 0 ♦ 3 months, followed by a progressively reduced growth rate between 3 ♦ 12 months. In addition, the posterior horn consistently outgrows the anterior horn. In contrast, the temporal changes of thickness of the mid-body are mainly from dorsal to ventral, with the fastest growth rate between 0 ♦ 3 months.

#### CONCLUSION

The LV growth exhibits both temporal and regional specific patterns during the first 18 months of life. Our results offer new insights into the unique growth patterns of human ventricle.

#### CLINICAL RELEVANCE/APPLICATION

This detailed normative spatiotemporal growth characteristics of LVs during the first 18 months of life provide important references for the delineation of early abnormal LV growth.

### SST11-04 • Whole Brain Volumetric and Morphometric Analysis of Patients with Maple Syrup Urine Disease

**Emilie R Muelly PhD** (Presenter) ; **Don Bigler** ; **Gregory J Moore MD, PhD** ; **Kevin Strauss** ; **D. Holmes Morton** ; **Julie A Mack MD**

#### PURPOSE

Maple syrup urine disease (MSUD) is an inherited metabolic disorder that impairs branched chain amino acid metabolism. Rapid elevations of circulating branched chain amino- and ketoacids cause life-threatening encephalopathy. Despite dietary treatment, achievement of metabolic control varies and patients remain at risk for acute decompensation. Liver transplantation has been shown to eliminate metabolic volatility. Reversible decreases in N-acetylaspartate (NAA) have been demonstrating using magnetic resonance spectroscopy during both acute and chronic states of disease. These findings may reflect structural or functional differences. Volumetric analysis may add value to interpretation of neurochemical findings.

#### METHOD AND MATERIALS

Quantitative proton magnetic spectra were obtained for 37 patients (26 on dietary therapy, 11 status-post liver transplantation) and 26 sibling controls using a Siemens Magnetom Trio 3 Tesla scanner. Whole brain and segmented volume calculations of the images were made using SPM5 in Matlab. Brain morphometry dimensional measurements were measured using Osirix. A three-way ANCOVA (accounting for age as a cofactor) with Tukey post-hoc testing were used to identify group differences.

#### RESULTS

Total brain parenchyma as a percentage of total brain volume was greater in patients on dietary therapy compared to controls (p = 0.02). Gray and white matter percentages of total brain volume individually did not differ between groups. Total whole brain volume and

morphometry did not differ between groups.

#### CONCLUSION

Our results support the hypothesis that low NAA levels in MSUD patients reflect impaired neuronal energy production rather than neuronal loss. However, our methods prevent us from detecting decreases in neuronal density that do not change tissue size and also do not specifically evaluate brain regions in which low NAA levels were detected. Furthermore, increased total brain parenchyma may reflect subtle chronic edema. Further study, such as analysis of T2\* and regional morphometric data, is needed to explore these possibilities.

#### CLINICAL RELEVANCE/APPLICATION

Patients with maple syrup urine disease have increased total brain parenchymal volume.

### **SST11-05 • DTI Correlates of Cognition in Conventional MRI Normal Appearing Brain in Patients with Vitamin B12 Deficiency**

**Rakesh K Gupta** MD, MBBS (Presenter) ; **Pradeep K Gupta** MSc ; **Ravindra K Garg** MD, MBBS ; **Bhaswati Roy** ; **Abhinav Yadav** BS ; **Yogita Rai** PhD ; **Ram K Rathore** DSc ; **Chandra M Pandey** PhD ; **Ponnada A Narayana** PhD

#### PURPOSE

Deficiency of vitamin B12 may result in neuronal degeneration and brain damage which influences the cognition. We hypothesized that patients with clinical symptoms of subacute combined degeneration (SACD) and biochemical evidence of Vitamin B12 deficiency should have a cognition decline and microstructural brain changes on advanced MRI even when conventional MRI appears normal.

#### METHOD AND MATERIALS

Patients with SACD of the cord were recruited for the study. Patients underwent nerve conduction velocity and biochemical analysis for serum Vitamin B12, and homocystine. Hematology including the type of anemia was also performed. All patients with Vitamin B12 deficiency and clinical features of SACD were subjected to the complete imaging cervical spine and brain imaging. Patients with normal brain MRI with or without imaging changes in the cervical spine were included for cognition tests. Based on these criteria, 51 patients and 46 age and sex matched controls were enrolled in this study. 3D-T1 weighted and DTI was performed in all these subjects. FSL based VBM and TBSS analysis were performed for volumetric and white matter fiber tracts changes quantification.

#### RESULTS

No significant changes in grey and white matter volumes were observed in patient compared to control using VBM. Significant reduction of FA and increase in MD and RD values were observed in various brain regions in patients compared to controls. Most of the Neuropsychological score were significantly altered in patients compared to controls and few of these showed significant correlation with FA and RD in some of the brain regions.

#### CONCLUSION

Decrease in FA and increase in MD and RD results of WM microstructure suggests its alteration probably due to demyelination of the fibers secondary to Vitamin B12 deficiency. These patients, though present clinically with SACD, have generalized involvement of the white matter of the CNS and have associated decline in cognition. Correlation of some of the NPT scores with region specific white matter changes confirms that the abnormalities in NPT relate to the changes in the white matter microstructures.

#### CLINICAL RELEVANCE/APPLICATION

Vitamin B12 deficiency has generalized effect on the CNS white matter even when it manifests as SACD as evidenced by cognition and brain microstructural alteration.

### **SST11-06 • Reliability of 3D Pseudo-continuous Arterial Spin-labeling MR Imaging for Measuring Visual Cortex Perfusion on Two 3T Scanners**

**Diandian Huang** (Presenter) ; **Xin Lou** MD, PhD ; **Lin Ma** MD ; **Bing Wu** ; **Kai-Ning Shi**

#### PURPOSE

The visual cortex cerebral blood flow (CBF) values are closely associated with visual perception. Perfusion MRI can be used to identify patients with ischemic changes of visual cortex who may benefit from reperfusion therapies. The risk of nephrogenic systemic fibrosis, however, limits the use of contrast agents. Our objective was to evaluate the reliability and reproducibility of three dimensional arterial spin labeling (3D pCASL), an alternative noninvasive perfusion technique, to detect CBF of visual cortex *in vivo*.

#### METHOD AND MATERIALS

Twelve healthy subjects were scanned three times on two 3.0T MR scanners with 3D pCASL technique. The 1st test and 3rd test were done on scanner-1, while the 2nd test was on scanner-2. Intervals between tests were among 10-15 days. The 3D pCASL data with two post labeling delay time (PLD) of 1.5 and 2.5 seconds was acquired during every scanning. Volumetric T1-weighted images were also acquired for image registration. The CBF values of visual cortex (included brodmann 17, brodmann 18, brodmann 19) were extracted for comparison. The intra- and inter-scanner reliability and reproducibility were evaluated with the intraclass correlation coefficient (ICC) and Bland-Altman plot.

#### RESULTS

The relative CBF values of visual cortex were 16-84 ml/min/100g (PLD=1.5s) and 27-75 ml/min/100g (PLD=2.5s). Compared with 1st test and 2nd test, the ICC was 0.685 at PLD=1.5s and 0.754 at PLD=2.5s. Compared with 2nd test and 3rd test, the ICC was 0.719 at PLD=1.5s and 0.903 at PLD=2.5s. Compared with 1st test and 3rd test, the ICC was 0.821 at PLD=1.5s and 0.831 at PLD=2.5s. Higher reliability (ICC=0.829) for PLD 2.5s compared to PLD 1.5s (ICC=0.743) were demonstrated in inter-scanners. At intra- and inter-scanner, the Bland-Altman showed the reproducibility at PLD=2.5s is better than that at PLD=1.5s.

#### CONCLUSION

Although inter-scanner reliability is slightly lower than intra-scanner, there is a very high similarity of the outcomes at different time from two scanners. The 3D pCASL technique is available for measuring the CBF at visual cortex with high reliability and reproducibility. It should be used for MR research on blood flow of visual cortex at multiple centers.

#### CLINICAL RELEVANCE/APPLICATION

The 3D pCASL can measure CBF values of visual cortex with high reliability and reproducibility and offers a noninvasive way to access the etiology and diagnosis of posterior visual pathway disease.

### **SST11-07 • Adaptation and Slow Recovery of Metabolic Activity in Human Visual Cortex Coupled with a Modest Change in Cerebral Blood Flow**

**Farshad Moradi** MD (Presenter) ; **Richard B Buxton** PhD

#### PURPOSE

We recently demonstrated sub-additive flow and metabolic response non-linearity in human visual cortex consistent with adaptation. A disproportionately larger adaptation of metabolic response compared to blood flow was observed. These results indicate an aspect of metabolic activity corresponding to neural adaptation (or fatigue) that has a different neurovascular coupling from stimulus driven activation. We examine if the adaptable aspect of metabolic activity is coupled with high flow and whether or not it recovers during inter-stimulus intervals.

#### METHOD AND MATERIALS

Six observers participated in the experiment. CBF and BOLD responses to continuous (46 s) and intermittent (7.6 s on and off x 3) peripheral gratings were measured using a dual gradient-echo optimized multipulse pseudo-continuous arterial spin labeling sequence. A 2x2 design (continuous vs. intermittent, two contrast levels) was used. The difference between initial and final 18 s of activity during each epoch (?CBF vs. ?BOLD) were determined. ?CMRO2 was estimated using a modified calibrated BOLD method.



## RESULTS

If the adaptable aspect of metabolic activity is coupled with high flow then the neurovascular-coupling ratio is expected to increase over time with prolonged stimulation in the continuous condition. If the adaptable aspect of metabolic activity recovers during interstimulus intervals then the neurovascular-coupling ratio should remain the same over time in the intermittent condition. A positive change in neurovascular coupling would result a  $\Delta$ BOLD that is disproportionately greater than  $\Delta$ CBF. Contrary to both predictions,  $\Delta$ BOLD was negative compared to  $\Delta$ CBF in all conditions, indicating a significantly lower neurovascular coupling ratio at the end of each epoch compared to the beginning.

## CONCLUSION

The adaptable aspect of metabolic activity is coupled with a lower flow modulation compared to the input-driven modulation and does not recover during short inter-stimulus intervals. Our findings are consistent with the hypothesis that cerebral blood flow in human visual cortex is driven by both metabolic activity and visual input via independent mechanisms.

## CLINICAL RELEVANCE/APPLICATION

Numerous pathologic conditions affect the regulation of cerebral blood flow. Our results provide insight into physiological modulations of neurovascular coupling and role of adaptation nonlinearity.

### SST11-08 • Evaluation of WBAA with Registration-based Cube Propagation for Brain Atrophy Quantification

**Martin Lillholm** MSc, PhD (Presenter) \* ; **Akshay Pai** ; **Lauge Sorensen** ; **Mads Nielsen** PhD \* ; **Jon Sparring** \* ; **Sune Darkner** ; **Erik B Dam** PhD \*

## PURPOSE

Atrophy for the whole brain and sub-structures is becoming common as study outcome in clinical trials assessing the efficacy of potential treatments of diseases involving dementia. In this study, we evaluated the sensitivity to change related to progression of Alzheimer's disease of a novel software framework, WBAA.

## METHOD AND MATERIALS

The recently defined Alzheimer's disease neuroimaging initiative (ADNI) standardized collection ('ADNI1:Annual 2 Yr 1.5T' at [adni.loni.ucla.edu](http://adni.loni.ucla.edu)) with 504 subjects (169 normals, 234 mild cognitively impaired, and 101 alzheimer) including baseline and 12-month 1.5T T1 magnetic resonance imaging (MRI) scans was used. The MRIs were processed using longitudinal FreeSurfer and the whole brain atrophy application (WBAA 1.0 by Biomediq) that performs non-rigid registration followed by atrophy estimation quantification using cube propagation (CP). The WBAA was also evaluated with CP replaced by the common Jacobian integration (JI) method. Sensitivity to change was evaluated by atrophy differences between healthy and Alzheimer subjects quantified using Cohen's D and required study sample sizes.

## RESULTS

As example, quantifications of the hippocampus atrophies estimated using WBAA were -1.3% and -0.6% for the Alzheimer and healthy subjects whereas the ventricle estimates were +9.3% and +4.1%, respectively. Corresponding Cohen's D for WBAA on these two regions were 1.1 and 1.0. For whole-brain, hippocampus, ventricles, and medial temporal lobe, the WBAA Cohen's D were 0.7, 1.1, 1.0, and 1.3. The corresponding sample sizes were 173, 124, 113, and 87. For WBAA with JI, Cohen's D were 0.5, 1.1, 1.0 and 1.2; with sample sizes 230, 139, 112, and 101. For longitudinal FreeSurfer, Cohen's D were 0.7, 1.0, 1.0, and 1.3; with sample sizes 183, 152, 118, and 102.

## CONCLUSION

The WBAA using CP for brain atrophy quantification provided sensitivity equal or superior to leading, competing methods. Specifically, the WBAA sample sizes were generally lower.

## CLINICAL RELEVANCE/APPLICATION

Unlike longitudinal FreeSurfer, WBAA allows quantification of final atrophy estimates directly after each visit. Adding the matching/improved sensitivity, WBAA seems appropriate for clinical trials.

### SST11-09 • Tumor Cellularity and the Extravascular-Extracellular Space: Using Quantitative Imaging to Evaluate Correlation Between ADC and DCE MRI in Human Gliomas, Meningiomas and Cerebral Lymphomas

**Hannu T Huhdanpaa** MD (Presenter) ; **Darryl Hwang** PhD ; **Naira Muradyan** PhD \* ; **Steven Cen** PhD ; **Michael Booker** ; **Alexander Lerner** MD ; **Deborah Commins** ; **Anandh G Rajamohan** MD ; **Paul E Kim** MD ; **Orest B Boyko** MD, PhD \* ; **John L Go** MD ; **Eu-Meng Law** MBBS \* ; **Mark S Shiroishi** MD

## PURPOSE

The apparent diffusion coefficient (ADC) determined from diffusion tensor (DTI) MR imaging can give an impression of the extravascular-extracellular space (EES) and has been shown to be inversely correlated with tumor cell density. Parametric maps such as the EES fraction ( $v_e$ ) derived from dynamic contrast enhanced (DCE) MRI also characterize EES. The purpose of this study was to determine if there is a correlation between ADC and DCE metrics such as  $v_e$ , blood-brain barrier transfer constant ( $K_{trans}$ ),  $K_{ep}$  ( $K_{trans}/v_e$ ), and fractional plasma volume ( $v_p$ ) for gliomas, cerebral lymphomas and meningiomas. Figure 1 demonstrates ADC and  $v_e$  parametric maps for a glioma.

## METHOD AND MATERIALS

18 gliomas (grade I-IV), 2 lymphomas and 5 meningiomas were retrospectively evaluated. DTI and DCE images were acquired during the same MRI exam. DCE-MRI images were postprocessed in CADvue. Metrics extracted from DCE MRI were:  $v_e$ ,  $v_p$ ,  $K_{trans}$ , and  $K_{ep}$ . ADC maps were generated by the MR scanner. DCE and ADC images were co-registered and 3-dimensional regions of interest were drawn on parametric maps. Voxel-wise correlation between ADC and DCE parameters were examined using scatter plots and tested by random effects model. Mean and median values were extracted using Spearman correlation.

## RESULTS

Overall, mean ADC correlated negatively with mean  $v_e$  ( $r = -0.48$ ,  $p = 0.03$ ) as well as with median  $v_e$  ( $r = -0.52$ ,  $p = 0.01$ ). The result of voxel level analysis using random effects model did not show significant correlation between ADC and  $v_e$  ( $r = 0.09$ ,  $p = 0.09$ ). No statistically significant correlation was observed between ADC and the other parameters,  $v_p$ ,  $K_{trans}$ , and  $K_{ep}$ .

## CONCLUSION

Our results showed a negative correlation between ADC and both mean as well as median  $v_e$ , and no significant correlation between ADC and the other DCE parameters. This is in agreement with a prior study performed in breast cancer, while another study in breast cancer as well as one in glioblastoma found no correlation. These results likely reflect limitations in our understanding of these metrics though limitations in imaging technique may be confounders.

## CLINICAL RELEVANCE/APPLICATION

Determination of the relationship between ADC and DCE MRI metrics such as extravascular-extracellular volume fraction ( $v_e$ ) may provide new imaging biomarkers of brain tumor cellularity

**Abbara, S.** - Consultant, Perceptive Informatics, Inc Author with royalties, Reed Elsevier Author with royalties, Amirsys, Inc  
**Abujudeh, H. H.** - Research Grant, Bracco Group Consultant, RCG HealthCare Consulting  
**Agliozzo, S.** - Researcher, im3D SpA  
**Altes, T. A.** - Research Grant, Vertex Pharmaceuticals Incorporated Research Grant, Novartis AG Research support, Siemens AG  
**Annapragada, A.** - Founder, Marval Biosciences Inc Stockholder, Marval Biosciences Inc Founder, Alzeca Biosciences LLC Stockholder, Alzeca Biosciences LLC Founder, Sensulin LLC Stockholder, Sensulin LLC Stockholder, Abbott Laboratories Stockholder, Johnson & Johnson Stockholder, Merck & Co, Inc  
**Avanaki, A. N.** - Employee, Barco nv  
**Averkiou, M. A.** - Consultant, Koninklijke Philips Electronics NV Consultant, Samsung Electronics Co Ltd  
**Awai, K.** - Research Grant, Toshiba Medical Sysmtes Research Grant, Hitachi Medical Corporation Research Grant, Bayer AG Research Consultant, DAIICHI SANKYO Group Research Grant, Eisai Ltd

## B

**Bae, K. T.** - Patent agreement, Covidien AG Patent agreement, Bayer AG  
**Baker, J. A.** - Research Consultant, Siemens AG  
**Bakic, P. R.** - Research collaboration, Barco nv Research collaboration, Hologic, Inc  
**Bamberg, F.** - Speakers Bureau, Bayer AG Speakers Bureau, Siemens AG Research Grant, Bayer AG Research Grant, Siemens AG  
**Bammer, R.** - Founder, iSchemaView, Inc Director, iSchemaView, Inc Stockholder, iSchemaView, Inc  
**Bankier, A. A.** - Author with royalties, Reed Elsevier Consultant, Olympus Corporation  
**Bauman, G. S.** - Research Grant, sanofi-aventis Group  
**Benzing, T. S.** - Research Grant, Eli Lilly and Company  
**Bert, A.** - Employee, im3D SpA  
**Biswal, S.** - Co-founder, SiteOne Therapeutics Inc Consultant, General Electric Company Stockholder, Atreus Pharmaceuticals Corporation  
**Bluemke, D. A.** - Research support, Siemens AG  
**Bosmans, H.** - Co-founder, Qaelum NV Research Grant, Siemens AG  
**Boyko, O. B.** - Consultant, Bracco Group Consultant, Patient Comfort Systems, Inc  
**Brown, M. S.** - Director, MedQIA Imaging Core Laboratory  
**Buls, N.** - Medical Advisory Board, General Electric Company

## C

**Carbonaro, L. A.** - Research Consultant, im3D SpA  
**Carr, J. C.** - Speaker, Lantheus Medical Imaging, Inc  
**Carrino, J. A.** - Research Grant, Siemens AG Research Grant, Carestream Health, Inc Research Consultant, General Electric Company  
**Chen, J.** - Research Grant, Pfizer Inc  
**Cho, S.** - Research support, Amgen Inc Research support, Peregrine Pharmaceuticals, Inc Research support, Algeta ASA  
**Choi, B.** - Research Consultant, Samsung Electronics Co Ltd  
**Chui, J. H.** - Research collaboration, Barco nv Research collaboration, Hologic, Inc  
**Chung, J. H.** - Research Grant, Siemens AG  
**Chung, M.** - Patent agreement, General Electric Company Patent agreement, Samsung Electronics Co Ltd  
**Clunie, D. A.** - Employee, Bioclinica, Inc Owner, PixelMed Publishing LLC Research support, Siemens AG  
**Cohan, R. H.** - Consultant, General Electric Company  
**Collins, J. D.** - Consultant, C. R. Bard, Inc  
**Coxson, H. O.** - Research Grant, GlaxoSmithKline plc Contract, GlaxoSmithKline plc Contract, Olympus Corporation Steering Committee, GlaxoSmithKline plc

## D

**Dam, E. B.** - Shareholder, Biomediq A/S Employee, Biomediq A/S  
**D'Anastasi, M.** - Travel support, Merck KGaA Travel support, Siemens AG  
**Danielsson, M.** - Stockholder, Koninklijke Philips Electronics NV Stockholder, Sectra AB Stockholder, Prismatic Sensors AB Stockholder, Innovicum AB Stockholder, Biovica International AB  
**Das, M.** - Research Consultant, Bayer AG Research Grant, Siemens AG Speakers Bureau, Siemens AG  
**De Koning, H.** - Research Grant, F. Hoffman-La Roche Ltd Equipment support, Siemens AG Medical Advisory Board, F. Hoffman-La Roche Ltd  
**De Mey, J.** - Research Grant, General Electric Company  
**Deyoe, E. A.** - Stockholder, Prism Clinical Imaging, Inc Board of Directors, Prism Clinical Imaging, Inc  
**Diehn, M.** - Research Consultant, Varian Medical Systems, Inc Research Grant, Varian Medical Systems, Inc  
**Dijkshoorn, M. L.** - Consultant, Siemens AG  
**Doraiswamy, P. M.** - Research Consultant, Bristol-Myers Squibb Company Research Consultant, Eli Lilly and Company Research Consultant, Neuronetrix, Inc Research Consultant, Medivation, Inc Research Grant, Bristol-Myers Squibb Company Research Grant, Eli Lilly and Company Research Grant, Neuronetrix, Inc Research Grant, Medivation, Inc Stockholder, Sonexa Therapeutics, Inc Stockholder, Clarimedix, Inc Speaker, Forest Medical, LLC  
**Drzegza, A.** - Research Consultant, Bayer AG Research Consultant, Eli Lilly and Company Research Consultant, General Electric Company Research Consultant, Piramal Enterprises Limited Speakers Bureau, Bayer AG Speakers Bureau, Eli Lilly and Company Speakers Bureau, General Electric Company Speakers Bureau, Siemens AG Research Grant, Bayer AG

## E

**Eckstein, F.** - Co-owner, Chondrometrics GmbH Co-founder, Chondrometrics GmbH CEO, Chondrometrics GmbH Consultant, Novartis AG Consultant, Merck KGaA Consultant, sanofi-aventis Group  
**Ehman, R. L.** - CEO, Resoundant, Inc  
**Erickson, B. J.** - Stockholder, Evidentia Health  
**Espig, K. S.** - Employee, Barco nv  
**Eusemann, C.** - Employee, Siemens AG  
**Evelhoch, J. L.** - Employee, Merck & Co, Inc Stockholder, Merck & Co, Inc

## F

**Faraggi, M.** - Consultant, Siemens AG  
**Faulhaber, P. F.** - Speaker, Koninklijke Philips Electronics NV Grant, Koninklijke Philips Electronics NV Medical Advisor, MIM Software, Inc  
**Fleischmann, D.** - Research support, Siemens AG Research support, General Electric Company  
**Flohr, T. G.** - Employee, Siemens AG  
**Frahm, J.** - Research collaboration, Siemens AG  
**Frey, K. A.** - Consultant, MIMvista Corp Consultant, General Electric Company Consultant, Eli Lilly and Company Consultant, Bayer AG Research funded, General Electric Company Research funded, Eli Lilly and Company Stockholder, General Electric Company Stockholder, Novo Nordisk AS Stockholder, Bristol-Myers Squibb Company Stockholder, Merck & Co, Inc

## G

**Galanaud, D. P.** - Research Consultant, Olea Medical  
**Gambhir, S. S.** - Research Grant, Bayer AG Research Grant, General Electric Company Research Grant, sanofi-aventis Group Research Consultant, Bracco Group Research Consultant, CytomX Therapeutics Research Consultant, Spectrum Dynamics Ltd Research Consultant, Enlight Biosciences Research Consultant, ImaginAb, Inc Research Consultant, FUJIFILM Holdings Corporation Speaker, Bracco Group Speaker, CytomX Therapeutics, Inc Speaker, Spectrum Dynamics Ltd Speaker, Enlight Biosciences Speaker, ImaginAb, Inc Speaker, FUJIFILM Holdings Corporation Stockholder, CellSight Technologies, Inc Stockholder, Endra, Inc Stockholder, Enlight Biosciences Stockholder, ImaginAb, Inc Stockholder, Lumen Therapeutics, LLC Stockholder, MagArray, Inc Stockholder, NinePoint Medical, Inc Stockholder, Prolume, Ltd Stockholder, RefleXion Medical Inc Stockholder, Spectrum Dynamics Ltd Stockholder, FUJIFILM Holdings Corporation Advisory Board, Enlight Biosciences Advisory Board, ImaginAb, Inc Advisory Board, FUJIFILM Holdings Corporation Spouse, Employee, CellSight Technologies, Inc

**Geyer, L. L.** - Speaker, General Electric Company  
**Ghaghada, K. B.** - Research Grant, Marval Biosciences Inc Consultant, Marval Biosciences Inc Shareholder, Marval Biosciences Inc  
**Giger, M. L.** - Stockholder, Hologic, Inc Shareholder, Quantitative Insights, Inc Royalties, Hologic, Inc Royalties, General Electric Company Royalties, MEDIAN Technologies Royalties, Riverain Technologies, LLC Royalties, Mitsubishi Corporation Royalties, Toshiba Corporation Researcher, Koninklijke Philips Electronics NV Researcher, U-Systems, Inc  
**Gill, R. R.** - Scientific Advisory Board, F. Hoffmann-La Roche Ltd  
**Glaser, K. J.** - Intellectual property, Magnetic Resonance Elastography Stockholder, Resoundant Inc  
**Goh, V. J.** - Research Grant, Siemens AG  
**Grant, K.** - Employee, Siemens AG  
**Graser, A.** - Speakers Bureau, Siemens AG Speakers Bureau, Bracco AG Grant, Bayer AG  
**Greiser, A.** - Employee, Siemens AG  
**Grimm, L. J.** - Board Member, Medscape, LLC Consultant, Medscape, LLC  
**Gulsun, M. A.** - Employee, Siemens AG

## H

**Hall, N. C.** - Consultant, Enlyton, Ltd  
**Hall, T. J.** - Equipment support, Siemens AG  
**Harloff, A.** - Speaker, Boehringer Ingelheim GmbH Speaker, Bayer AG  
**Harvey, J. A.** - Researcher, Hologic, Inc Researcher, Pfizer Inc Shareholder, Matakina International Ltd Shareholder, Hologic, Inc  
**Heinemann, V.** - Research Grant, Merck KGaA  
**Henkel, K. W.** - Employee, MedQIA Imaging Core Laboratory  
**Huisman, H.** - Stockholder, QView Medical, Inc

## I

**Isgum, I.** - Research Grant, Pie Medical Imaging BV Research Grant, 3mensio Medical Imaging BV

## J

**Jack, C. R. Jr** - Consultant, Bristol Meyer Squibb Consultant, General Electric Company Consultant, Siemens Healthcare Consultant, Elan Corporation, plc Researcher, Allon Therapeutics Inc Researcher, Baxter International Inc  
**Jaffray, D. A.** - Research Grant, Koninklijke Philips Electronics NV Research Grant, Elekta AB Research Grant, Raysearch Laboratories AB Research Grant, IMRIS Inc Research Grant, Varian Medical Systems, Inc Research Grant, Modus Medical Devices Inc Royalties, Raysearch Laboratories AB Royalties, Modus Medical Devices Inc Royalties, Elekta AB Royalties, IMRIS Inc  
**Johnson, K. S.** - Research Consultant, Siemens AG

## K

**Kamel, I. R.** - Research support, Bracco Group Research support, Bayer AG  
**Kaplan, S. S.** - Advisory Panel, Hologic, Inc  
**Karczmar, G. S.** - Research Consultant, Perceptive Informatics, Inc Research Consultant, BioClinica, Inc  
**Karssemeijer, N.** - Shareholder, Matakina International Limited Scientific Board, Matakina International Limited Shareholder, QView Medical, Inc Research Grant, Riverain Medical  
**Kauczor, H.** - Research Grant, Boehringer Ingelheim GmbH Research Grant, Siemens AG Speakers Bureau, Boehringer Ingelheim GmbH Speakers Bureau, Bayer AG Speakers Bureau, Siemens AG  
**Khatonabadi, M.** - Research Support, Siemens AG  
**Kimpe, T.** - Employee, Barco nv  
**Kinahan, P. E.** - Research Grant, General Electric Company Co-founder, PET/X LLC  
**Kohan, A.** - Research support, Koninklijke Philips Electronics NV  
**Korporaal, J. G.** - Employee, Siemens AG  
**Kotter, E. C.** - Editorial Advisory Board, Thieme Medical Publishers, Inc  
**Krauss, B.** - Employee, Siemens AG  
**Krestin, G. P.** - Consultant, General Electric Company Research Grant, General Electric Company Research Grant, Bayer AG Research Grant, Siemens AG Speakers Bureau Siemens AG  
**Kripfgans, O. D.** - Research support, General Electric Company Equipment support, General Electric Company  
**Kuhl, C. K.** - Advisory Board Member, Bayer AG  
**Kuo, M. D.** - Shareholder, Confluence Life Sciences, Inc  
**Kurhanewicz, J.** - Research Grant, General Electric Company

## L

**Lassau, N. B.** - Speaker, Toshiba Corporation Speaker, Bracco Group Speaker, Novartis AG Speaker, Pfizer Inc Speaker, F. Hoffmann-La Roche Ltd  
**Laubender, R. P.** - Research Grant, Merck KGaA  
**Law, E.** - Speakers Bureau, Toshiba Corporation Medical Advisory Board, Bayer AG Medical Advisory Board, Bracco Group Medical Advisory Board, FUJIFILM Holdings Corporation  
**Lee, T.** - Grant, General Electric Company Royalties, General Electric Company  
**Leen, E.** - Equipment support, Koninklijke Philips Electronics NV Equipment support, General Electric Company Equipment support, SuperSonic Imagine Research Consultant, General Electric Company Speakers Bureau, Bracco Group Speakers Bureau, Koninklijke Philips Electronics NV Speakers Bureau, AngioDynamics, Inc Speakers Bureau, General Electric Company  
**Lehman, C. D.** - Consultant, Bayer AG Consultant, General Electric Company Research Grant, General Electric Company  
**Leiner, T.** - Speakers Bureau, Koninklijke Philips Electronics NV Consultant, Bayer AG Research Grant, Bracco Group  
**Levenson, R.** - Consultant, Aspect Medical Systems, Inc Consultant, Zymera, Inc  
**Lillholm, M.** - Employee, Biomediq A/S Shareholder, Biomediq A/S  
**Link, T. M.** - Research Grant, General Electric Company Research Grant, InSightec Ltd  
**Loo, B. W. JR** - Speaker, Varian Medical Systems, Inc Speaker, General Electric Company  
**Lynch, D. A.** - Research support, Siemens AG Scientific Advisor, Perceptive Informatics, Inc Consultant, Actelion Ltd Consultant, InterMune, Inc Consultant, Gilead Sciences, Inc Consultant, F. Hoffmann-La Roche Ltd  
**Lynghjem, J.** - Research Grant, Merck KGaA

## M

**Macmahon, H.** - Shareholder, Hologic, Inc Consultant, Riverain Technologies, LLC Royalties, UCTech  
**Macura, K. J.** - Research Grant, Siemens AG  
**Madabhushi, A.** - Research partner, Siemens AG Research partner, General Electric Company Research partner, F. Hoffman-La Roche Ltd Founder and President, IbRiS, Inc  
**Mahnken, A. H.** - Speaker, Bayer AG  
**Maidment, A. D.** - Research support, Hologic, Inc Research support, Barco nv Spouse, Employee, Real-Time Radiography, Inc Spouse, Stockholder, Real-Time Radiography, Inc  
**Majumdar, S.** - Research Grant, Merck & Co, Inc  
**Maravilla, K. R.** - Research Grant, Bayer AG Research Grant, Bracco Group Research, Guerbet SA Speaker, Bracco Group Consultant, Guerbet SA  
**Marchessoux, C.** - Employee, Barco nv  
**Mayo, J. R.** - Speaker, Siemens AG  
**McConathy, J. E.** - Research Consultant, GLG Consulting Speakers Bureau, Eli Lilly and Company Research Consultant, General Electric Company  
**McNitt-Gray, M. F.** - Institutional research agreement, Siemens AG Research support, Siemens AG

**Miles, K.** - Director, TexRAD Limited Shareholder, TexRAD Limited  
**Minoshima, S.** - License agreement, General Electric Company Research Grant, Koninklijke Philips Electronics NV Research Grant, Hitachi, Ltd Research Consultant, Hamamatsu Photonics KK Grant, Nihon Medi-Physics Co, Ltd Research Grant, Astellas Group Research Grant, Seattle Genetics, Inc  
**Morra, L.** - Researcher, im3D Spa  
**Mukherjee, P.** - Research Grant, General Electric Company  
**Muradyan, N.** - Employee, iCAD, Inc  
**Muzic, R.** - Research Grant, Koninklijke Philips Electronics NV

## N

**Newstead, G. M.** - Medical Advisory Board, Bayer AG Consultant, Three Palm Software LLC  
**Nguyen, T.** - Research Grant, Bayer AG Research Consultant, Bayer AG  
**Nichols, K.** - Royalties, Syntermed, Inc Consultant, Gilead Sciences, Inc  
**Nielsen, M.** - Stockholder, Biomediq A/S Research Grant, Nordic Bioscience A/S Research Grant, SYNARC Inc Research Grant, AstraZeneca PLC  
**Nishikawa, R. M.** - Royalties, Hologic, Inc Royalties, Mitsubishi Corporation Royalties, MEDIAN Technologies Royalties, Toshiba Corporation Royalties, Riverain Technologies, LLC Consultant, iCAD, Inc  
**Ntziachristos, V.** - Stockholder, iThera Medical GmbH

## O

**O'Connell, T.** - President, Resolve Radiologic Ltd

## P

**Padhani, A. R.** - Consultant, IXICO Limited Advisory Board, Acuitus Medical Ltd Advisory board, Siemens AG  
**Park, S.** - Research Consultant, INFINITT Healthcare Co, Ltd Research Grant, DONGKOOK Pharmaceutical Co, Ltd Research Grant, General Electric Company  
**Partovi, S.** - Research Grant, Koninklijke Philips Electronics NV  
**Petrella, J. R.** - Advisory Board, Johnson & Johnson Speakers Bureau, Quintiles Inc Advisory Board, Piramal Enterprises Limited  
**Pillai, J. J.** - Medical Advisory Board, Prism Clinical Imaging, Inc Research Grant, Siemens AG  
**Plecha, D. M.** - Advisory Board, Hologic, Inc Research Grant, SuperSonic Imagine  
**Priatna, A.** - Research Consultant, Siemens AG Employee, Siemens AG  
**Prokop, M.** - Speakers Bureau, Bayer AG Speakers Bureau, Bracco Group Speakers Bureau, Toshiba Corporation Speakers Bureau, Koninklijke Philips Electronics NV Research Grant, Toshiba Corporation

## Q

**Quon, A.** - Speakers Bureau, Lilly USA/Avid Pharmaceuticals Research Consultant, Phillips Healthcare

## R

**Ratib, O.** - Research Consultant, Koninklijke Philips Electronics NV  
**Reiter, G.** - Employee, Siemens AG  
**Remy-Jardin, M. J.** - Research Grant, Siemens AG  
**Robson, M. E.** - Advisory Board, Pfizer Inc Advisory Board, Abbott Laboratories Advisory Board, sanofi-aventis Group Advisory Board, General Electric Company Research funded, AstraZeneca PLC  
**Romman, Z.** - Employee, Koninklijke Philips Electronics NV  
**Rubbert, C.** - Fellowship funded, Koninklijke Philips Electronics NV  
**Rubin, D. L.** - Grant, General Electric Company Grant, Siemens AG  
**Rybicki, F. J. III** - Research Grant, Toshiba Corporation Research Grant, Bracco Group

## S

**Saam, T.** - Research Grant, Diamed Medizintechnik GmbH Research Grant, Bayer AG  
**Schmidt, B.** - Employee, Siemens AG  
**Schoenberg, S. O.** - Institutional research agreement, Siemens AG  
**Schoepf, U.** - Research Grant, Bracco Group Research Grant, General Electric Company Research Consultant, Siemens AG Research Grant, Siemens AG  
**Sedlmair, M. U.** - Employee, Siemens AG  
**Siegel, E. L.** - Research Grant, General Electric Company Speakers Bureau, Siemens AG Board of Directors, Carestream Health, Inc Research Grant, XYBIX Systems, Inc Research Grant, Steelcase, Inc Research Grant, Anthro Corp Research Grant, RedRick Technologies Inc Research Grant, Evolved Technologies Corporation Research Grant, Barco nv Research Grant, Intel Corporation Research Grant, Dell Inc Research Grant, Herman Miller, Inc Research Grant, Virtual Radiology Research Grant, Anatomical Travelogue, Inc Medical Advisory Board, Fovia, Inc Medical Advisory Board, Vital Images Medical Advisory Board, McKesson Corporation Medical Advisory Board, Carestream Health, Inc Medical Advisory Board, Bayer AG Research, TeraRecon, Inc Medical Advisory Board, Bracco Group Researcher, Bracco Group Medical Advisory Board, Merge Healthcare Incorporated Medical Advisory Board, Microsoft Corporation Researcher, Microsoft Corporation  
**Siewerdsen, J. H.** - Research Grant, Siemens AG Consultant, Siemens AG Research Grant, Carestream Health, Inc Royalties, Elekta AB  
**Sirlin, C. B.** - Research Grant, Bayer AG Research Grant, General Electric Company Research Grant, Bracco Group Contract, Isis Pharmaceuticals, Inc Contract, Pfizer Inc Speakers Bureau, Bayer AG Consultant, Bayer AG Medical Advisory Board, Bayer AG Consultant, Merck & Co, Inc Medical Advisory Board, General Electric Company Consultant, sanofi-aventis Group Consultant, Synageva BioPharma Corporation Contract, Profil Consultant, Takeda Pharmaceutical Company Limited Contract, Siemens AG  
**Sosna, J.** - Consultant, ActiViews Ltd Research Grant, Koninklijke Philips Electronics NV  
**Sporring, J.** - Co-founder, DigiCorpus ApS Shareholder, DigiCorpus ApS  
**Stalder, A. F.** - Employee, Siemens AG  
**Stayman, J. W.** - Research Grant, Varian Medical Systems, Inc  
**Strecker, R.** - Employee, Siemens AG  
**Summers, R. M.** - Royalties, iCAD, Inc Grant, iCAD, Inc Stockholder, Johnson & Johnson Grant, Viatronix, Inc

## T

**Tanifum, E.** - Stockholder, Alzeca Biosciences LLC

## V

**Van Tosh, A.** - Consultant, Pfizer Inc Consultant, Bracco Group Consultant, Cardinal Health, Inc Consultant, Ion Beam Applications, SA  
**Vercher-Conejero, J. L.** - Research Grant, Koninklijke Philips Electronics NV  
**Viergever, M. A.** - Research Grant, Koninklijke Philips Electronics NV Research Grant, Pie Medical Imaging BV  
**Vlahos, I.** - Consultant, Siemens AG Consultant, General Electric Company

## W

**Wahl, R. L.** - Patents, Naviscan, Inc Patents, GlaxoSmithKline plc Patents, Spectrum Pharmaceuticals, Inc Research Consultant, GlaxoSmithKline plc Research Consultant, Nihon Medi-Physics Co, Ltd Research support, General Electric Company Research support, Molecular Insight Pharmaceuticals, Inc Research support, Cell Point LLC  
**Weber, M.** - Research Grant, Bayer AG Research Grant, Guerbet SA Research Grant, Bracco Group Research Grant, Siemens AG  
**Weissman, I. L.** - Co-founder, StemCells, Inc Director, StemCells, Inc Stockholder, Amgen Inc

**Wolterink, J. M.** - Research Grant, Pie Medical Imaging BV

**Woodard, P. K.** - Research support, Siemens AG Meeting travel, Siemens AG Research support, Astellas Group Consultant, Medtronic, Inc Consultant, BIOTRONIK GmbH & Co KGC Consultant, GE Healthcare

**Wu, A. M.** - Stockholder, ImaginAb, Inc Research Grant, ImaginAb, Inc Consultant, ImaginAb, Inc. Consultant, DAIICHI SANKYO Group Consultant, sanofi-aventis Group

## X

**Xthona, A.** - Employee, Barco nv

**Xu, J.** - Employee, Siemens AG

## Y

**Yang, K.** - Employee, MedQIA Imaging Core Laboratory

**Yao, J.** - Royalties, iCAD, Inc

**Yorkston, J.** - Employee, Carestream Health, Inc

**Yoshida, H.** - Patent holder, Hologic, Inc Patent holder, MEDIAN Technologies

## Z

**Zaharchuk, G.** - Research Grant, General Electric Company

**Zbijewski, W.** - Research Grant, Carestream Health, Inc